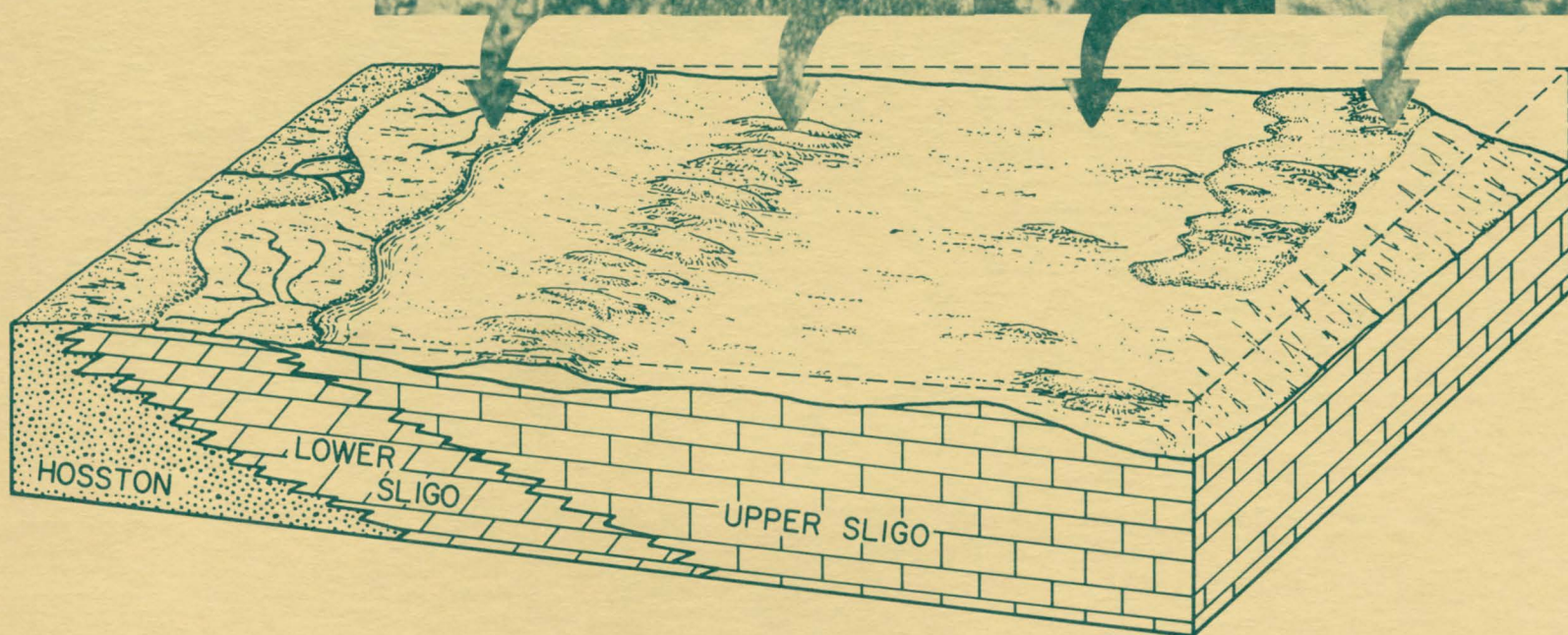


DEPOSITIONAL AND DIAGENETIC HISTORY OF THE SLIGO AND HOSSTON FORMATIONS (LOWER CRETACEOUS) IN SOUTH TEXAS

by Don G. Bebout
David A. Budd
Richard A. Schatzinger



1981



Bureau of Economic Geology
The University of Texas at Austin
Austin, Texas 78712

W. L. Fisher, Director

QAe4010

DEPOSITIONAL AND DIAGENETIC HISTORY OF THE SLIGO AND HOSSTON FORMATIONS (LOWER CRETACEOUS) IN SOUTH TEXAS

by **Don G. Bebout**
David A. Budd
Richard A. Schatzinger

1981



Bureau of Economic Geology
The University of Texas at Austin
Austin, Texas 78712

W. L. Fisher, Director

CONTENTS

ABSTRACT	1	Sligo shelf-lagoon and oolite-shoal complex ..	44
INTRODUCTION	2	<i>Submarine stage</i>	45
General remarks	2	<i>Early meteoric-phreatic stage</i>	45
Objectives	2	<i>Late meteoric-phreatic stage</i>	46
Paleogeographic setting	3	<i>Deep subsurface stage</i>	47
General geologic history — Trinity Group ..	4	Sligo shelf-margin grainstones	47
Previous work	10	<i>Submarine stage</i>	47
DEPOSITIONAL ENVIRONMENTS	11	<i>Early meteoric-phreatic stage</i>	48
Hosston and lower Sligo environments	11	<i>Late meteoric-phreatic to deep</i>	
Upper Sligo environments	14	<i>subsurface stage</i>	61
FACIES	29	Sligo shelf-margin wackestones and	
General remarks	29	packstones	61
Facies distribution	32	Summary: Sligo diagenesis	61
Hosston and lower Sligo facies	32	Hosston Formation	62
Upper Sligo facies	36	Siliciclastics	62
<i>Regional facies patterns</i>	36	Carbonates	62
<i>Oolite-shoal complex</i>	37	CONCLUSIONS	64
<i>Shelf margin</i>	40	ACKNOWLEDGMENTS	65
DIAGENESIS	44	REFERENCES	65
Sligo paragenetic sequences	44	APPENDIX I: Materials and Procedures	68

Figures

1. Cretaceous stratigraphy, Central and South Texas	2
2. Location of study area, South Texas	2
3. Sligo gas fields, South Texas	3
4. Sligo and Hosston wells and cores, South Texas	4
5. Previous Bureau of Economic Geology studies, Sligo and Hosston Formations, South Texas	5
6. Early Cretaceous paleogeography, South Texas	5
7. Seismic lines across Lower Cretaceous shelf margins, South Texas	6
8. Trinity Group of Central and South Texas	7
9. Regional lithologies and depositional environments, Sligo and Hosston Formations, South Texas	8
10. Transgressive-progradational cycles in the Sligo and Hosston Formations, South Texas	8
11. Electric-log section of the Lower Cretaceous Series, South Texas	9
12. Structure-contour map, top of Sligo Formation, South Texas	9
13. Regional fossil abundance and diversity within the Sligo and Hosston Formations, South Texas	10
14. Sligo and Hosston depositional environments	13
15. Hosston and lower Sligo tidal-flat complex	13
16. Oolite-shoal complex, upper Sligo	15
17. Sligo shelf margin	15
18. Burrowed dolomite mudstone and pellet-mollusk dolomite wackestone	16
19. Burrowed sandstone and laminated sandstone	17
20. Laminated siltstone and intraclast dolomite wackestone	18
21. Laminated dolomite mudstone and skeletal dolomite grainstone	19
22. Pellet dolomite grainstone and conglomeratic sandstone	20
23. Silty lime mudstone, miliolid wackestone, mollusk-miliolid wackestone, and echinoid-mollusk-miliolid wackestone	21
24. Pellet grainstone and fossiliferous lime mudstone	22
25. Oyster-miliolid wackestone, toucasid wackestone, and oncolite packstone	23
26. Laminated lime mudstone and coated-grain packstone	24
27. Pellet packstone and skeletal grainstone	25
28. Oolite grainstone	26
29. Caprinid grainstone, coral-caprinid grainstone, and caprinid-coral packstone/wackestone	27

Figures (cont.)

30. Coral-caprinid packstone/wackestone, caprinid packstone/wackestone, and coralgall boundstone	28
31. Hosston and lower Sligo dip section B-B'	in pocket
32A. Progradational sequences in the Hosston clastic tidal flats	34
32B. Hosston siliclastic tidal flats	35
33A. Progradational sequences in the Hosston dolomitic tidal-flat deposits	36
33B. Hosston dolomitic tidal flat	37
34A. Progradational cycles of the lower Sligo tidal-flat deposits	38
34B. Lower Sligo dolomitic tidal-flat sequence	39
35. Dip section B-B', Sligo and Hosston Formations	39
36. Regional dip section C-C' through the upper Sligo Formation	40
37. Dip section D-D' through the upper Sligo oolite-shoal complex	40
38. Dip section E-E' through the upper Sligo oolite-shoal complex	41
39. Regional strike section F-F' along the Sligo shelf margin	42
40. Regional strike section G-G' behind the Sligo shelf margin	43
41. Submarine diagenesis and syntaxial overgrowths	49
42. Skeletal dissolution, isopachous rim cement, and compaction	50
43. Collapsed rim cements and compacted pellets	51
44. Progressive dolomitization	52
45. Timing of dolomitization and euhedral calcite	53
46. Coarse-crystalline calcite and baroque dolomite	54
47. Baroque dolomite and anhydrite	55
48. Anhydrite and authigenic quartz	56
49. Submarine diagenesis of shelf-margin grainstones	57
50. Radial cement, skeletal dissolution, and fine-crystalline early meteoric-phreatic cement	58
51. Radial cement	59
52. Radial cement, coarse-crystalline calcite, and diagenesis in shelf-margin packstone/wackestone facies	60
53. Sequence of diagenetic events in the upper Sligo oolite-shoal complex and adjacent shelf facies	61
54. Sequence of diagenetic events in the Sligo shelf-margin grainstones and wackestones/packstones facies	61
55. Anhydrite and gypsum, Hosston tidal-flat facies	63

Tables

1. Sligo gas fields, South Texas	3
2. Facies descriptions, Sligo and Hosston Formations	12
3. Facies and depositional environments, Sligo and Hosston Formations	30
4. Comparison of tidal-flat sequences, Hosston and lower Sligo Formations	38

ABSTRACT

The Sligo and Hosston Formations of Aptian age occur over thousands of square miles in the subsurface of South Texas. These two formations consist of three major coeval parts, Hosston, lower Sligo, and upper Sligo, all three of which were deposited contemporaneously to produce a time-transgressive wedge of sediment. Superimposed on the overall transgressive sequence are numerous progradational cycles composed of shoaling-upward sequences.

Thirty facies were deposited in six major environments: (1) alluvial plain, (2) tidal-flat complex, (3) inner-shelf lagoon, (4) oolite-shoal complex, (5) outer-shelf lagoon, and (6) shelf margin. Shelf-margin facies include coral-caprinid wackestone, grainstone, and coralgall boundstone deposited in organic banks and associated sand shoals. Back-reef facies are dominated by oyster, *toucasid*, and miliolid wackestones and oncolite packstones, all deposited in low- to moderate-energy settings. The inner- and outer-shelf facies are low-energy, highly burrowed, skeletal wackestones. Oolite and skeletal grainstones deposited in mobile sand shoals and coated-grain and pellet packstones deposited in stabilized grain flats compose the oolite-shoal complex.

In the Hosston tidal-flat complex, laminated sandstone, dolomite mudstone, and anhydrite were deposited on a broad sabkha. The lower Sligo tidal-flat complex, however, is characterized by abundant subtidal and intertidal deposits, including burrowed dolomite mudstone and pellet-mollusk dolomite wackestone. Supratidal facies in the lower Sligo Formation include not only laminated dolomite mudstone but also skeletal and pellet grainstones deposited as beach ridges and channel levees.

Four stages of diagenesis are apparent in Sligo and Hosston rocks: submarine, early meteoric-phreatic, late meteoric-phreatic, and deep subsurface. The significance of each of these stages to the diagenetic histories of the oolite-shoal complex, inner- and outer-shelf deposits, and shelf-margin complex varies considerably, however. Except at the shelf margin, submarine diagenesis was minimal, consisting primarily of micrite rim formation, deposition of internal sediment, and grain breakage. At the shelf margin, isopachous aragonite cement was

precipitated in some of the grainstone facies. Some less widespread Mg-calcite submarine cement also formed.

Two ubiquitous early meteoric-phreatic events were the dissolution of aragonite allochems and the precipitation of syntaxial overgrowths on echinoderms. Excellent preservation of original oolite structure suggests that their original mineralogy was Mg-calcite and that therefore the oolites did not undergo dissolution. Rocks of the oolite-shoal complex and adjacent subtidal shelf deposits show evidence of meteoric-phreatic diagenesis, including precipitation of finely crystalline isopachous calcite, compaction and collapse of micrite rims, presence of more isopachous calcite, and mixing-zone dolomitization. Dolomitization is most pronounced in the skeletal and pelletal wackestone facies.

Meteoric-phreatic diagenesis is also significant in the shelf-margin facies. An isopachous, fine-crystalline, equant calcite precipitated only where marine cements were lacking. Pore-filling fine-crystalline calcite spar is limited to skeletal molds; the dominant feature is bladed radial cement. Some of this cement is the product of the inversion of aragonitic submarine cement and rudist shells; however, much appears to have been primary pore-filling cement.

A coarsely crystalline, equant calcite spar was precipitated throughout the Sligo Formation as a late meteoric-phreatic product. This is the final diagenetic product in the shelf-margin facies. However, in the oolite-shoal complex and adjacent subtidal shelf deposits, dolomitization (yielding successively larger rhombs), replacement by anhydrite, cementation by pore-filling baroque dolomite, anhydrite, and euhedral calcite, and formation of authigenic quartz all occur as deep subsurface (below 610 m [2,000 ft]) diagenetic products.

The diagenetic history revealed in the dolomitic tidal-flat facies resembles the diagenetic sequences documented for the oolite-shoal complex. Complete dolomitization of all units to a fine- to medium-crystalline, inclusion-rich dolomite in the tidal-flat facies is the only difference.

Significant hydrocarbon production from the Sligo Formation in South Texas is restricted to three gas fields. Two reservoirs are in shelf-margin facies and the other is in shelf-platform facies. In addition, four inactive gasfields occur in the area.

INTRODUCTION

General Remarks

The Sligo and Hosston Formations of Aptian age (fig. 1) are the lowermost Cretaceous rocks in Texas. In South Texas the Sligo and Hosston Formations occur solely in the subsurface for thousands of square miles (fig. 2) and represent a basal Cretaceous transgressive wedge of carbonates and sandstones, respectively. Directly overlying the Sligo and Hosston Formations are, in ascending order, the Pearsall and Glen Rose Formations and the Edwards Group.

Information about these rocks in the subsurface is limited to oil and gas drilling data. Oil and gas recovery from the Sligo Formation in South Texas is restricted to seven gas fields (table 1, fig. 3), but only three fields are presently producing. Reservoirs occur in shelf-margin and outer-shelf facies of the Sligo, but all wells have shallower pay horizons also. Other well-known lowermost Cretaceous reservoirs (Sligo equivalents) include the Black Lake field of northern Louisiana (Myerhoff, 1967), and Pemex discoveries at Anahuac and Totonaca in northern Mexico (Cook, 1979).

CRETACEOUS	Upper	Turonian	Eagle Ford			
		Cenomanian				
	Lower	Albian	Washita	Buda		
				Del Rio		
				Georgetown		
			Edwards	Stuart City		
			Glen Rose			
		Aptian	Trinity Group	Pearsall		
		Barremian		Sligo		
		Hauterivian				
					? - - - - -	

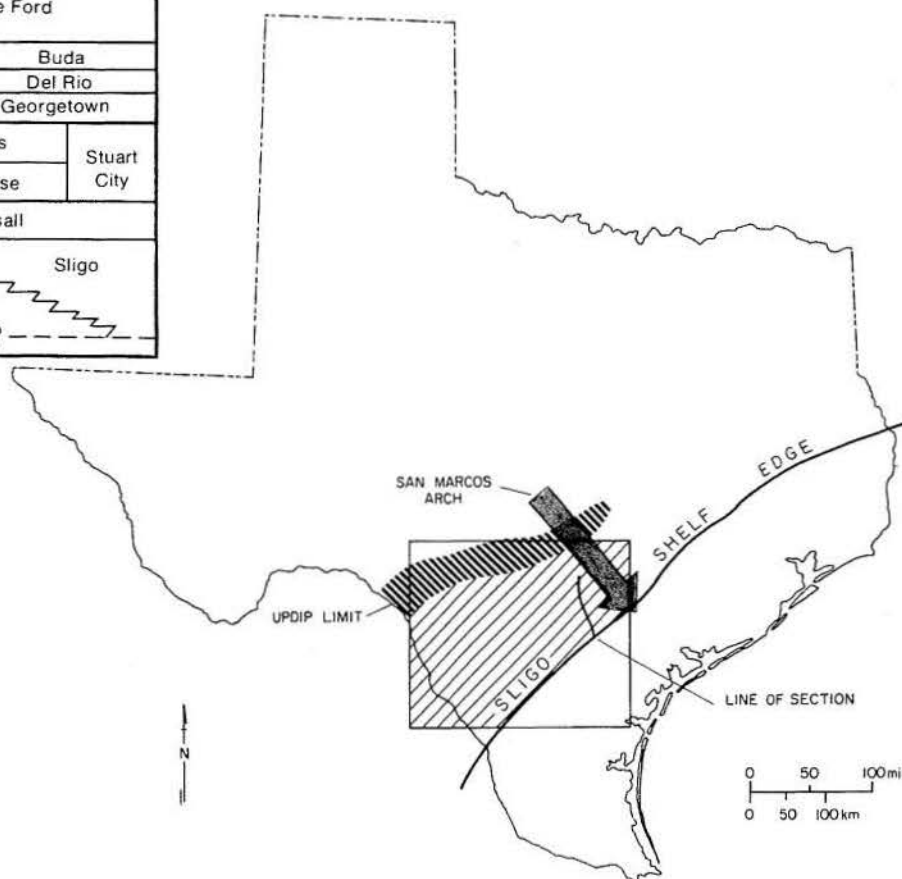
Figure 1. Lower Cretaceous formations and age correlations, Central and South Texas (modified from Bebout and Loucks, 1977).

Figure 2. Study area bounded updip by the Sligo pinch-out, downdip by the shelf edge, to the northeast by the San Marcos Arch, and to the southwest by the international boundary with Mexico. The line of section is shown in figure 11.

More than 200 wells have been drilled into the Sligo Formation in South Texas (fig. 4), but more than three-fourths penetrate only the upper 15 to 30 m (50 to 100 ft). Cores were obtained from 50 wells in the vicinity of the Sligo shelf margin and in a cluster in Atascosa, Frio, Medina, and Zavala Counties. The latter are largely the result of extensive exploration by Tenneco Oil Company.

Objectives

Hydrocarbon exploration in Lower Cretaceous strata in South Texas has been active for the last ten years. These Cretaceous carbonates and the older Jurassic strata represent one of the last drilling frontiers on the Texas Gulf Coast. Therefore over the past six years geologists of the Bureau of Economic Geology have studied the Lower Cretaceous in South Texas, bringing together the available core and summarizing depositional facies, environments, diagenetic histories, and porosity types. Previous Bureau reports (fig. 5) include analyses of the Stuart City Trend (Bebout and Loucks, 1974), the Pearsall Formation (Loucks, 1977), and the Sligo and Hosston Formations (Bebout, 1977; Bebout and Schatzinger, 1978); a symposium on the



Cretaceous of Texas and Mexico (Bebout and Loucks, 1977); and various papers on the diagenesis of the Stuart City Trend (Bebout, 1974; Bebout and others, 1977).

This report completes the analysis of the Sligo and Hosston Formations of South Texas by presenting the depositional facies and

environments, diagenetic histories, and porosity development of the entire sequence. A depositional-diagenetic model for the Sligo Formation in South Texas is directly applicable to exploration activity in Lower Cretaceous rocks around the entire Gulf of Mexico. In addition, extensive carbonate shelves and shelf-margin

banks also developed along the margins of many other basins around the world during Early Cretaceous time. A knowledge of the geologic history of the Sligo and Hosston Formations may lead to a better understanding of similar shelves elsewhere.

Table 1. Sligo gas fields, South Texas.*

Field Name	County	Total No. Wells	Total Prod. Wells	Initial Prod. Year	Present Status (1979)	Cum. Prod. (mcf)
Kenedy, S. W.	Karnes	1	1	1974	Active	2,557,226
Pawnee	Bee	3	2	1968	Active	7,556,876
Kincaid-Winn	Maverick	1	1	1972	Active	1,350,309+ 2,312 bbls
Nordheim, N.	De Witt	1	0	1970	Inactive (1975)	1,934,640
Chittim	Maverick	1	0	1963	Inactive (1971)	224,707
Los Cuatros	Maverick	1	0	1976	Inactive (1977)	30,698+ 27 bbls
Doering Ranch	Frio	0	0	1976	Inactive (1977)	3,676
						13,658,132+ 2,339 bbls

*Based on Texas Railroad Commission, Oil and Gas Division, Annual Reports through 1979.

Paleogeographic Setting

During deposition of the Sligo and Hosston Formations, a broad, shallow shelf up to 160 km (100 mi) wide extended across South Texas (fig. 6). This shelf was bordered to the north

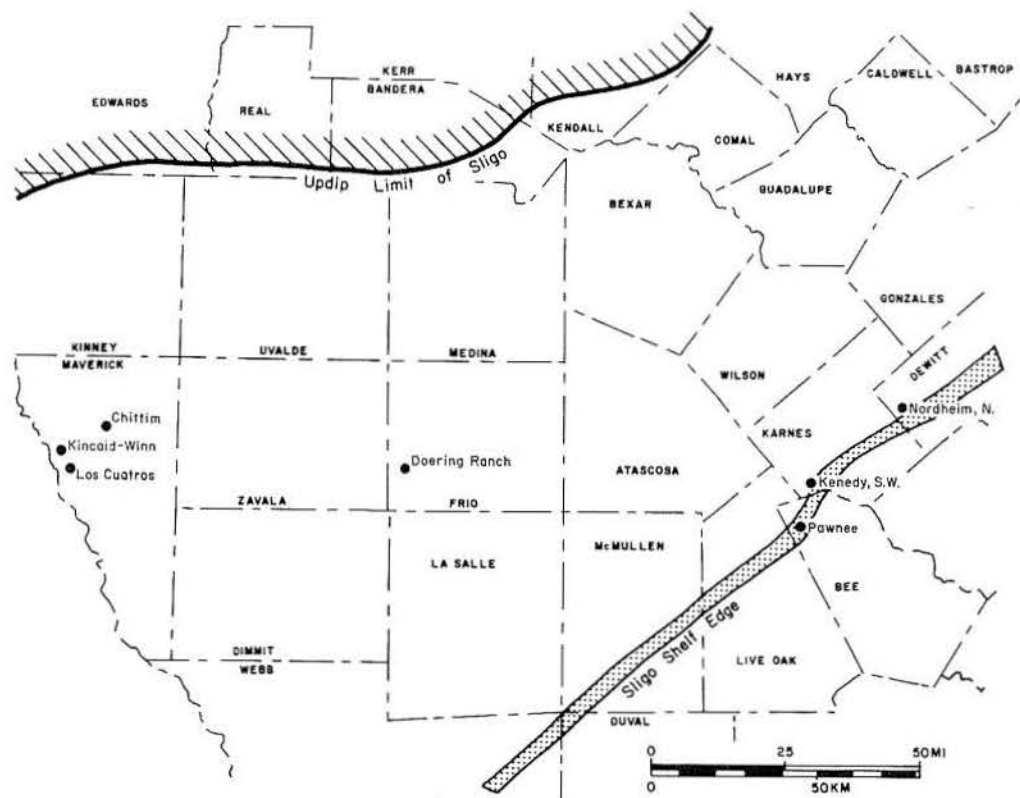


Figure 3. Location of Sligo gas production in the South Texas study area. See table 1 for drilling and production data.

by the Llano Uplift and to the northwest by the Devil's River Uplift. The Hosston Formation overlies these uplifts.

The San Marcos Arch is a low structure trending southeast from the Llano Uplift. The arch was active during Early Cretaceous time, subsiding more slowly than the East Texas Basin to the northeast and Maverick Basin to the southwest (Loucks, 1977). The Pearsall Arch projected into the Maverick Basin from the northeast and localized the deposition of an oolite-sand shoal complex in the upper Sligo Formation (Bebout and Schatzinger, 1978).

The Sligo and Hosston shelf was bordered to the west in Mexico by the Tamaulipas Platform. To the southeast, a shelf-margin complex separated the shelf wedge from the deep, ancestral Gulf of Mexico Basin. Seismic lines indicate that this shelf-margin complex extended farther gulfward than the later Stuart City Trend, whereas to the north the Stuart City Trend is nearly superimposed on the Sligo reef (fig. 7). In both areas the slope in front of the Sligo shelf edge appears to have been much steeper, and it exhibits major post-Sligo marine onlapping sequences.

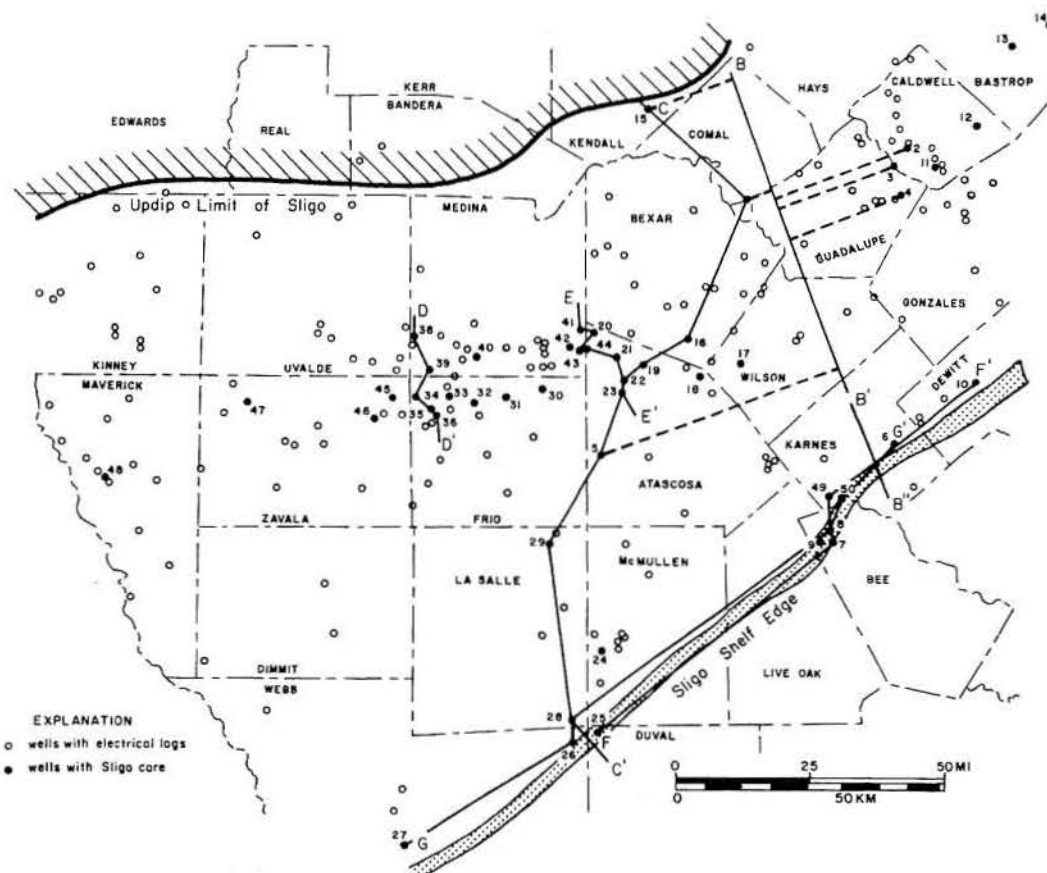
General Geologic History — Trinity Group

The Sligo and Hosston Formations comprise the first of three major transgressive cycles of sedimentation in the Trinity Group (fig. 8; Stricklin and others, 1971). Each cycle was deposited progressively farther landward than the preceding cycle and is separated from the succeeding cycle by a disconformity in the updip outcrop area (Stricklin and others, 1971).

In the Central Texas outcrop area each cycle is a terrigenous clastic-carbonate couplet (Stricklin and others, 1971). Downdip, at the Cretaceous shelf edge, only two major cycles can be recognized — the Sligo and Stuart City Formations (Bebout and Loucks, 1974; Loucks, 1977). Carbonate deposition dominated in this area, and sedimentation occurred concurrently with the relative rise in sea level, resulting in aggradation and progradation of the Stuart City reef.

Bebout (1977) recognized the upper Sligo Formation, composed primarily of limestone, and the lower Sligo Formation, composed primarily of dolomite and anhydrite (fig. 9). The Hosston

Figure 4. Well and core control and location of detailed cross sections B-B' through G-G'. Names of wells with core are listed in Appendix I.



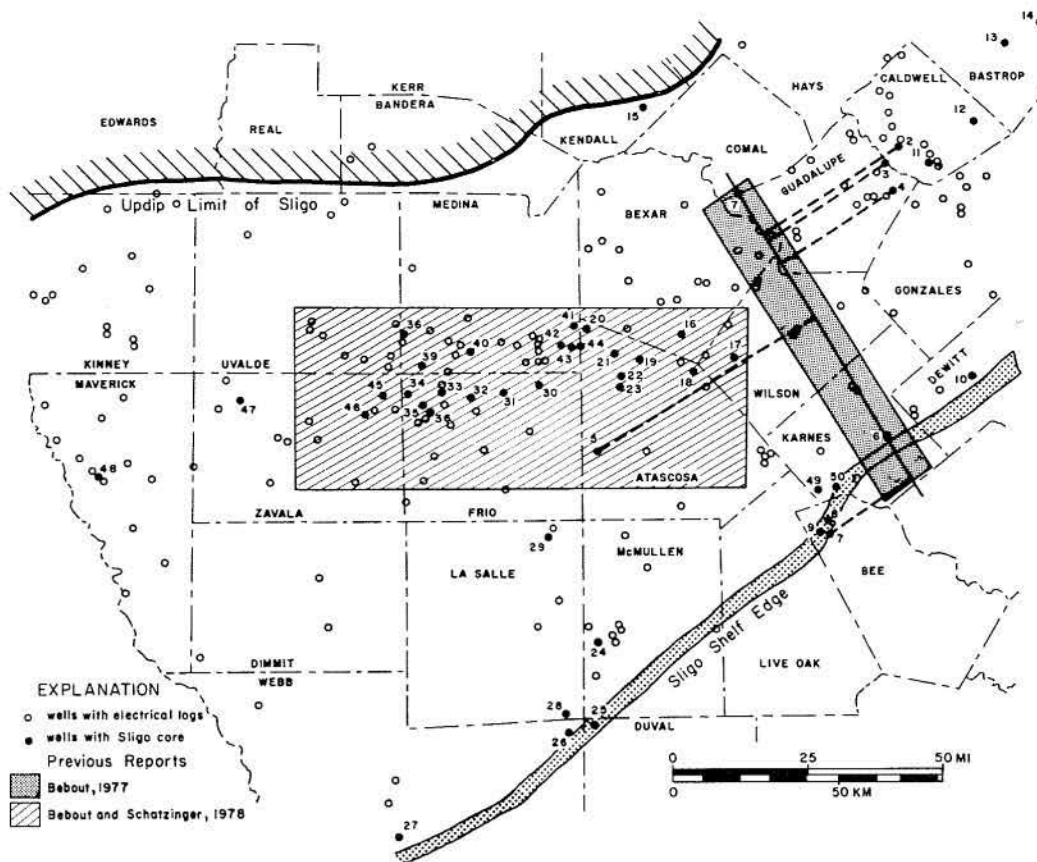


Figure 5. Areas of Sligo and Hosston Formations described and discussed in previous Bureau of Economic Geology studies (Bebout, 1977; Bebout and Schatzinger, 1978).

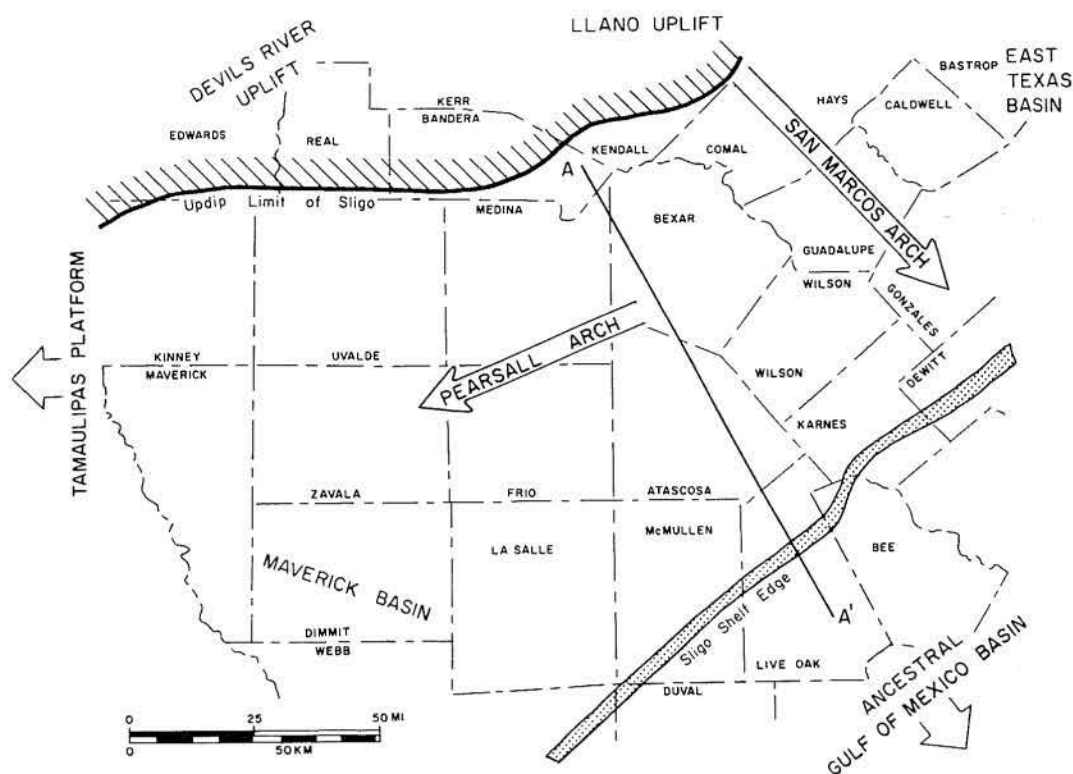
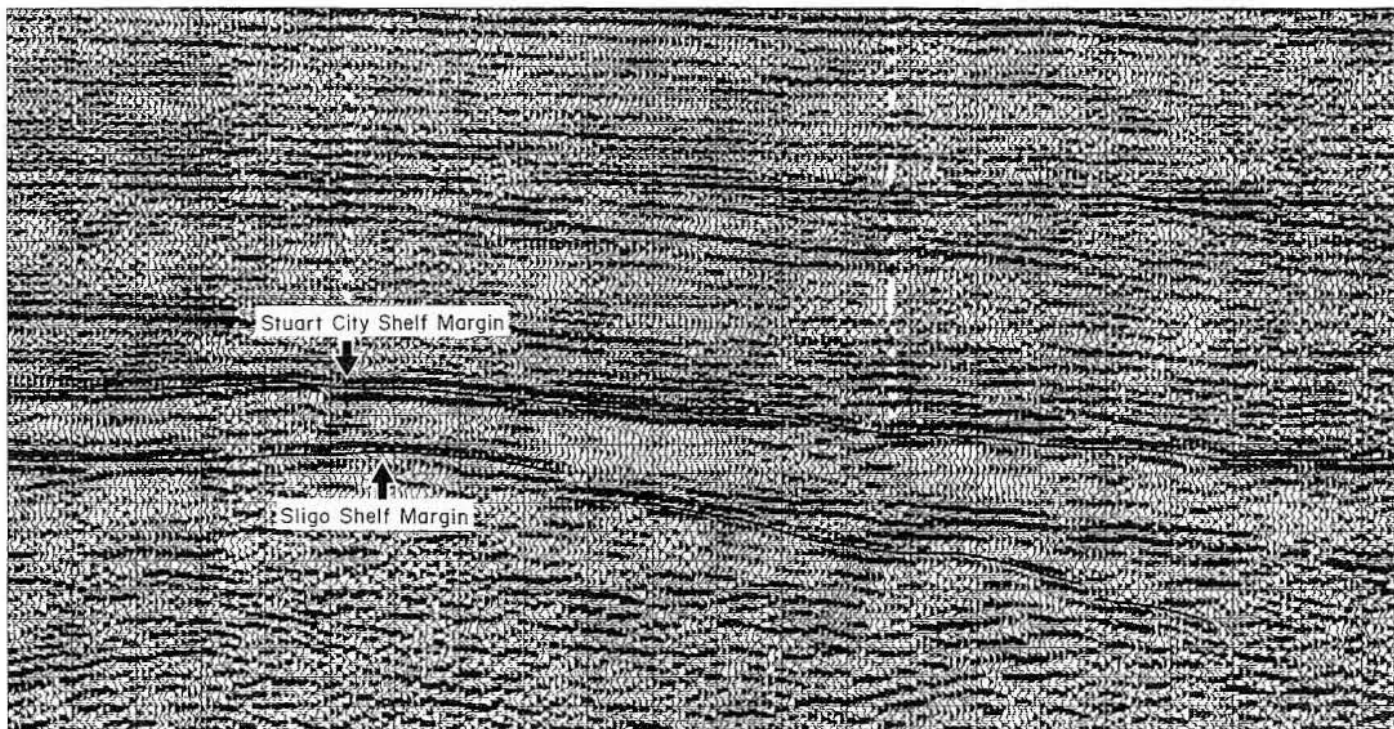


Figure 6. Paleogeography of the Early Cretaceous of South Texas (modified from Loucks, 1977). The line of section, A-A', is shown in figure 8.



NW

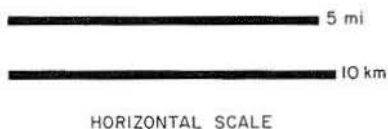
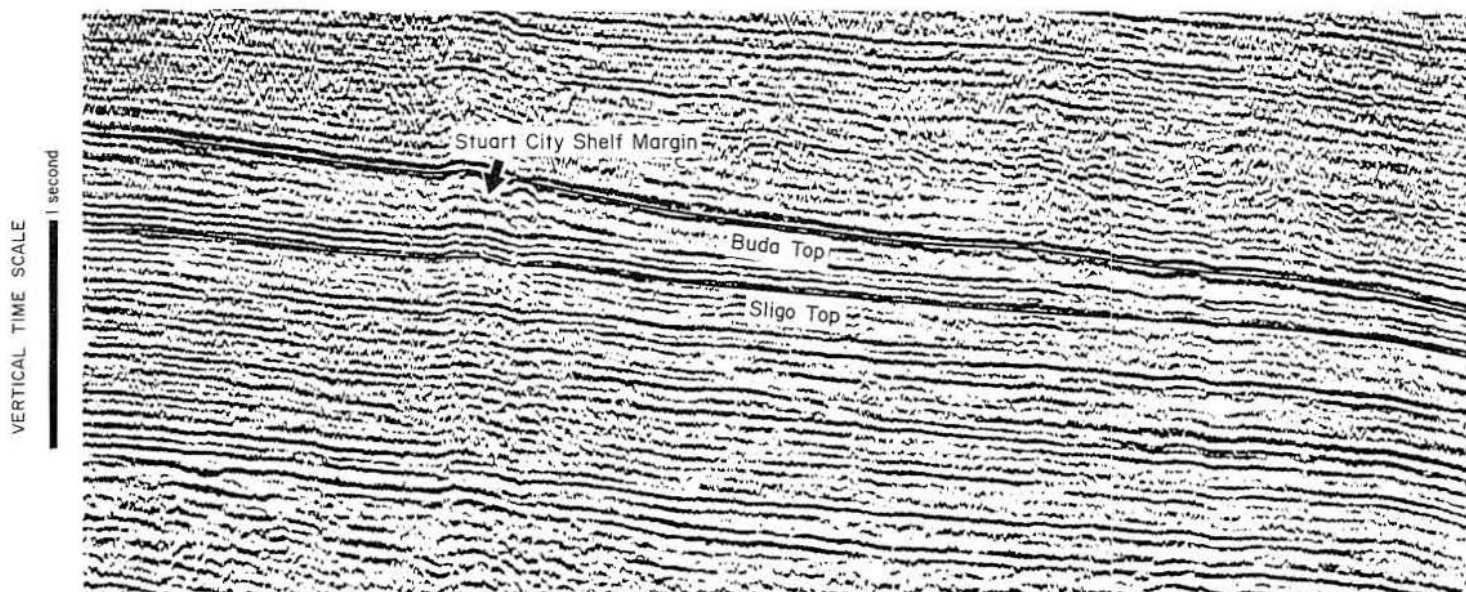


Figure 7. Seismic sections across the Sligo and Stuart City shelf margins in the southern (lower) and northern (upper) portions of the study area. The sections are shown with the tops of the Sligo and Buda Formations (approximately one cycle above the top of the Stuart City Formation) on the lower section and the tops of the Sligo and Stuart City Formations on the upper section. Note that the Sligo shelf edge occurs nearly 40 km (25 mi) to the southeast of

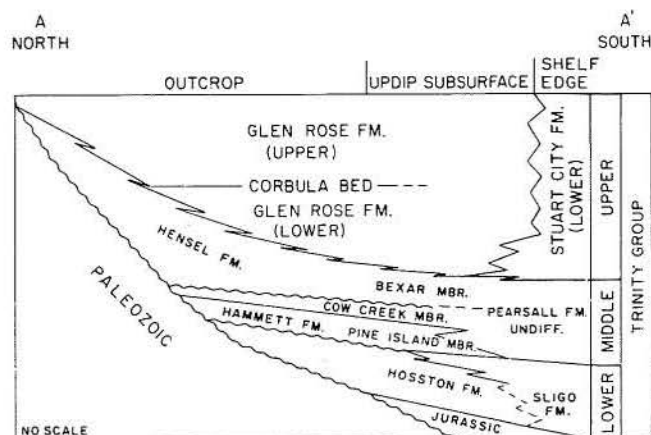
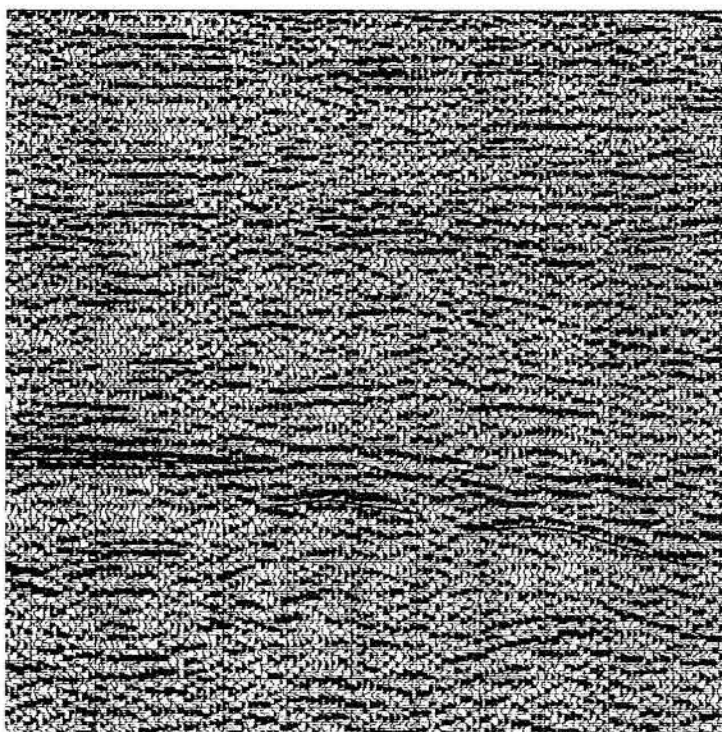


Figure 8. Stratigraphic diagram of the Trinity Group, Central and South Texas. General location of diagram is shown in figure 6 (modified from Stricklin and others, 1971; Loucks, 1977).

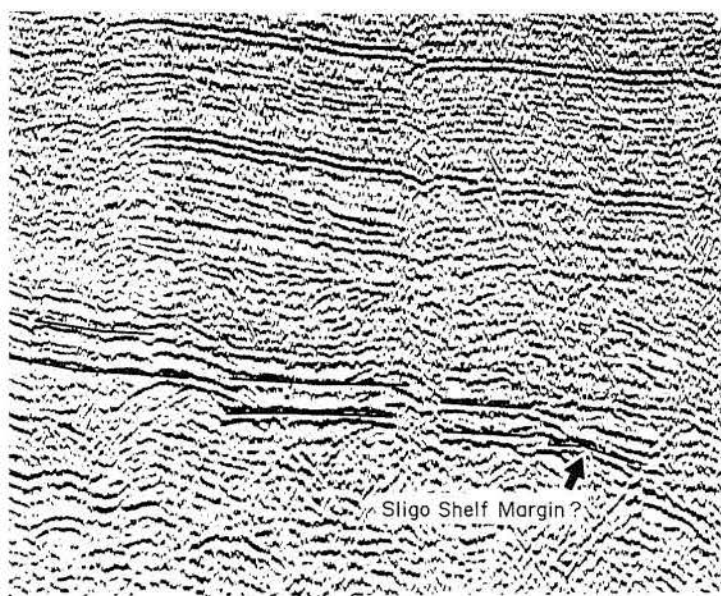
Formation consists of siliciclastic sandstone and dolomite. Contacts between these units are time-transgressive and represent major facies and depositional environment transitions (fig. 9). Basal sandstones of the Hosston Formation unconformably overlie folded Paleozoic strata in outcrop and shallow subsurface (Stricklin and others, 1971). Downdip, the Hosston Formation onlaps marine Jurassic carbonates (Bebout and Loucks, 1974).

Bebout (1977) documented numerous progradational cycles within the overall time-transgressive Sligo and Hosston sedimentary wedge. The progradational cycles are represented by many shoaling-upward sequences (fig. 10). Amsbury (1974) and Loucks (1977) found evidence of the subaerial exposure of the top of the Sligo Formation as far downdip as northern Frio County. This exposure created an erosional unconformity on which the Hammett and Pine Island Shales were deposited (fig. 8), but this contact appears to be gradational farther basinward (Bebout, 1977).

Regional subsidence that occurred during the Early Cretaceous along the Texas Gulf Coast produced substantial thickening of the Sligo and Hosston wedge from its pinch-out near the outcrop to greater than 300 m (1,000 ft) downdip at the shelf edge (fig. 11). Continued subsidence during the Tertiary is indicated on the structure-contour map of the top of the Sligo Formation (fig. 12), which shows an increase in depth from 300 to 4,900 m (1,000 to 16,000 ft) in less than 160 km (100 mi).

The middle part of the Trinity Group (fig. 8) outcrop consists of the Hammett Shale (below) and the Cow Creek Limestone (above) and is equivalent to the subsurface Pearsall Formation (Stricklin and others, 1971; Loucks, 1977). The

SE



Seismic section courtesy of Teledyne Exploration Company

the Stuart City shelf edge in the lower section, whereas they are nearly superimposed on the upper section. The upper section is oblique to the strike of the Stuart City shelf edge. Interpretations on the lower line by John B. Sangree, Exxon Company, U.S.A., and on the upper line by Charles D. Winker, Bureau of Economic Geology.

Figure 9. Regional lithologies and depositional environments of the Sligo and Hosston Formations. This cross section is highly generalized and the formational contact (dashed lines) is time-transgressive and interfingering.

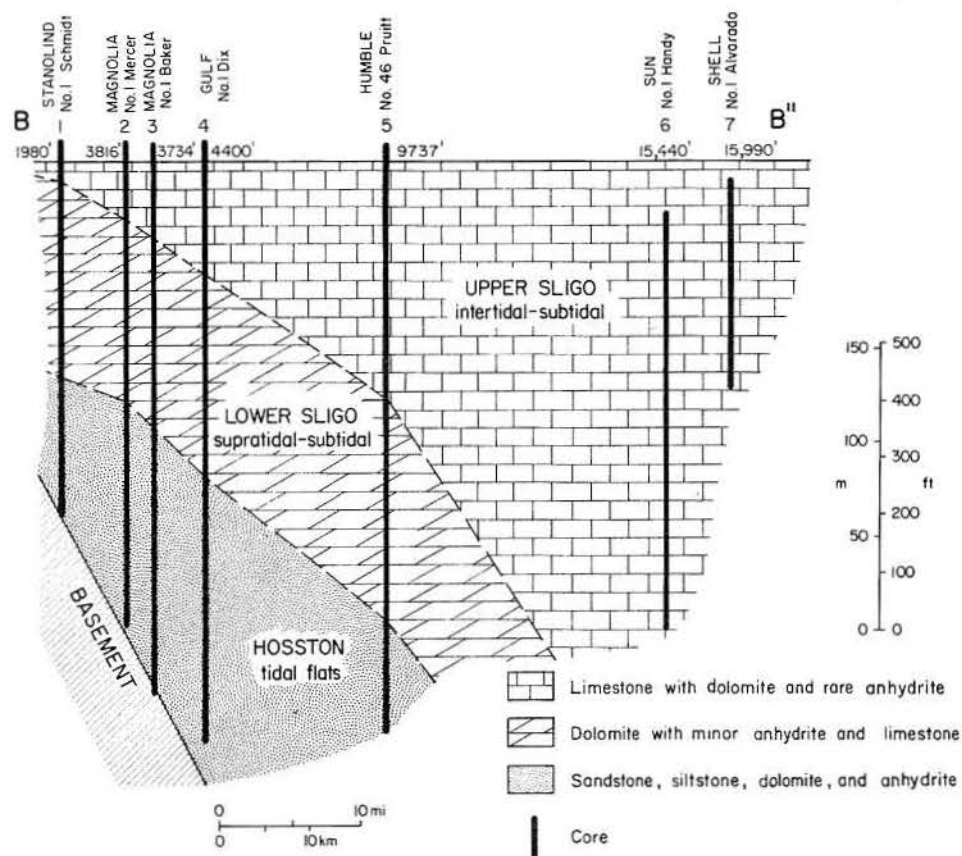
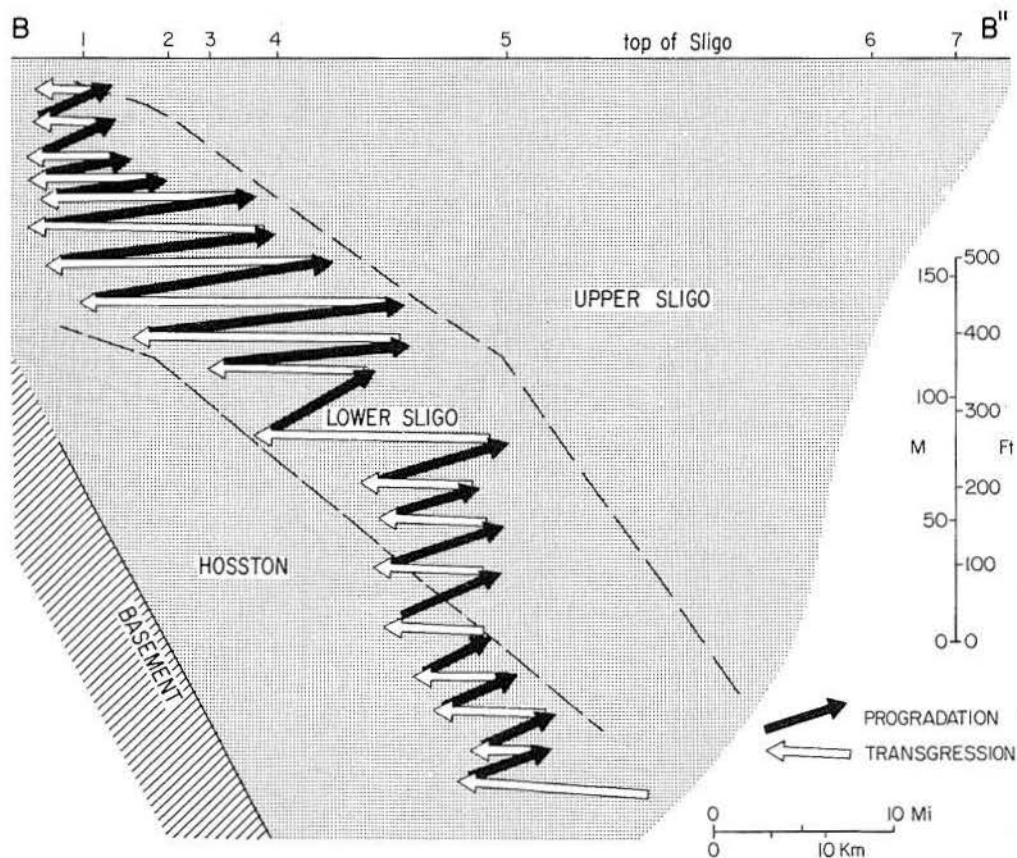


Figure 10. Diagrammatic relationship of the numerous progradational cycles to the overall transgressive, onlapping nature of the Sligo and Hosston depositional wedge. This cross section is highly generalized and formational contact (dashed line) is time-transgressive and interfingering.



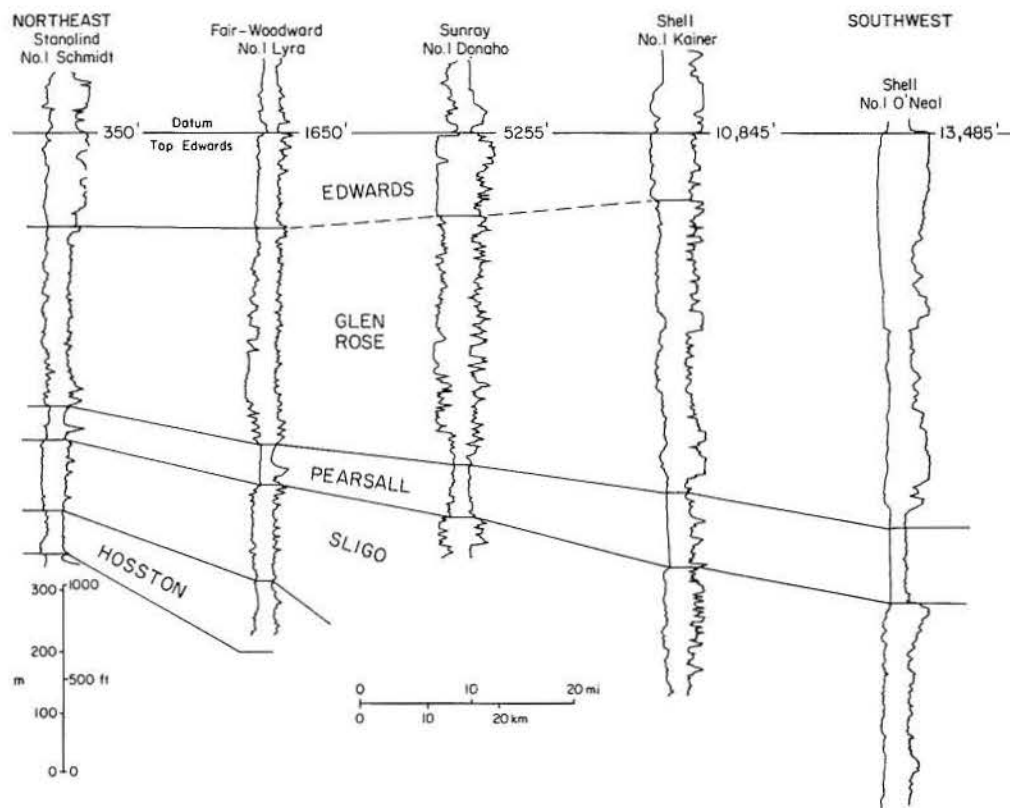


Figure 11. Electric-log section of the Lower Cretaceous Series, South Texas. See figure 2 for the line of section.

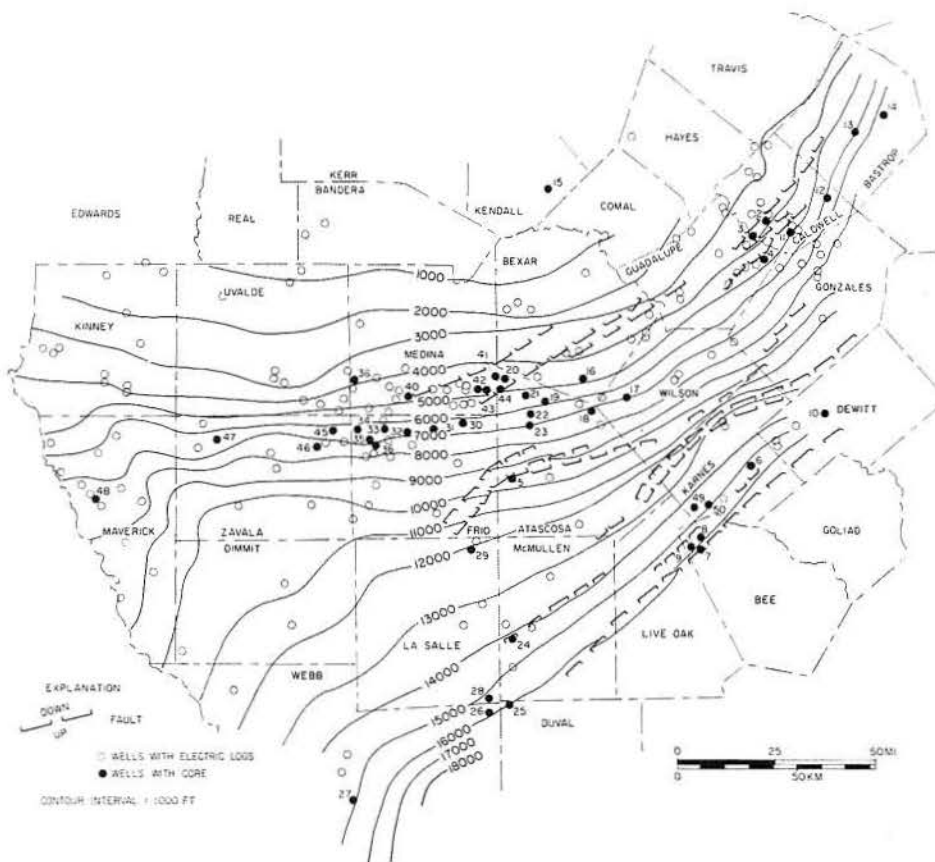


Figure 12. Simplified regional structure on the top of the Sligo Formation. Only major fault zones are shown.

upper Trinity Group (fig. 8) outcrop is divided into the Hensel Sandstone and Glen Rose Limestone (Stricklin and others, 1971). At the shelf margin this couplet is represented by transgression through the upper Pearsall and lower Stuart City Formations and by progradation of the upper Stuart City Formation. This cycle extends into the Fredericksburg Group (Bebout and Loucks, 1974).

Previous Work

Previous investigations of the Sligo and Hosston Formations in South Texas examined smaller study areas than does this report. They concentrated either on a particular depositional environment, such as the Sligo oolite-shoal complex (Bebout and Schatzinger, 1978) and Sligo shelf margin (Achauer, 1977), or on a specific geographic area, such as outcrop exposures (Stricklin and others, 1971; Amsbury, 1974) and the area flanking the San Marcos Arch (McBride and others, 1979). Interpretations vary among these studies, but these disparities are probably a result of dissimilar study areas. The conclusions of this report do not differ significantly from those of previous investigations; instead, they provide a regional synthesis of facies and diagenesis in the Sligo and Hosston Formations.

Stricklin and others (1971) and Amsbury (1974) reported on the facies and depositional environments of the outcropping Sycamore Sandstone and the shallow subsurface Sligo and Hosston Formations of south-central Texas. Their most downdip well was the Stanolind No. 1 Schmidt. These authors interpreted the Sycamore Sandstone to be an alluvial valley-fill deposit in which Amsbury (1974) recognized point bars, alluvial fans, and caliche-soil profiles. Amsbury concluded that the Sycamore Sandstone grades downdip into small fan-delta deposits transitional to the Hosston Formation. Amsbury (1974) regarded the Hosston Formation as low-energy, brackish, lagoon and tidal-flat deposits. The lower Sligo Formation is considered to be the seaward extension of this low-energy lagoon and tidal-flat system. Upward across this gradational contact there is a decrease in terrigenous sediments, an increase in carbonate sediments, and an increase in burrows of marine organisms. According to Amsbury (1974), the upper Sligo Formation is less than 12.2 m (40 ft) thick updip and consists of a higher energy sequence of normal-marine conditions, dominated by oolitic and skeletal grainstones.

McBride and others (1979) examined the Hosston Formation over the San Marcos Arch and

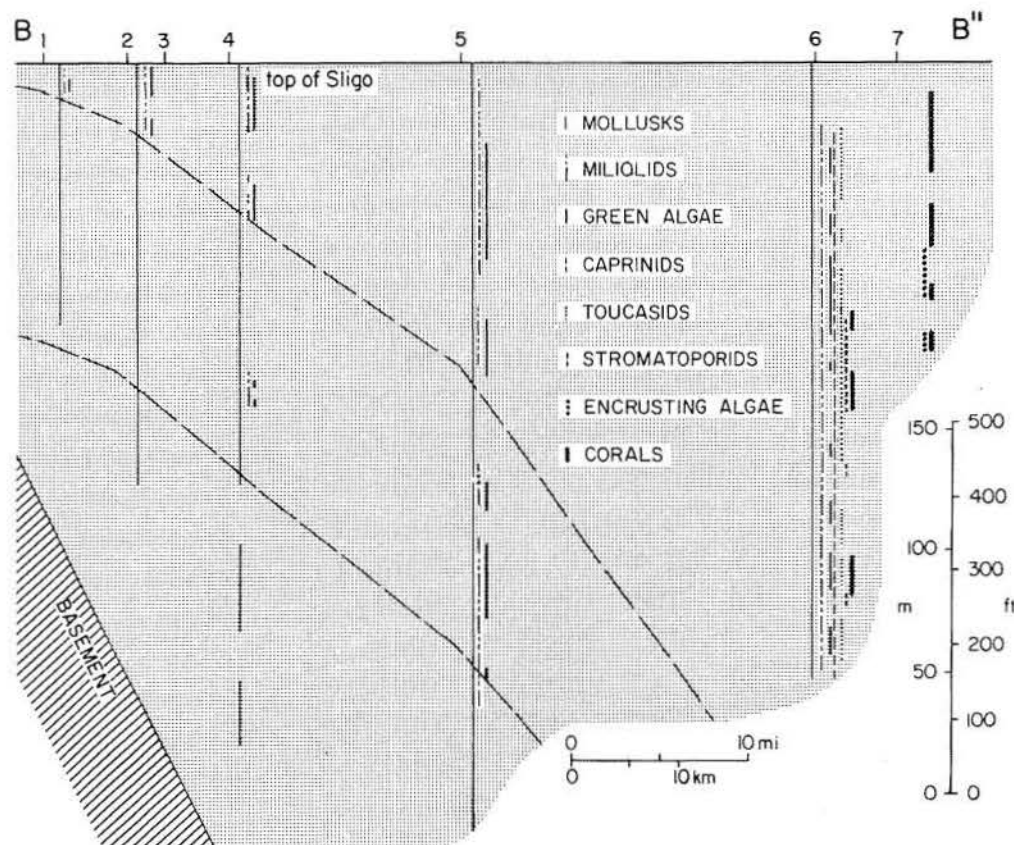


Figure 13. Fossil distribution in the Sligo and Hosston depositional wedge, demonstrating the overall onlapping nature. Increased diversity upward and downdip reflect more normal marine conditions. This cross section is highly generalized and the contact (dashed line) is time-transgressive and interfingering.

on its flanks. They distinguished four general genetic facies: (1) fluvial sandstone, (2) deltaic and/or strandline sandstone, (3) interdistributary and/or lagoon-marsh mudstone and siltstone, and (4) intertidal to supratidal dolomite. On the southwestern flank of the arch the tidal-flat dolomite transgresses over the deltaic/strandline sandstone.

Bebout (1977) outlined regional depositional patterns of the Sligo and Hosston Formations in the South Texas area using seven wells with nearly continuous cores throughout the formation (fig. 9). Most of these wells are located in the northeastern part of the study area on the flank of the San Marcos Arch (fig. 5). The updip-most well of Bebout's (1977) study is the Stanolind No. 1 Schmidt, which correlates with but does not overlap Amsbury's (1974) study area. Bebout (1977) concluded that the Hosston Formation is an arid tidal-flat deposit and that the lower Sligo Formation represents numerous cycles of subtidal to supratidal carbonates. These onlapping progradational cycles clearly demonstrate the overall transgressive nature of the Sligo Formation (fig. 10). An increase in fossil abundance and diversity upward in the section and basinward (fig. 13) resulted from this transgression of normal-marine environments (Amsbury, 1974; Bebout, 1977).

Bebout (1977) interpreted the upper Sligo Formation to be a normal-marine shelf deposit, characterized by burrowed wackestones and oolitic and skeletal grainstones. Bebout and Schatzinger (1978) documented the oolitic-sand shoals on the shelf platform, noting their

transgressive nature even within the upper 15.3 m (50 ft) of the Sligo Formation. Downdip, at the shelf edge, a high-energy complex of grainstones and bafflestones is widespread. These banks aggraded vertically throughout the transgression (Bebout, 1977).

Achauer (1977) examined cores from five wells along the Sligo shelf edge. He recognized a reef tract of organic boundstones (corals, rudists, hydrozoans, and algae) and their associated debris (skeletal grainstones). Achauer also distinguished a back-reef environment consisting of skeletal wackestones with abundant pellets, lumps, and algal fragments, all interbedded with subordinate amounts of reef-derived grainstones. He concluded, however, that there was not enough core for detailed delineation between reef facies and back-reef facies in the vicinity of the Sligo shelf edge.

Several studies of the age-equivalent Cupido Formation in the Sabinas Basin of northern Mexico have also been completed (Wilson and Piali, 1977; Stabler and Marquez, 1977; Conklin and Moore, 1977). These authors described the Cupido as representing a prograding carbonate platform. Carbonate environments identified from nearshore to basin are lagoon, restricted lagoon, and sabkha; near-reef tidal-flat and sand shoals; organic reefs of corals, red algae, requeniids, and caprinids; forereef talus slope; and open-marine basin. The organic reef facies is commonly highly altered by fracturing and dolomitization, and a true reef framework cannot be distinguished.

DEPOSITIONAL ENVIRONMENTS

The environmental interpretations presented here are based on facies relationships within the cores studied and comparison with those of modern carbonate environments. Table 2 shows the relationship between the facies and environmental setting.

Six major depositional environments are recognized: alluvial plain, tidal-flat complex, inner-shelf lagoon, oolite-shoal complex, outer-shelf platform, and shelf margin (fig. 14). These environments indicate that a broad, shallow, very gently sloping ($<1^\circ$) shelf existed across the study area during the time of Sligo and Hosston deposition. Changes from one major environment to another range from abrupt to gradational.

Downdip, on the outer shelf and along the shelf margin, a single facies extends vertically through time, whereas updip the transitions from alluvial-plain facies through supratidal, tidal-flat, and shelf-lagoon facies are abrupt and commonly reoccur vertically within a few meters (<20 m) of core.

Hosston and Lower Sligo Environments

The seaward edge of an alluvial plain consisting of braided streams and fan deltas extends into the study area (fig. 15). Both dolomitic and siliciclastic tidal-flat units are present, although the siliciclastic sequence rarely is supratidal. The evaporative supratidal flat consists of laminated dolomite mudstone (algal marsh) with nodular to mosaic anhydrite, intraclasts, bird's-eye structures, and mud cracks. These features and their stratigraphic position seem similar to those of the

Table 2. Facies and depositional environments, Sligo and Hosston Formations.

Facies	Depositional environment
LOWER SLIGO AND HOSSTON FORMATIONS	
Burrowed dolomite mudstone	Subtidal restricted lagoon
Burrowed sandstone	
Pellet-mollusk dolomite wackestone	Intertidal flats, ponds, and channels
Laminated sandstone	
Laminated siltstone	
Intraclastic dolomite wackestone	Sabkha
Laminated dolomite mudstone	
Skeletal dolomite grainstone	Beach ridges, levees, tidal channels, and deltas
Pellet dolomite grainstone	
Conglomeratic sandstone	Alluvial plain
UPPER SLIGO FORMATION	
Silty lime mudstone	Inner shelf lagoon
Miliolid wackestone	
Mollusk-wackestone	
Mollusk-miliolid wackestone	Outer shelf
Echinoid-mollusk-miliolid wackestone	
Pellet grainstone	
Fossiliferous lime mudstone	"Back-reef" shelf including oyster banks and local tidal flats
Oyster-miliolid wackestone	
Toucasid wackestone	
Oncolite packstone	Stable-grain flat
Laminated lime mudstone	
Coated-grain packstone	Oolite-shoal complex
Pellet packstone	
Oolite grainstone	Mobile grain belts, tidal bars, beaches, spits, and channels
Skeletal grainstone	
Coral-caprinid grainstone	
Caprinid grainstone	Shelf-margin complex
Coral-caprinid packstone/ wackestone	
Caprinid packstone/wackestone	Reefs, banks, and upper shelf- slope biohermal zones
Coralgal boundstone	

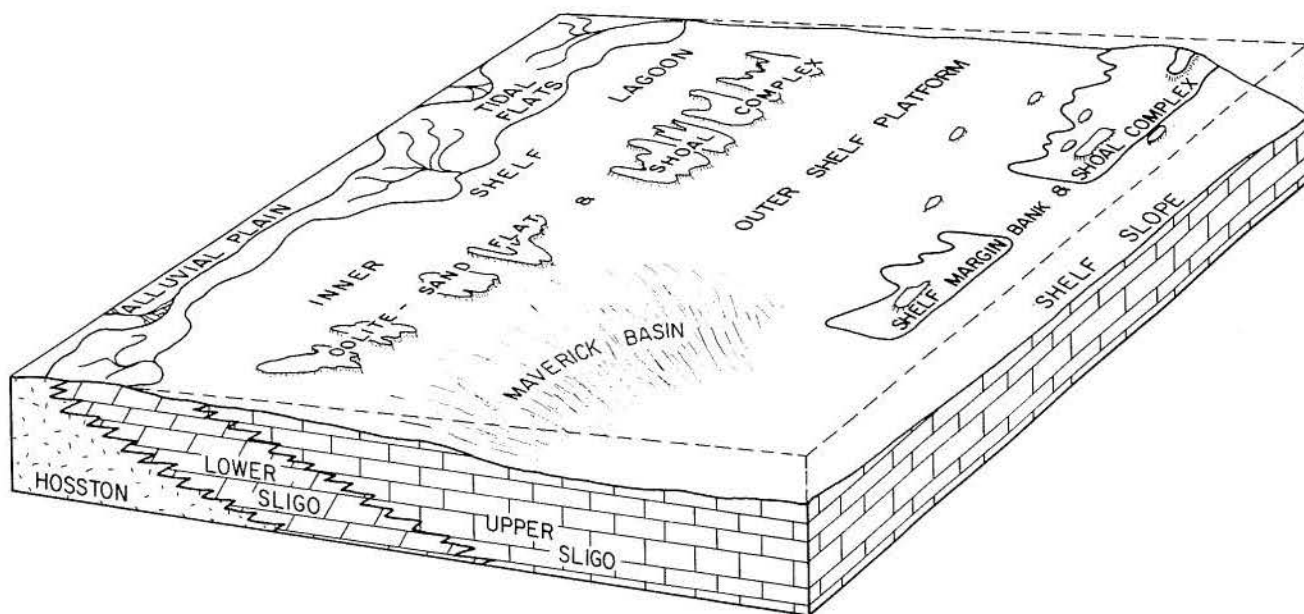


Figure 14. Interpreted environmental setting on the Early Cretaceous platform during deposition of the Sligo and Hosston sedimentary wedge.

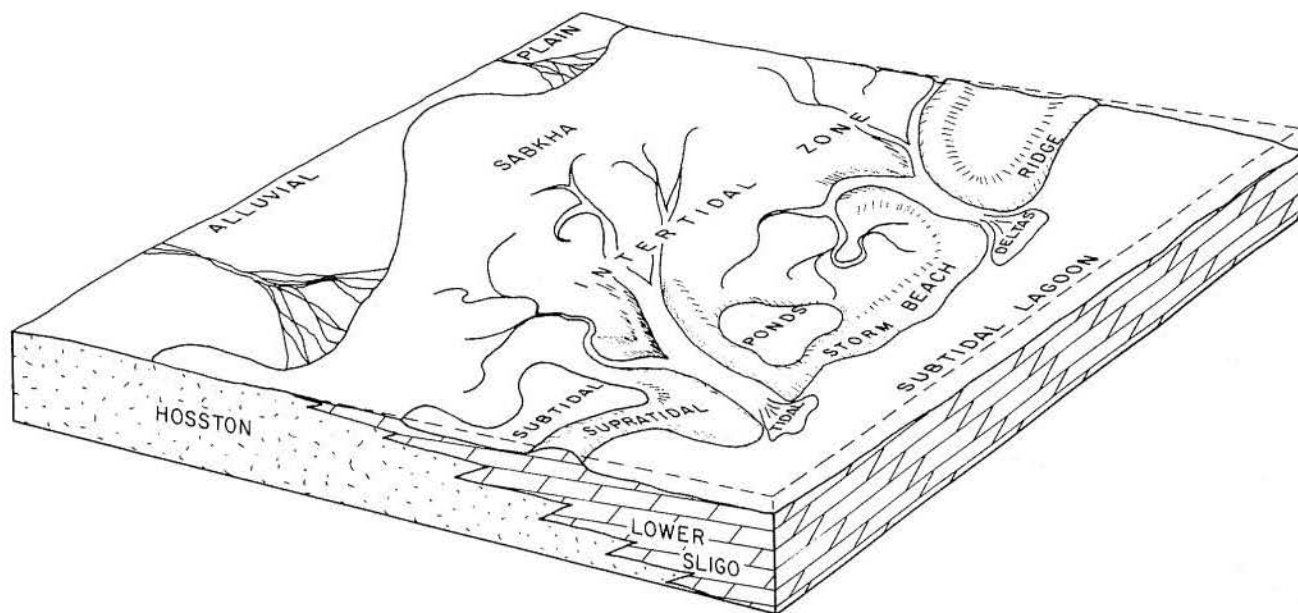


Figure 15. Idealized environments of the Hosston and lower Sligo tidal-flat deposits.

modern sabkhas of the Trucial Coast of the Persian Gulf (Kendall and Skipworth, 1969; Evans and others, 1969; Purser and Evans, 1973).

In the siliciclastic tidal flats the scarcity of argillaceous mud and dominance of fine sand resulted in limited grain-size variation between the upper and lower tidal flat. However, the lower flat consists of massive sandstones with low-angle crossbedding, laminations, and rippled cross-stratification, whereas mud cracks, algal laminations, intraclasts, and clay drapes

characterize the slightly finer grained sandstones of the upper tidal flat. Channels vary from minor runnels a few centimeters deep to fining-upward sequences 4.6 m (15 ft) thick. Highly burrowed sandstone, siltstone, and shale interpreted as pond deposits are also present.

Dolomitic tidal flats in the Hosston Formation have much less sandstone and siltstone although lateral transitions into the clastic tidal flats do occur. A highly burrowed, organic-rich, argillaceous dolomite mudstone of an intertidal

pond deposit intercalates with lower intertidal-flat sediments. The latter are characterized by a decrease in burrows and an increase in preserved laminations (wispy irregular to parallel). Storm beds of intraclasts are common. The upper intertidal-flat facies consists of laminated dolomite mudstone and storm beds but lacks burrowing. The harshness of the upper intertidal-flat environment appears to have severely limited the activity of most organisms. The previously described supratidal marsh caps the Hosston dolomite tidal-flat facies.

Tidal-flat deposits of the lower Sligo Formation, although quite similar to those of the Hosston Formation, contain more burrows and a molluscan fauna, two indications of more marine conditions in the Sligo. The supratidal sediments were probably deposited on topographic highs within the intertidal zone. Lower Sligo tidal flats represent the seaward extension of the complex and thus are characterized by more intertidal sedimentation. Hosston tidal flats are the more landward and thus were dominated by supratidal (sabkha) sedimentation.

The lower Sligo intertidal zone consisted of supratidal beach ridges, channel levees, channel bars, tidal deltas, tidal-flat marshes, and ponds. The Andros Island, Bahamas, tidal flats have a similar suite of environments (Shinn and others, 1969; Hardie and Garrett, 1977). However, this modern analog probably exists in a more humid climate than that which prevailed during deposition of the lower Sligo tidal flat. The marsh deposits are algal-laminated dolomite mudstones with rip-up clasts and small tidal channel-fill strata. Pond sediments are highly burrowed dolomite mudstones that contain flecks of oxidized organics. Shallow ponds were only a few (<3) meters deep but were maintained for long periods of time. Commonly, the lateral change from pond to intertidal flat to supratidal beach was transitional. Burrowed packstones within this transition represent overwash into the pond. Dolomitized grainstones compose the higher energy beach ridges, channel levees, channel bars, and tidal deltas. The fossil assemblage consists of fine, generally monotypic, molluscan debris. This low diversity results from the high-stress environment of the tidal flat. The abundance of burrows indicates the presence of an extensive crustacean or other soft-bodied fauna.

A restricted subtidal lagoon bordered the tidal-flat complex. The carbonate mudstone from this lagoon is highly burrowed and commonly pelleted. The molluscan fauna resembles that of the tidal flats, and thus the intertidal pond and subtidal lagoon are hard to differentiate. A similar

pelleted and burrowed carbonate mud occurs adjacent to the tidal-flat complex of Andros Island, Bahamas (Purdy, 1963; Shinn and others, 1969).

Upper Sligo Environments

Carbonate mud-rich sediments were deposited in a low-energy, shallow-water lagoon seaward of the lower Sligo carbonate tidal flats (figs. 16 and 17). This inner-shelf lagoon is probably analogous to the modern Florida Bay (Ginsburg, 1956, 1964; Enos and Perkins, 1979). Highly burrowed, silty, lime mudstones characterize this environment. Across the lagoon, conditions varied from open marine to restricted, and the fauna consisted of varying numbers of echinoids, mollusks, and miliolids. Small islands, typified by bird's-eye structures in laminated lime mudstones, formed on local highs in bottom topography. Oyster banks were often associated with these islands where water depths were probably less than 6 m (~20 ft). The influx of terrigenous sediment decreases seaward through these lagoonal sediments.

This lagoon was barred from the higher energy conditions of the more open-marine outer shelf by a series of strike-trending oolite-shoal complexes (Bebout and Schatzinger, 1978, fig. 16). Size, shape, and orientation of individual oolite shoals, as well as facies composition and juxtaposition, are strikingly similar to those of Joulter's Cay, Bahamas (Harris, 1979). On the windward margin, a skeletal grain belt formed as a result of shoaling by wave- and tidal-current processes. Crossbedded sediment of oolite bars, up to 9.2 m (30 ft) thick, developed in shallow water along the high-energy belt. Oolites and skeletal grains were swept landward onto a highly burrowed grain flat and deposited there as a result of the sediment-baffling and stabilizing effects of algae. Carbonate mud content increased landward across the grain flat, resulting in the development of a muddy sand flat with abundant pellets on the lee side. Small tidal creeks drained the sand flats through large passes along the margins. The shoals' geographic position is a result of the impingement of wave and tidal-current energies established by the large fetch across the broad outer shelf.

Seaward of the oolite-shoal complexes, muddy sediments accumulated, and skeletal wackestones and fossiliferous lime mudstones dominate. Thin, discontinuous skeletal and/or pellet grainstones were deposited by high-energy pulses. A diverse fauna of mollusks, miliolids, echinoids, green algae, serpulid worms, and tucasids indicates

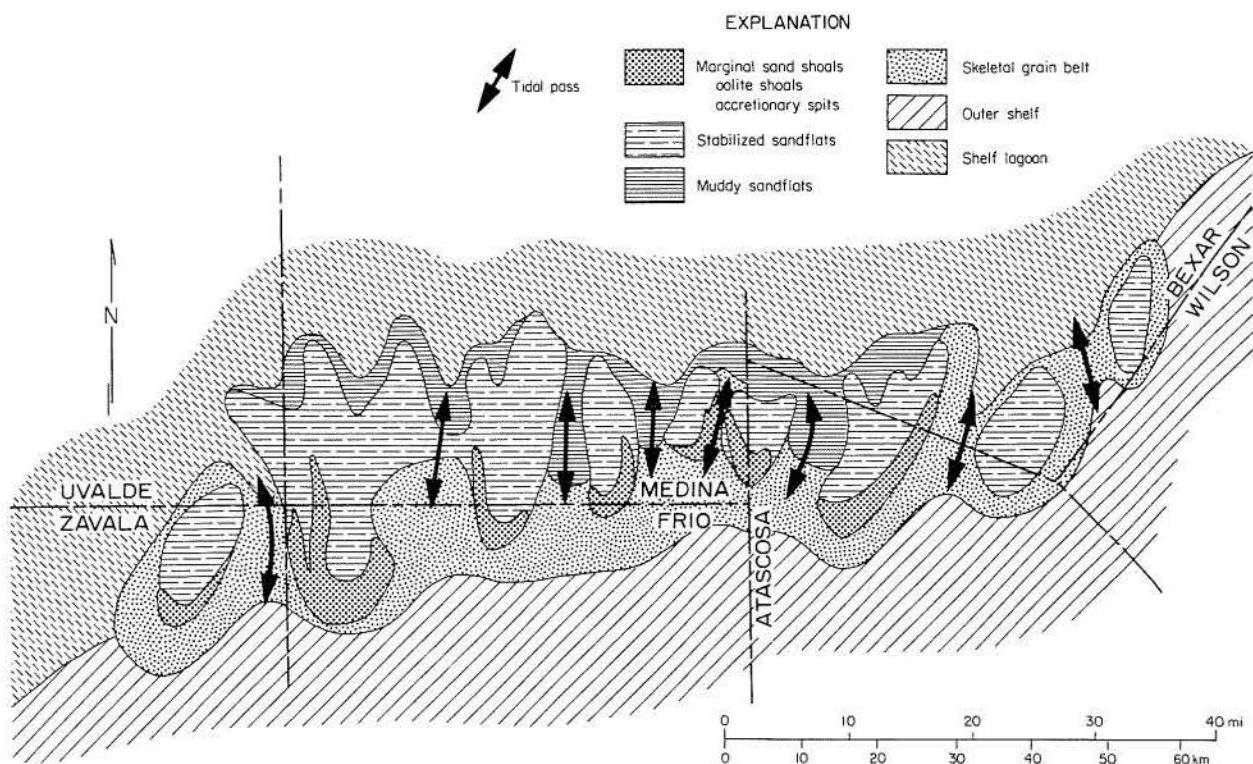


Figure 16. Depositional environments within the upper Sligo oolite-shoal complex, South-Central Texas.

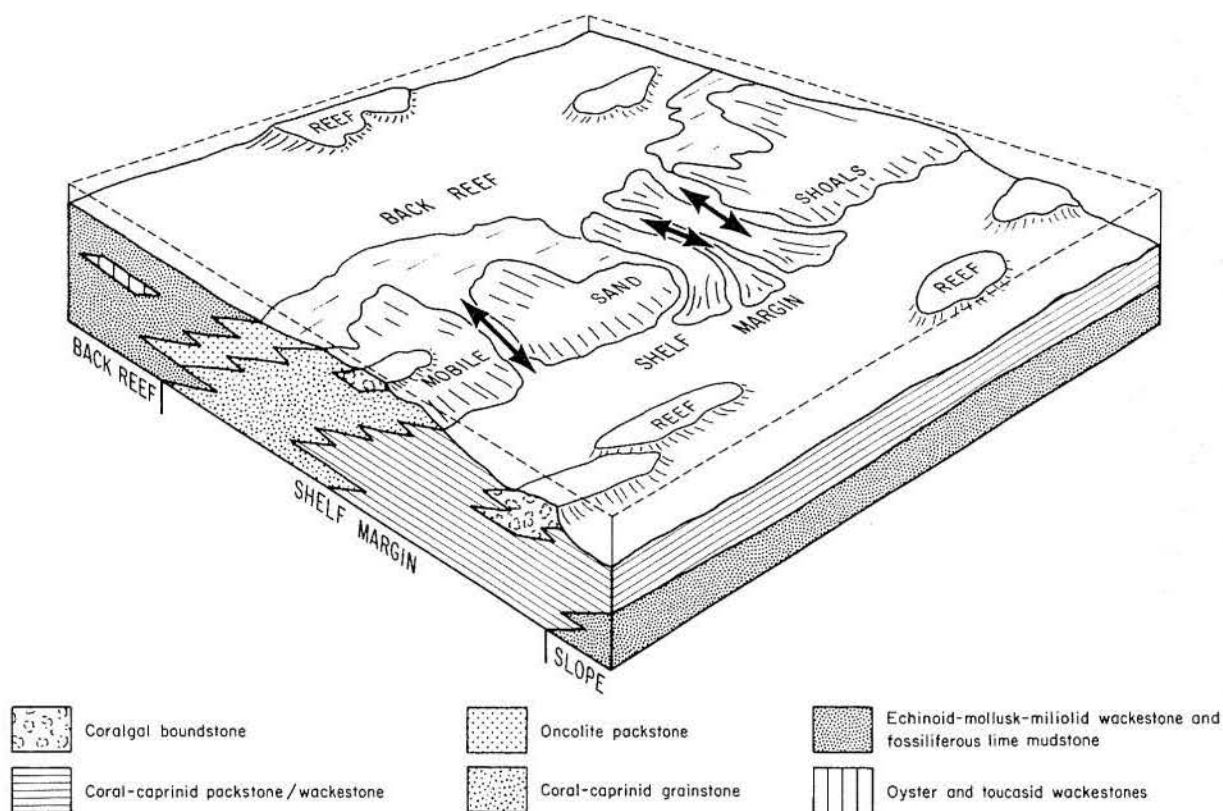
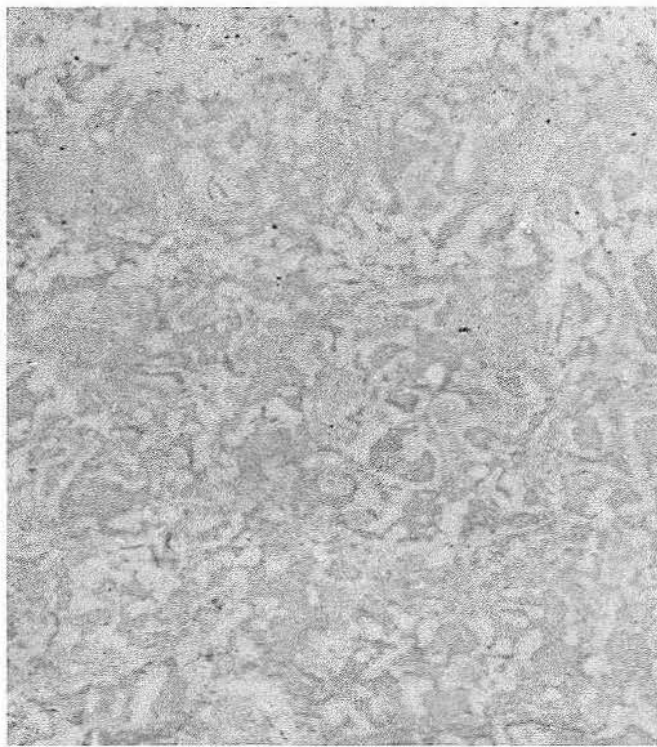
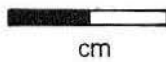


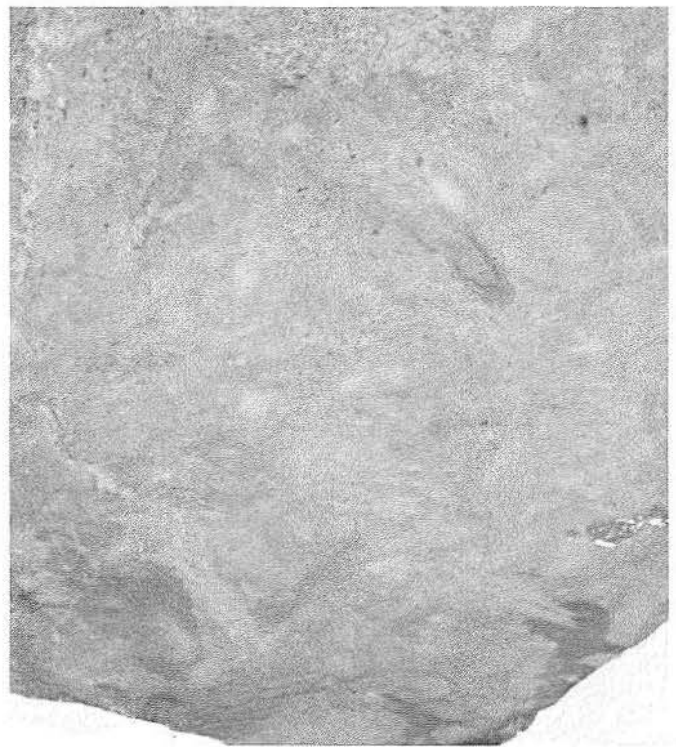
Figure 17. Idealized facies tract along the Sligo shelf margin. Depositional settings are interpretive and include shelf-margin sand shoals, organic banks, tidal passes, and "back-reef" environments.



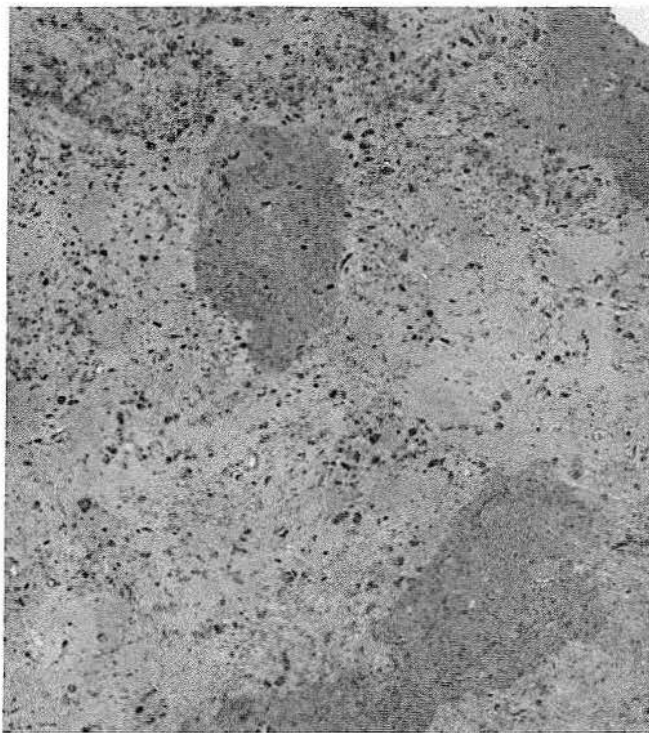
a



cm



b

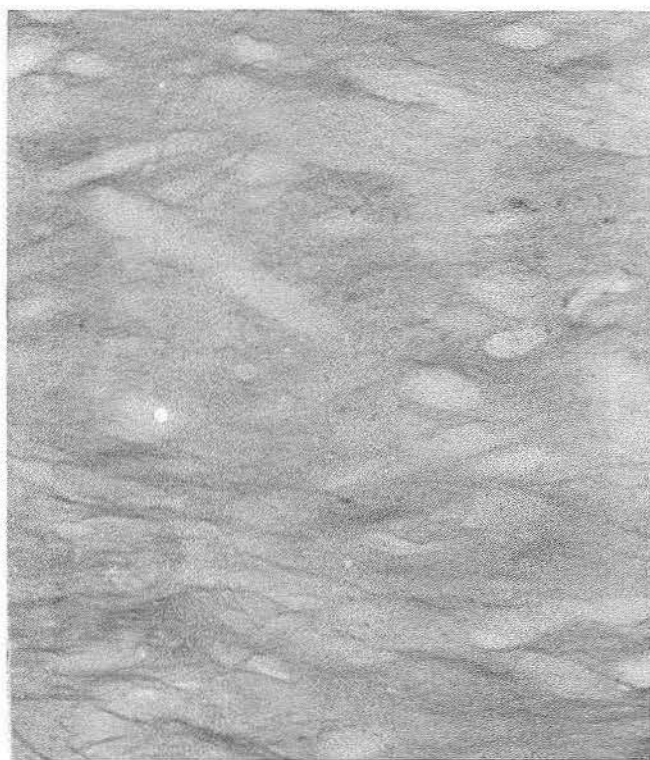


c

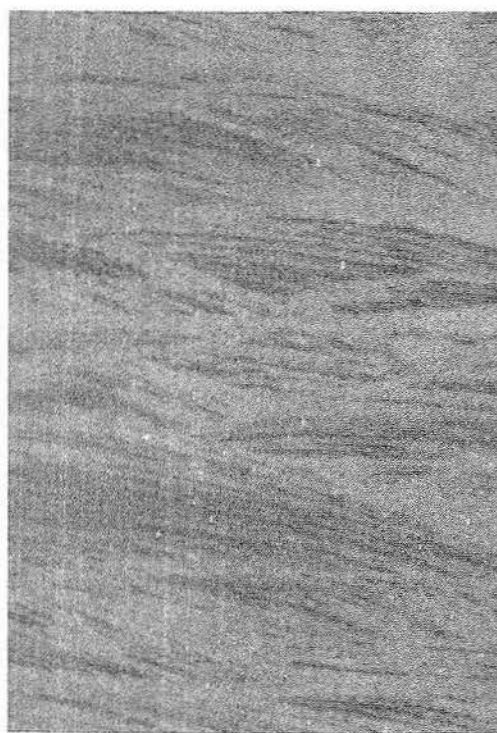


d

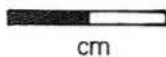
Figure 18. Burrowed dolomite mudstone: a. Very abundant burrows with oxidized rims suggest intertidal to supratidal deposition; b. Due to extensive burrowing, only minor original wispy lamination remains. Pellet-mollusk dolomite wackestone: c. Greater than 10 percent fossil moldic porosity exists, mainly between the large dark burrows; d. About 10 percent moldic porosity evenly distributed within and between burrowed areas.



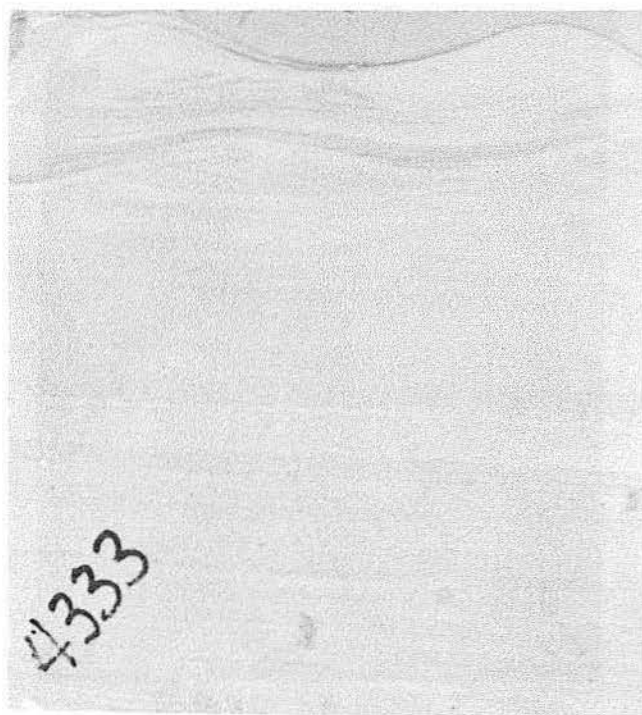
a



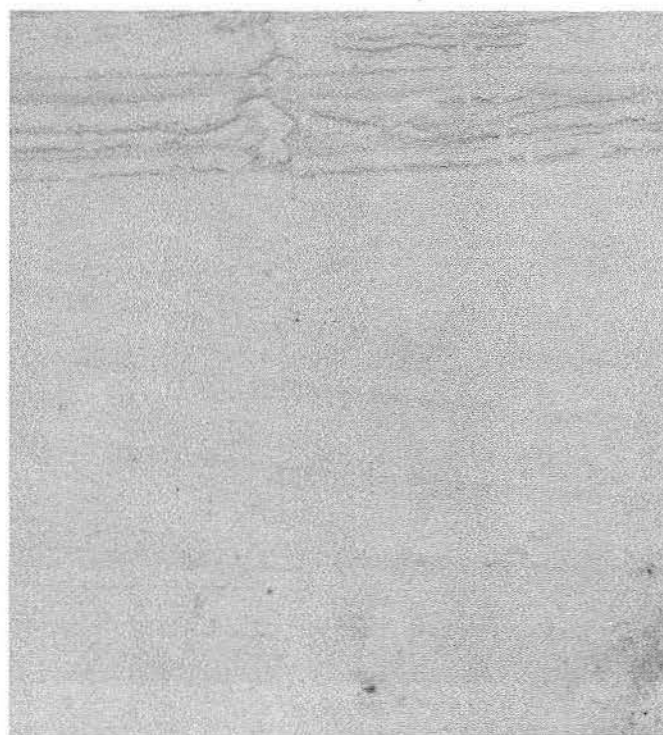
b



cm



c

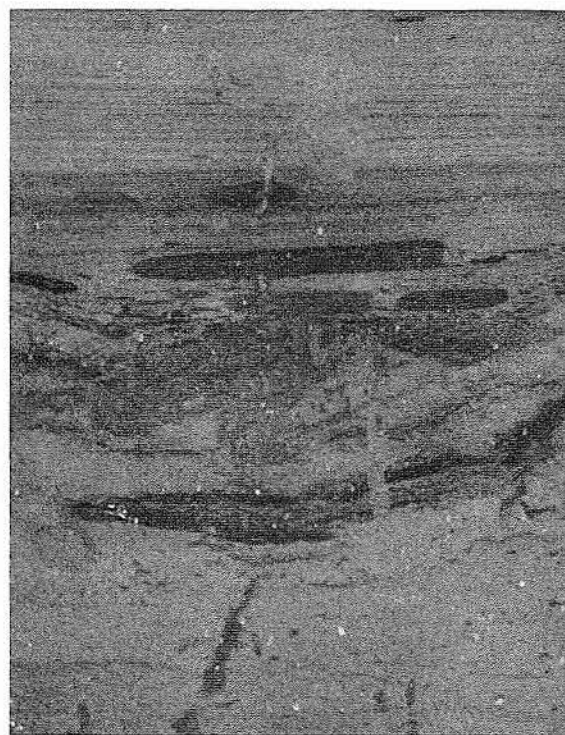
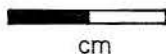


d

Figure 19. Burrowed sandstone: a. Small amounts of shale deposited in wispy laminations enhance appearance of extensive burrowing. Laminated sandstone: b. Slab with well-developed ripple cross-laminations; c. Parallel-laminated sandstone grades upward into ripple laminated sandstone with a dark organic drape; d. Possible escape burrow in thinly laminated sandstone of tidal-flat origin. Overlying sandstone shows low-angle cross-stratification.



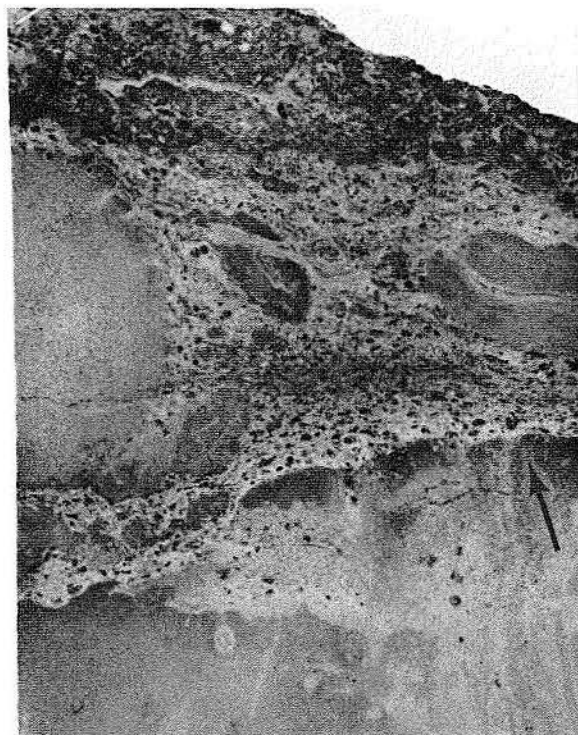
a



b



c

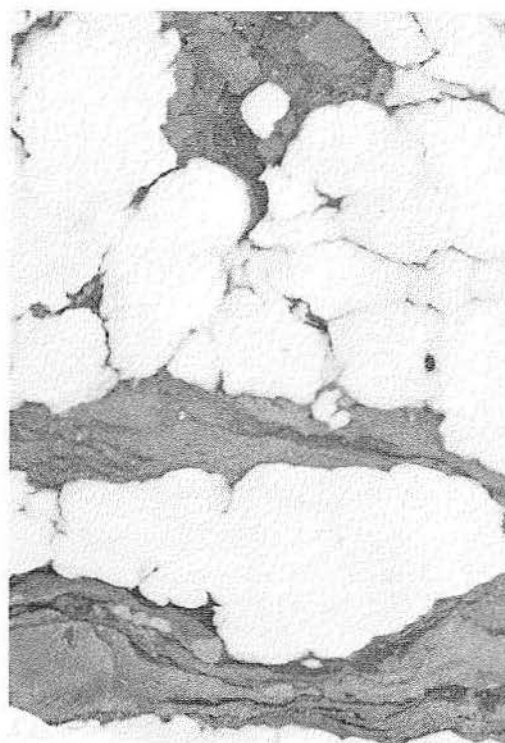


d

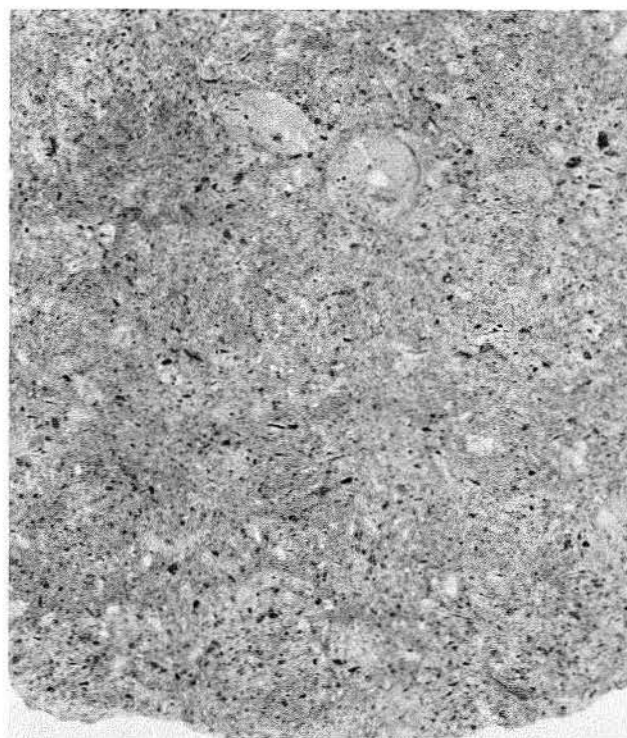
Figure 20. Laminated siltstone: a. Organic-rich laminae between ripple cross laminations indicate current was dominantly from right to left; b. Parallel-laminated sandstone with large shale clasts. This sample also contains abundant hematite and is red. Intraclast dolomite wackestone: c. Poorly sorted dolomite lithoclasts with irregularly shaped anhydrite (white). Anhydrite probably filled early pores that resulted from rapid deposition, possibly during a storm; d. Massively bedded dolomite mudstone (below) with a bored hardground on the upper surface (arrow). Overlying intraclast dolomite wackestone shows poorly developed laminations accentuated by pellets and small dark intraclasts. Sequence represents storm lag deposit over a hardground.



a



b

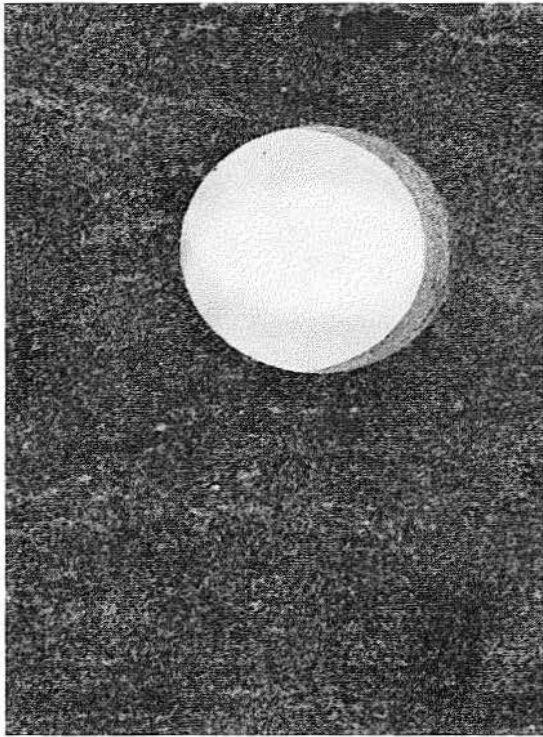


c



d

Figure 21. Laminated dolomite mudstone: a. Burrows disrupt oxidized laminae and possibly mud cracks (arrow) of this typical intertidal-supratidal dolomite mudstone; b. Nodular anhydrite in contorted organic-rich dolomite mud. Texture is characteristic of tidal-flat dolomite being replaced or displaced by anhydrite in the supratidal zone. Skeletal dolomite grainstone: c. Nearly 15 percent moldic porosity due to leached pellets. Original bedding completely destroyed by burrowing; d. Core slab very similar to (c) showing aligned and leached molluscan shells in pellet-rich matrix.



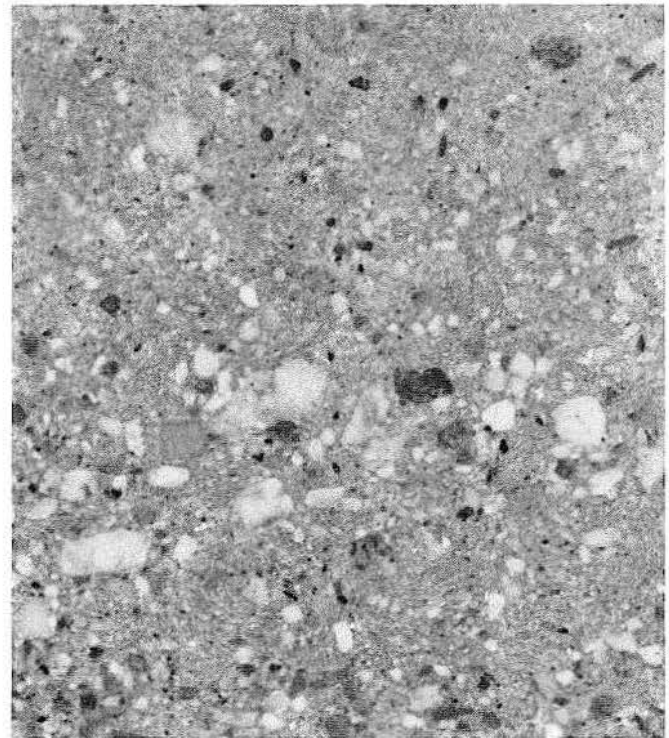
a



b



c

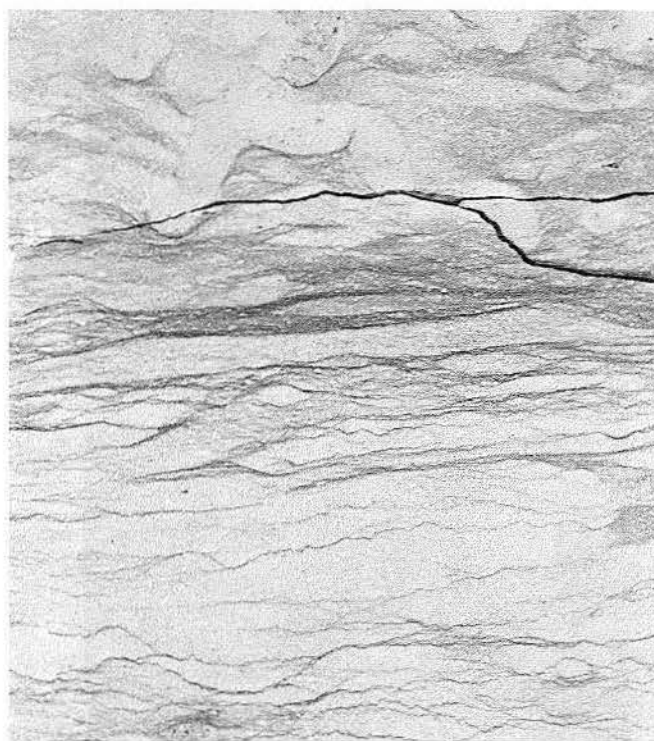


d

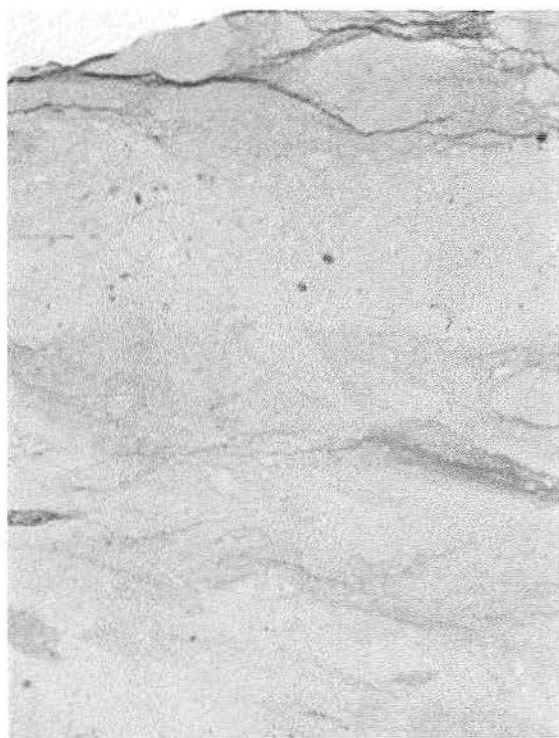
Figure 22. Pellet dolomite grainstone: a., b. Cross-laminated dolomite grainstone. Intraclasts at the top of (a) probably represent lag on a beach ridge; c. Lower cross-laminated grainstone overlain by a middle unit that consists of burrowed homogenized, intraclastic, pellet grainstone. The sequence is capped by an upper laminated pellet grainstone. Conglomeratic sandstone: d. There are two fining-upward sedimentation units in this arkosic sandstone.



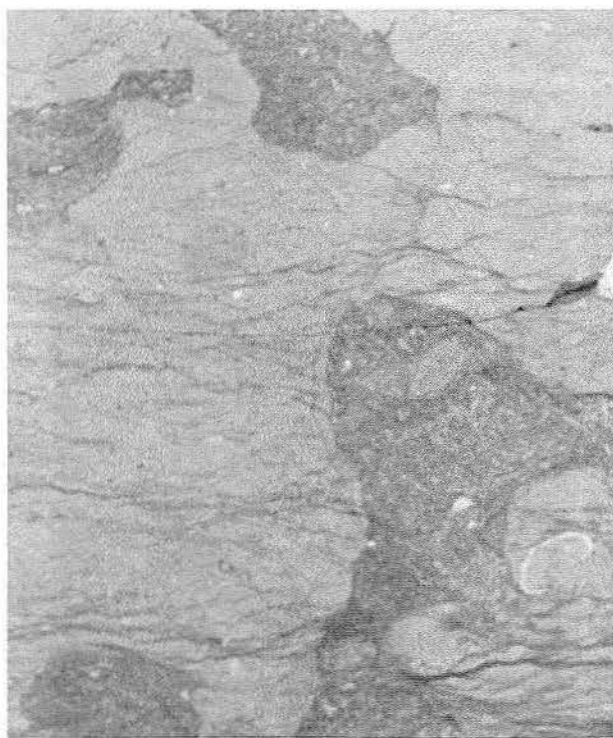
a



b

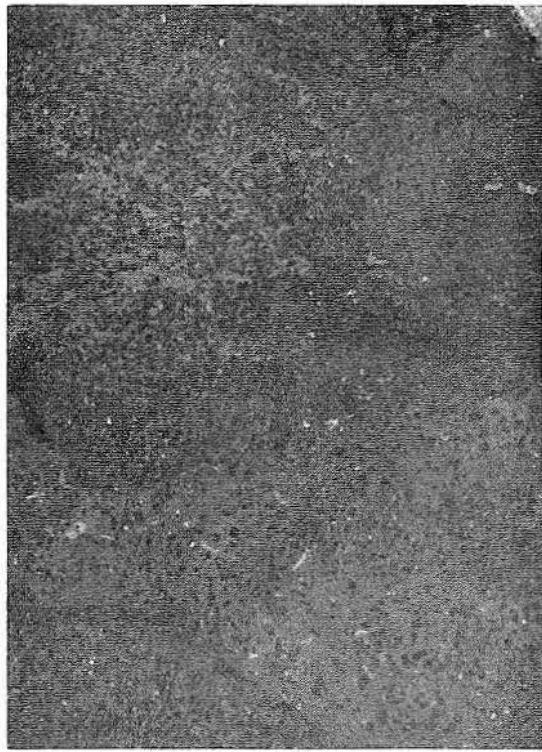


c

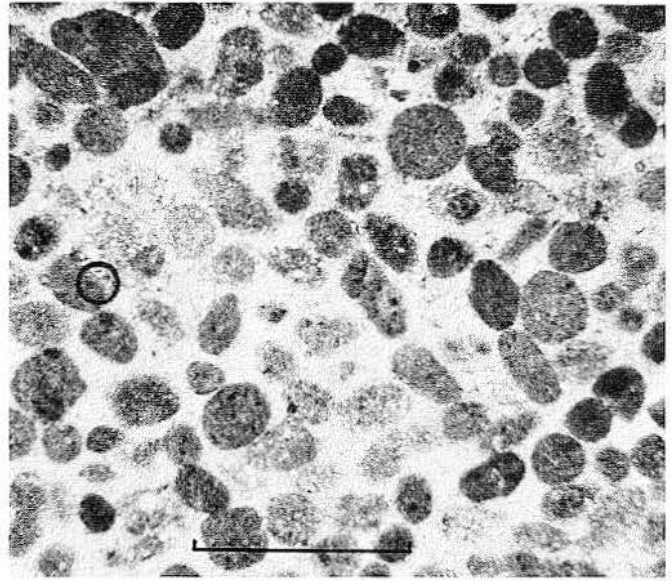


d

Figure 23. Silty lime mudstone: a. Very silty mudstone (dark) with nonsilty (light) laterally discontinuous fossiliferous mudstone laminae and burrows. Echinoid remains are relatively common in this slab. Miliolid wackestone: b. Numerous organic-rich, irregularly laminated, microstylolite-bearing sequences are overlain by a burrowed zone. Note burrows tend to lack abundant organic matter that is common in the unburrowed matrix. Mollusk-miliolid wackestone: c. Highly burrowed texture is common. Microstylolites in bottom of picture are concentrated in argillaceous laminae. Echinoid-mollusk-miliolid wackestone: d. Irregular laminae accentuated by microstylolites and well preserved darker burrows.



a



b



c

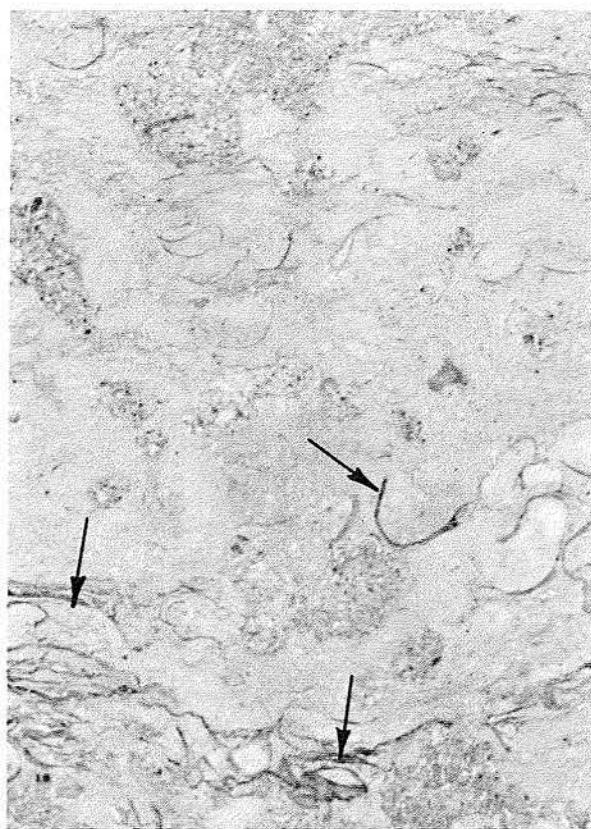


d

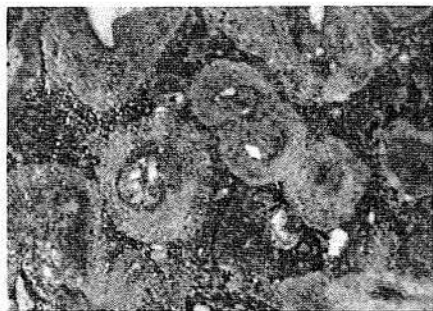
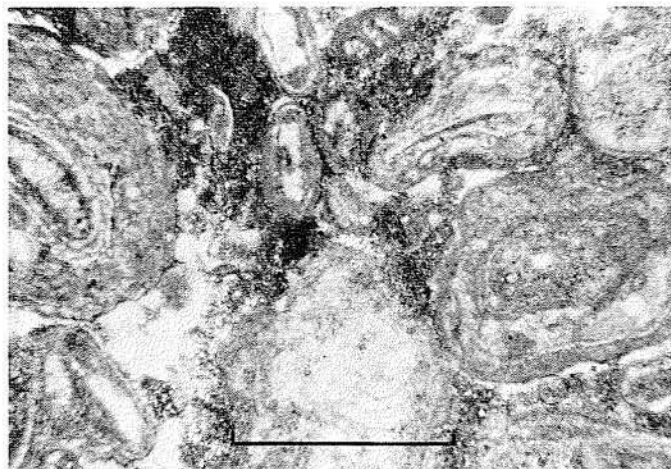
Figure 24. Pellet grainstone: a. Lighter areas are probably mud-filled irregular burrows that have destroyed much of the original bedding; b. Photomicrograph of a. Uncompacted pellets are the result of early calcite cementation. Bar represents 0.5 mm. Fossiliferous lime mudstone: c. Well-developed horizontal burrows were possibly made by echinoids. The burrows are only slightly compacted; d. Fossiliferous mudstone that is slightly shaly in the darker burrowed areas (burrow fill) shows an accumulation of echinoderm debris (right) and vertical burrows (left).



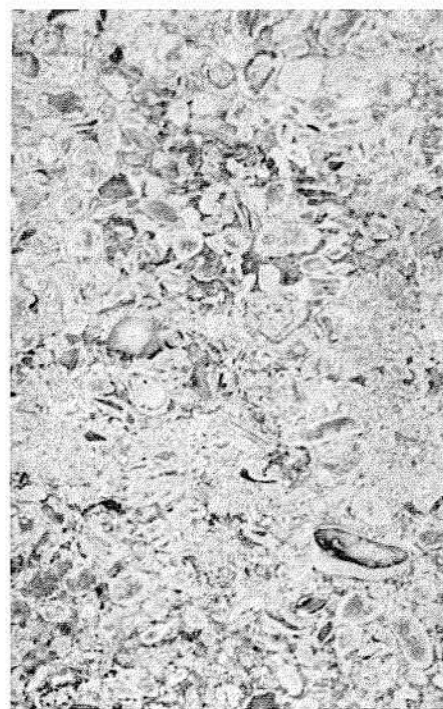
a



b



d



e

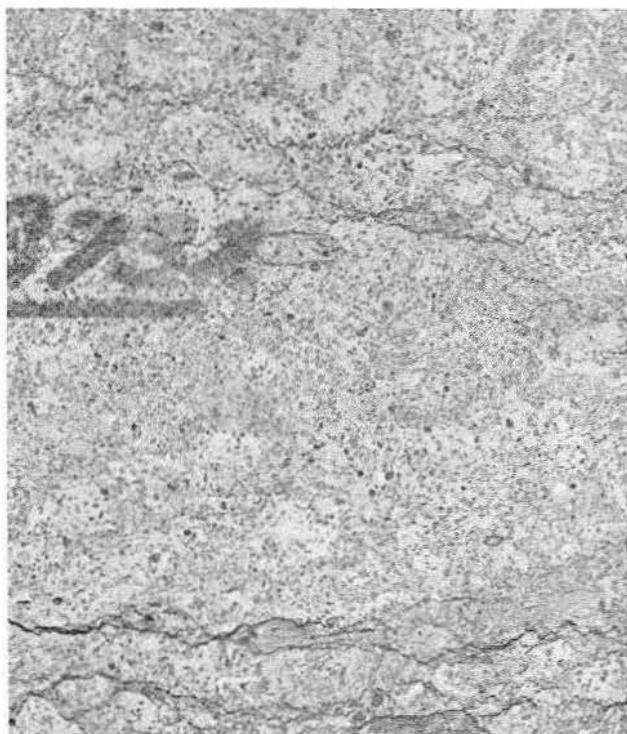
Figure 25. Oyster-miliolid wackestone: a. Whole *Chondrodonta*-like oysters abound in these slabs. Toucasid wackestone: b. Toucasid wackestone in which large burrows filled with skeletal packstone are associated with layers rich in toucasids (arrows). Oncolite packstone: c., d. Irregular to ovate oncolites are closely packed in a pellet-rich matrix. Bar in (c) represents 0.5 mm: e. Packed oncolites and superficially coated grains occur with micrite rims.



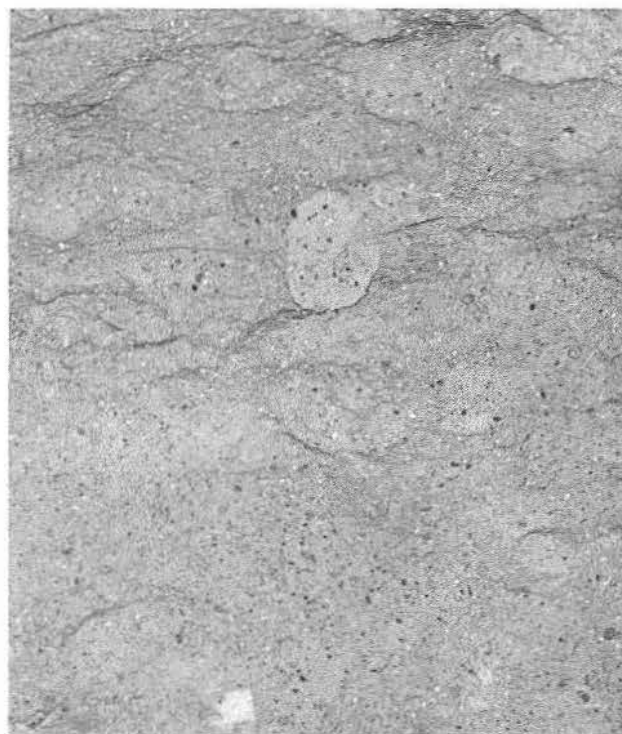
a



b



c



d

Figure 26. Laminated lime mudstone: a. Burrowed laminated mudstone (algal mat?) overlain by highly burrowed, pellet- and small intraclast-rich wackestone. Abundant burrowers did not completely destroy the original laminations in the upper unit; b. Desiccation-cracked and -crusted (algal?) chips. Slab probably represents algal mats growing in the high intertidal or supratidal zones that originated on intermittently exposed sand shoals and tidal flats. Coated-grain packstone: c., d. Both slabs show stylolites and accumulation of insolubles in the bottom half of the slab associated with a well burrowed upper portion. Intraclasts, pellets, and most skeletal material show rounding and moderate to good sorting.

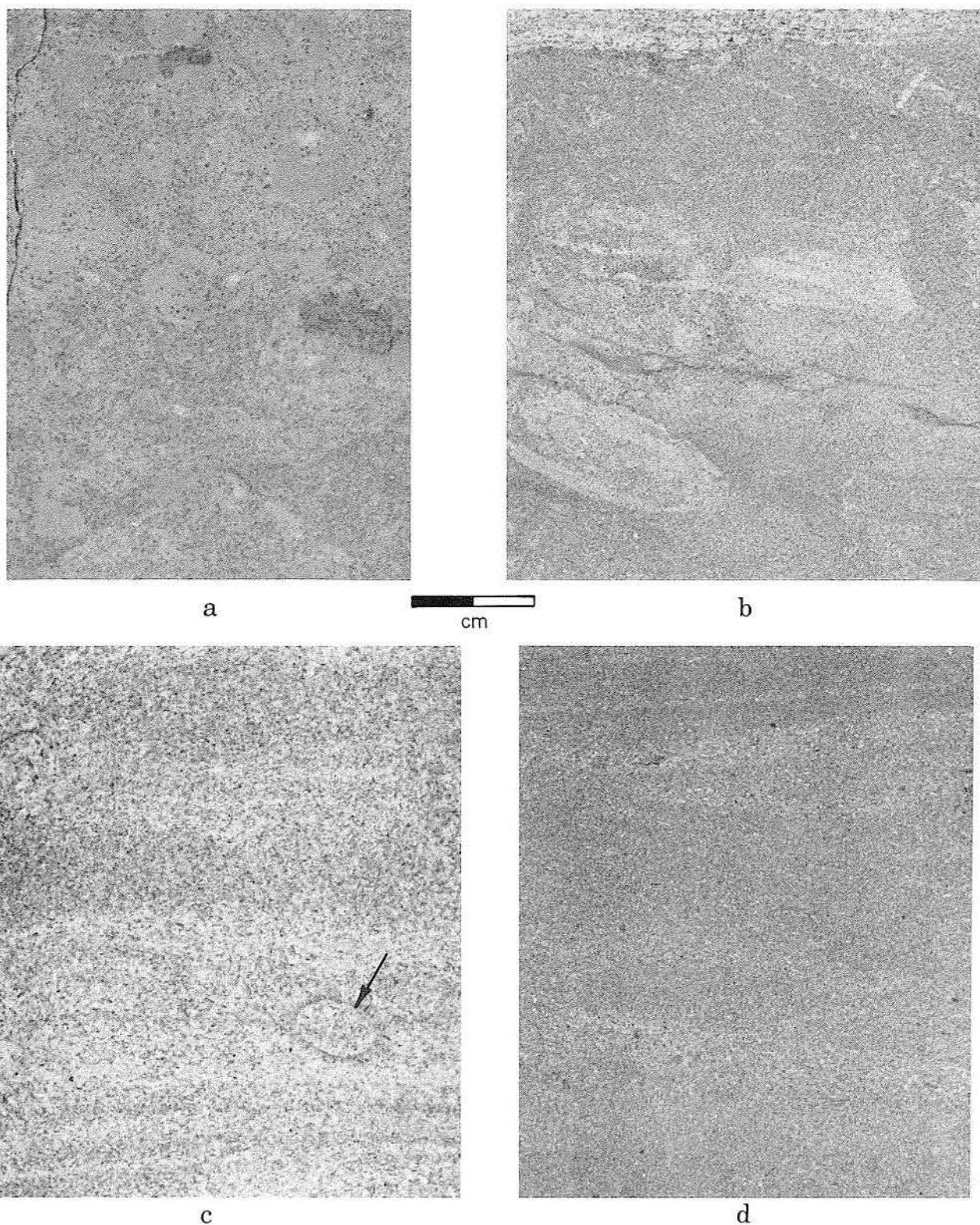
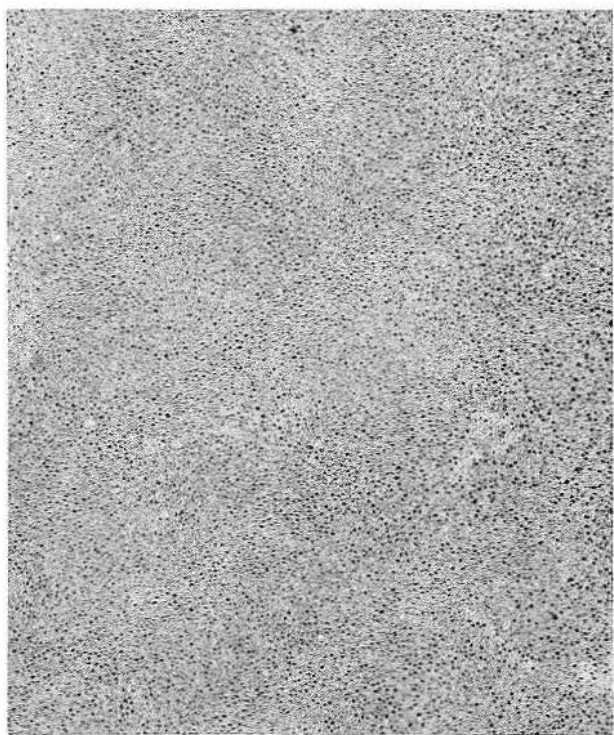
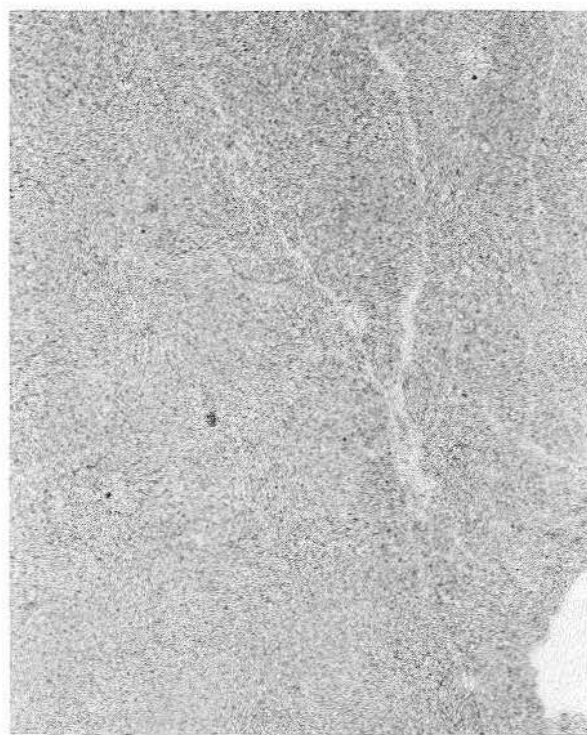
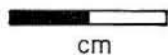


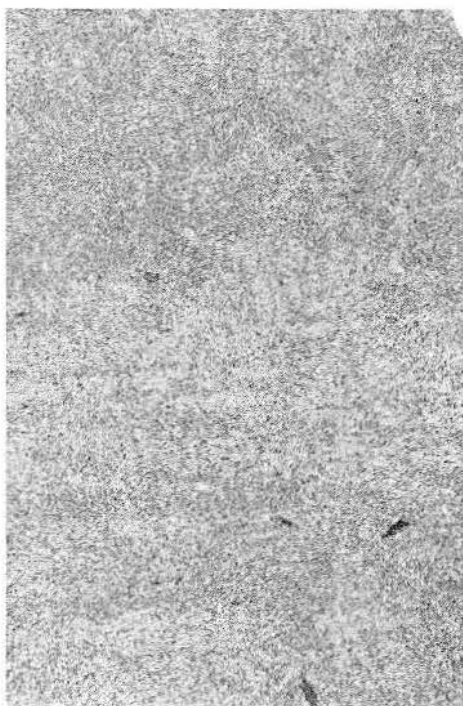
Figure 27. Pellet packstone: a. Large pellets are more common between burrows than within them. Note general absence of fossils in both (a) and (b); b. Burrowing in the lower half has partly destroyed the original cross-laminated texture that is still visible in the upper half. Skeletal grainstone: c. Parallel-laminated to low-angle cross-stratification characterizes this facies. A single burrow (arrow) illustrates the lack of infauna in this high-energy facies. The abundance of skeletal grains, especially mollusks, indicates dominance of reworking and concentration of skeletal debris in the mobile grain belt; d. Fine-grained skeletal grainstone (darker) interfingering with lenses of skeletal packstone (lighter). Fine grain size, sorting, and rounding reflect extensive reworking on beaches, bars, and spits.



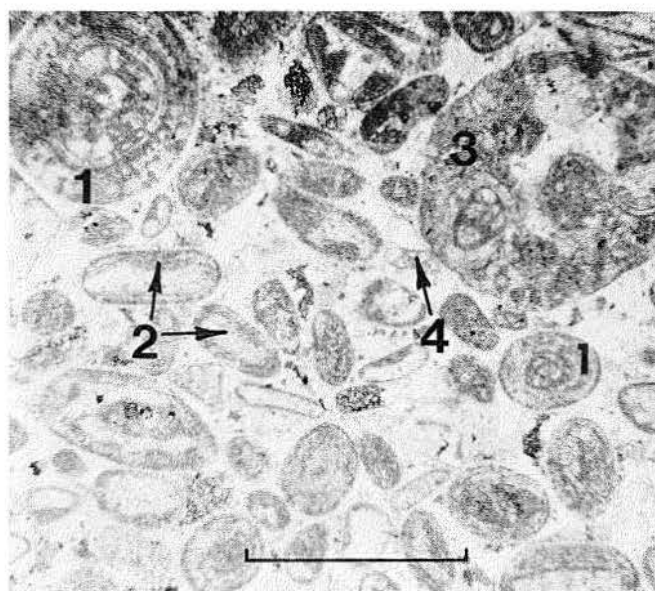
a



b



c



d

Figure 28. Oolite grainstone: a. Porous oolite grainstone homogenized by burrowing. Leaching of oolites has resulted in more than 50 percent moldic porosity. Permeability is excellent because the oomolds are connected by intercrystalline porosity; b. Oolite grainstone with numerous calcite-cemented vertical fractures. Primary bedding is completely obliterated; c. Burrowing destroyed the cross laminae in the upper half of this slab, producing a mottled massive bed similar to that in (b); d. Oolites (1), superficially coated molluscan shell debris (2), rounded foraminifer-rich intraclasts (3), and uncoated foraminifers (4) compose this uncompacted grainstone. Such a texture could only be preserved by very early cementation. Bar represents 0.5 mm.

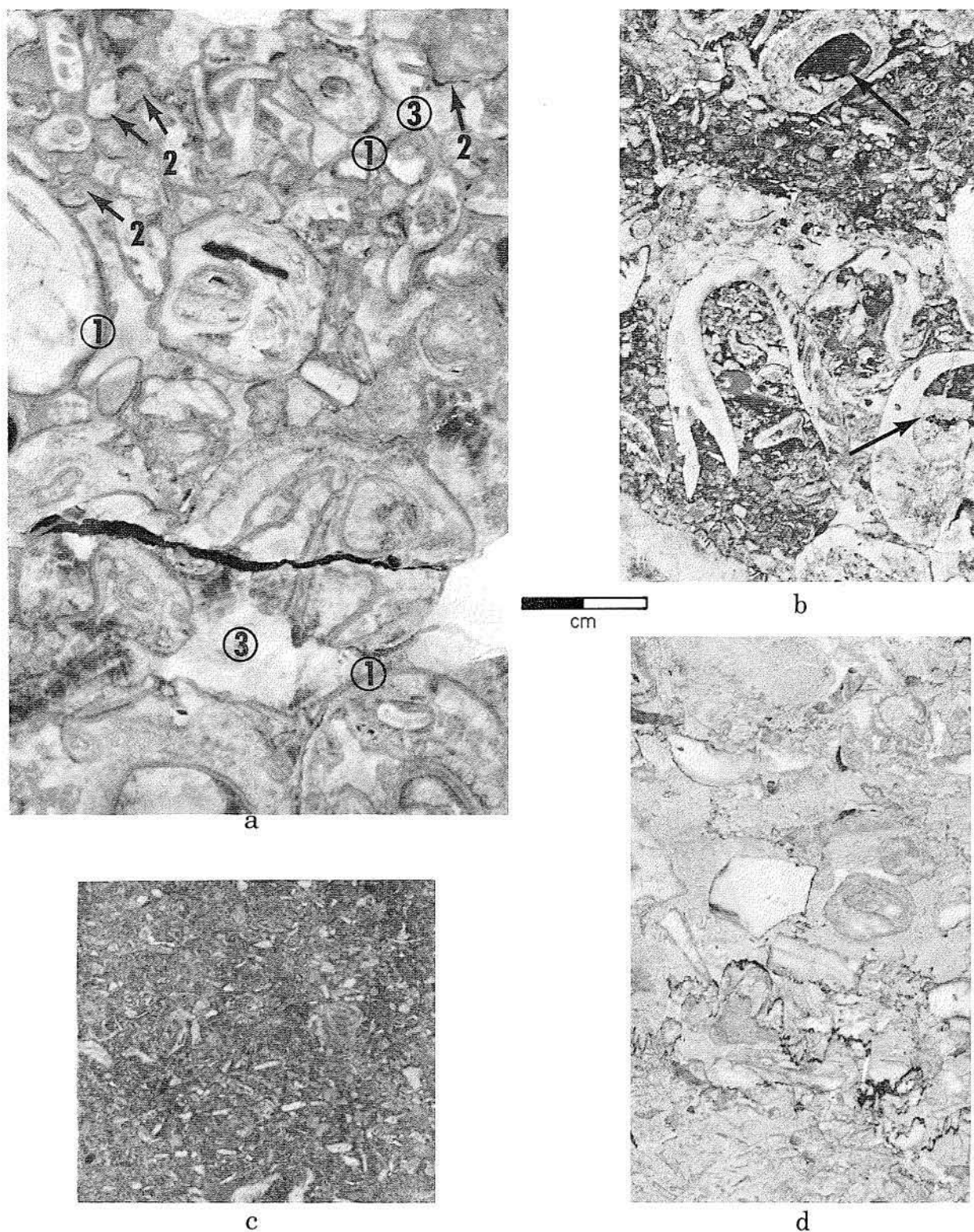


Figure 29. Caprinid grainstone: a. Gravel-sized, fining-upward accumulation of caprinids. Although original porosity was great, it is now virtually nonexistent. Thick radiaxial cement layer (1) postdates darker dripstone cement (2). Coarse, equant calcite (3) fills remaining pores; b. Bimodality of grain size is probably due to periodic (storm) debris being swept onto strong current-swept shoals. Note geopetal structures within caprinid body cavities (arrows). Coral-caprinid grainstone: c. Better sorting and finer grain size than in (a) and (b) above indicate greater reworking and transport. Deposition was probably on beaches, bars, or spits distal to organic reefs or banks. Caprinid-coral packstone/wackestone; d. Stylolites separate coarse-grained caprinid-coral wackestone from lower, finer grained caprinid-coral packstone.

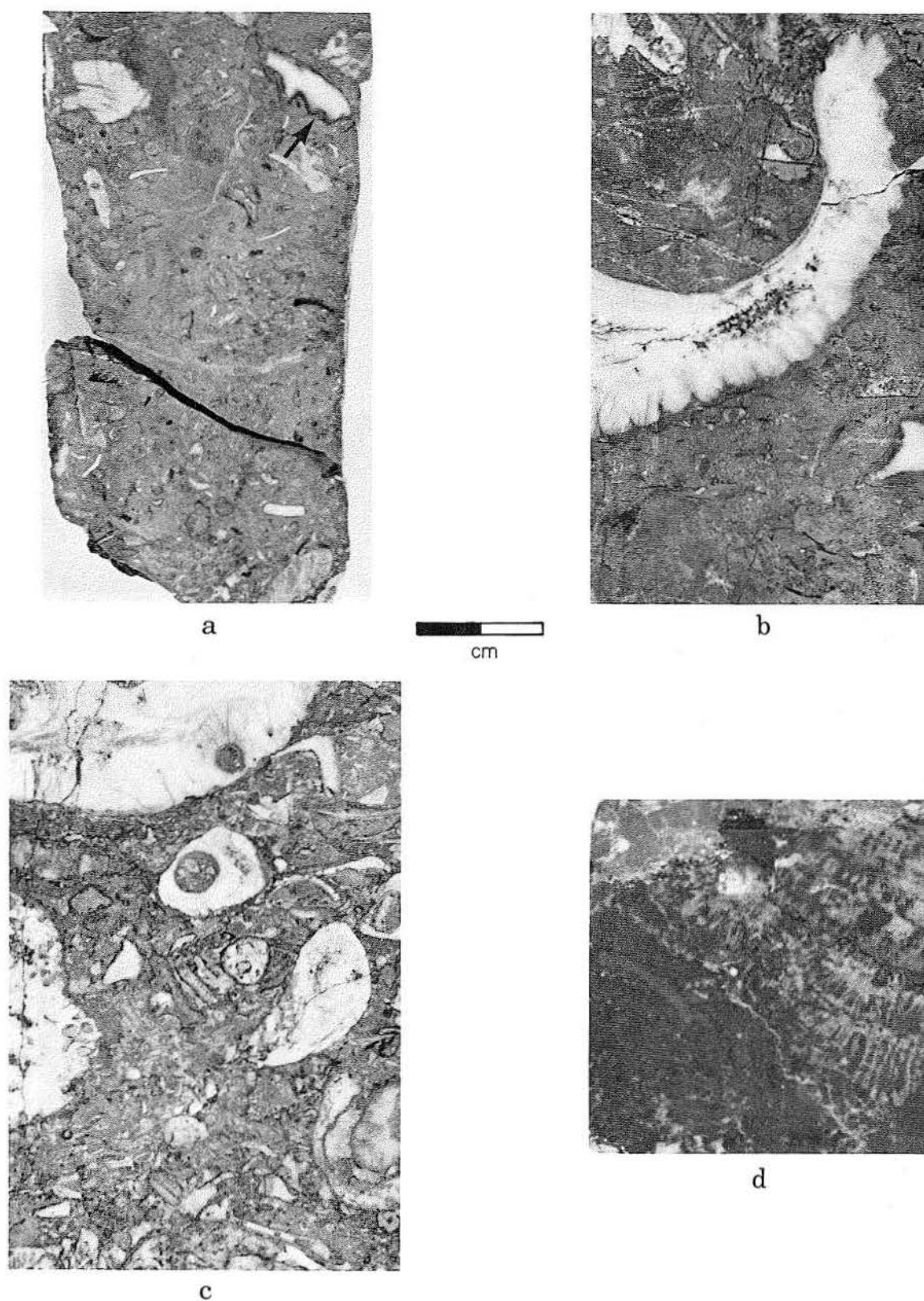


Figure 30. Coral-caprinid packstone/wackestone: a. Grain breakage, rounding, and boring by microorganisms (arrow) indicate deposition at some distance from organic reefs or banks yet still in relatively quiet water, as indicated by the mud matrix. Caprinid packstone/wackestone: b, c. Massive caprinids (white) contrast with much finer abraded skeletal remains. Such bimodality and fractures, like the ones on the left of c, typify this facies. Corallgal boundstones: d. A large stromatoporoid-like structure dominates the slab.

open-marine conditions. Variations in fauna across the shelf were a function of local restrictions of water movement. Oyster reefs and hardgrounds developed locally. Bioturbation was the dominant sedimentary process. Water depths varied greatly across this shelf platform and probably ranged from 3 to over 20 m (10 ft to more than 65 ft). An increase in oyster reefs and *toucasid* wackestone and a decrease in fossiliferous lime mudstone marks the seaward transition from the outer shelf into the "back-reef" area of the shelf margin. Locally, an increase in number and extent of islands in the "back-reef" area is reflected in the presence of thinly laminated tidal-flat mudstones.

The shelf margin consisted of a complex of organic banks, tidal passes, sand shoals, and accretionary sand spits (fig. 17). These shelf-edge environments are generally similar to those of the younger Stuart City shelf margin (Bebout and Loucks, 1974) and would fit the windward-bank margin type 1, reef- and shoal-complex model of Hine and Neumann (1977) or the organic reef rim shelf-margin model of Wilson (1974). Burrowing, encrusting, and localized framebuilding were the dominant biological processes, whereas the reworking, winnowing, and concentrating of skeletal debris by wind, waves, tides, and storms were the major physical processes.

Grainstones consisting of fragments of mollusks, corals, and caprinids were deposited by physical processes in mobile grain belts. Poorly sorted, coarse debris was deposited in tidal channels and flanking beds of small organic banks. Well-sorted fine skeletal grainstone represents extensive reworking on beaches and spits. Coated-grain packstone and oncolite packstone were deposited in quieter water

landward of these shelf-margin shoals as a result of stabilization of the shoal.

Coral and caprinid packstone to wackestone (associated with stromatoporoids, encrusting algae, and mollusks) represents discontinuous reefs, banks, and biostromes (Heckel, 1974) on the shelf margin. These deposits are the result of dominantly biological processes. Coralgal boundstones also occur in this setting in the Shell No. 1 Brown well. Energy conditions were moderate to high and most facies were deposited in shallow water, probably less than 3 m (10 ft) deep but possibly as deep as 10 m (33 ft).

The Sligo shelf margin is narrow, less than 1.6 km (1 mi) long, elongate, and discontinuous. The entire complex is characterized by abundant bioclastic debris from prolific local organic growth. Actual preserved reefs are few. The sand shoals represent the topographically high, shelf-edge structures.

No exact modern analogs of the Sligo outer-shelf and shelf-margin environments are known. The barrier-reef tracts of northern Belize (Pusey, 1975) and Australia (Maxwell, 1968) are probably only approximations. Lack of carbonate mud along the Great Barrier Reef (Maxwell, 1968, p. 197) and the importance of terrigenous siliciclastics and antecedent topography along both tracts limit the analogy. The facies tract of the South Florida shelf margin (Enos, 1977, p. 57) resembles that of the Sligo shelf margin; however, the narrowness of the South Florida outer shelf and shelf margin, 8 km (5 mi), clearly limits the similarity. An individual reef and associated sand shoal from any of these three modern shelf margins should compare well to a single reef and sand shoal complex of similar areal extent along the Sligo shelf margin.

FACIES

General Remarks

A facies is considered here as a group of rocks which are similar in mineralogy, biological composition, petrography, sedimentary structures, color, geometry, or combinations of these features. The depositional environment can be inferred from these properties and from its vertical and lateral relationships with other facies. Facies variations are a result of local and temporal fluctuations by the controlling depositional processes. In addition, the diagenetic overprint on a lithologic unit may alter significantly one or more properties.

To delineate the facies within the Sligo and Hosston Formations more than 2,765 m (9,069 ft) of core from 50 wells were logged (fig. 4; Appendix I). These cores were described according to lithology, color, texture, sedimentary structures, faunal content, porosity, and composition. These features were then analyzed and the facies were distinguished. These facies are listed in table 2 according to the inferred depositional environment and described in table 3. Some facies differ from each other in only subtle features and have similar origins; such facies are thus described together.

The facies are named according to Dunham's (1962) textural classification. Texture within some facies is variable, and only the dominant type is generally used in a facies name. Both the

Table 3. Facies and depositional environments,

Description and Figure	Lithology	Color	Texture	Fossils	Thickness
Burrowed dolomite mudstone Fig. 18 A, B	Dolomite, rarely silty or shaly, up to 20% nodular anhydrite	Cream, light to dark brown. Red oxidation rims often line burrows	Mudstone. Organic matter (generally oxidized) abundant	Minor occurrences of small mollusks	1 to 12 ft (0.3 to 3.7 m)
Pellet-mollusk dolomite wackestone Fig. 18 C, D	Dolomite and dolomitic limestone. Silty and up to 30% nodular anhydrite, traces of pyrite locally	Light to dark gray, light to medium brown	Wackestone, often coarsening into a thin (< 1 ft) packstone, rarely a mudstone. Pellets very common, up to 50% of grains	Mollusks are common and characterize this facies. Ostracodes and miliolids are occasionally present	1 to 40 ft (0.3 to 12.2 m), generally no more than 20 ft (6.1 m)
Burrowed sandstone Fig. 19 A	Terrigenous siliciclastics, usually dolomitic, rarely 5% nodular anhydrite	Medium to dark gray, cream	Generally a very fine sand, often silty, commonly shaly	None observed	1 to 8 ft (0.3 to 2.4 m)
Laminated sandstone Fig. 19 B, C, D, and Laminated siltstone Fig. 20 A, B	Terrigenous siliciclastics, often dolomitic, rarely shaly. Up to 40% nodular anhydrite locally in thicker units	Light to medium gray, cream, or rarely red	Generally well sorted sand or silt. Some units transitional between siltstone and sandstone.	None observed	1 to 100 ft (0.3 to 30.5 m), generally 2 to 15 ft (0.6 to 4.6 m)
Intracast dolomite wackestone Fig. 20 C, D	Dolomite	Brown	Wackestone, locally a packstone. Characterized by intracasts, up to 30% pellets	Mollusk skeletal debris makes up as much as 20 to 40% of the grains	1 to 3 ft (0.3 to 0.9 m)
Laminated dolomite mudstone Fig. 21 A, B	Dolomite, rarely dolomitic limestone. Silty, often sandy, with up to 80% nodular and nodular-mosaic anhydrite	Cream, light brown, rarely light gray. Red oxidation rims often line burrows	Mudstone. Organic matter (generally oxidized) and intracasts common	Generally absent; minor occurrence of mollusks	1 to 20 ft (0.3 to 6.1 m), generally less than 10 ft (3 m) in lower Sligo Formation and 10 to 20 ft (3 to 6.1 m) in the Hosston Formation
Skeletal dolomite grainstone Fig. 21 C, D	Dolomite, locally up to 10% nodular anhydrite, rarely silty	Light to dark brown	Grainstone, locally a packstone. Pellets common	Mollusks dominate; miliolids, worm tubes, and green algae are also present	Normally about 5 ft (1.5 m) to 25 ft (7.6 m) observed
Pellet dolomite grainstone Fig. 22 A, B, C	Dolomite with up to 30% interbedded nodular to mosaic anhydrite. Rarely silty	Light to dark brown	Grainstone, locally a packstone. Small rounded intracasts common	Miliolids, mollusks, and ostracodes are common	1 to 8 ft (0.3 to 2.4 m)
Conglomeratic sandstone Fig. 22 D	Terrigenous siliciclastics (arkosic). Pebbles of limestone and chert	Red	Poorly sorted sandy gravels and gravelly sand. Fining-upward sequences	None observed	30 ft (9.2 m) in Baker 2 ft (0.6 m) in Schmidt
Silty lime mudstone Fig. 23 A	Silty limestone; locally very sandy	Medium to dark gray	Mudstone, locally wackestone with up to 20% pellets. This facies is characterized by having a 10% or greater terrigenous silt component	None observed	2 ft (0.6 m)
Miliolid wackestone (fig. 23 B), Mollusk wackestone mollusk-miliolid wackestone (fig. 23 C), and echinoid-mollusk-miliolid wackestone (fig. 23 D)	Limestone; locally dolomitic and argillaceous, rare pyrite. In lower Sligo Formation, occasionally dolomitized completely and with up to 25% nodular anhydrite	Light to dark brown, light to dark gray, black in O'Neal	Dominantly wackestone, locally packstone. Commonly up to 10% superficially coated grains or up to 20% pellets or up to 20% intracasts	Mollusks, miliolids, worm tubes, sparse ostracodes, green algae, questionable red algae, and rare planktonic foraminifers. Corals, caprinids and oncolites are occasionally observed near the shelf margin	2 to 25 ft (0.6 to 7.6 m)
Pellet grainstone Fig. 24 A, B	Dolomitic limestone and limestone with traces of pyrite	Dark brown, medium to dark gray	Grainstone, locally a packstone	Miliolids, mollusks, ostracodes, echinoid fragments, and encrusting algae are common	1 to 8 ft (0.3 to 2.4 m)
Fossiliferous lime mudstone Fig. 24 C, D	Limestone; locally dolomitic, shaly, and pyritic	Medium to dark brown to black basinward	Mudstone, occasionally with minor pellets	Although fossils never make up more than 10% of this facies, echinoid spines and miliolids are relatively common. Less common are mollusks, whole oysters, and ostracodes	1 to 18 ft (0.3 to 5.5 m); commonly 1 to 4 ft (0.3 to 1.2 m) thick, thickest part toward the shelf edge
Oyster-miliolid wackestone Fig. 25 A	Limestone and slightly dolomitic limestone. Slightly pyritic	Light to dark brown to black	Wackestone dominant but packstone common. Rarely up to 30% pellets and 30% intracasts	Dominantly Chondrodonta-like oysters and miliolids. Less common are other kinds of mollusks, algal oncolites, serpulid worm tubes, small benthic foraminifers, dasycladacean green algae, and toudasids	1 to 22 ft (0.3 to 6.7 m) with thickest intervals toward the shelf edge
Toucasid wackestone Fig. 25 B	Limestone, traces of pyrite	Medium to dark gray	Wackestone, locally packstone. Allochems make up 10 to 30% of grains and include pellets, rounded intracasts, and coated grains	Toucasids characterize the facies. Mollusks, oysters, miliolids, oncolites, and encrusting algae are also present	1 to 5 ft (0.3 to 1.5 m). Thinner beds are locally interbedded with mollusk-miliolid wackestones and oyster-miliolid wackestones
Oncolite packstone Fig. 25 C, D, E	Limestone, locally shaly with traces of pyrite	Black, dark brown	Packstone, locally a wackestone. Grains are mainly skeletal but up to 30% are pellets	Oncolites characterize this facies. Skeletal material includes oysters, caprinids, corals, green algae, red algae, worm tubes, forams, mollusks and miliolids. Stromatoporoids and bryozoa are rare	4 to 25 ft (1.2 to 7.6 m)
Laminated lime mudstone Fig. 26 A, B	Limestone, locally shaly and pyritic	Light gray to dark gray	Mudstone, occasionally with pellets	Although fossils never make up more than 10% of this facies, miliolids and mollusks are common. Less common are oysters and oncolites	1 to 10 ft (0.3 to 3 m), commonly 2 to 4 ft (0.6 to 1.2 m)

Sligo and Hosston Formations.

Structures	Porosity	Occurrence	Associated Facies	Depositional Environments
Burrows totally dominate this facies	Commonly 5% intercrystalline and up to 10% vuggy or moldic porosity	Schmidt, Baker, Mercer, Dix, and Pruitt	Laminated dolomite mudstone, pellet-mollusk dolomite wackestone, pellet dolomite grainstone, skeletal dolomite grainstone, mollusk miliolid wackestone, laminated siltstone, burrowed and laminated sandstones, intraclast dolomite wackestone	Abundant burrows with oxidation rims, organic debris, and sparse fauna suggest deposition in a very shallow, low-energy intertidal pond or lagoon
Burrows very characteristic; wavy laminations and stylolites also abundant	Up to 20% vuggy, moldic, and interparticle porosity, but generally less than 5%	Schmidt, Baker, Mercer, Dix, and Pruitt	Burrowed mudstone, laminated mudstone, mollusk-miliolid wackestone, echinoid-mollusk-miliolid wackestone, skeletal dolomite grainstone, pellet dolomite grainstone, intraclast dolomite packstone and siltstone	Sparse fauna and heavy burrowing indicate deposition in a shallow, restricted subtidal environment probably adjacent to tidal flats. Storm, tidal, and wind currents occasionally winnowed the grains into a coarser deposit
Extensively bioturbated, dominantly horizontal burrows	Up to 5% interparticle porosity rare	Schmidt, Mercer, Baker, Dix, and Pruitt	Laminated sandstone and siltstone, laminated and burrowed dolomite mudstones	Abundant burrows are indicative of shallow, low-energy subtidal conditions, either adjacent to the tidal flats or as ponds within the intertidal zone
Parallel laminations, ripples, and crossbedding most common. Burrows, graded bedding, clay drapes, mudcracks, and scour also observed	None observed in the siltstone; 5% interparticle porosity common in the sandstone	Mercer, Baker, Dix, Schmidt, and Pruitt	Burrowed sandstones, conglomeratic sandstone, pellet-mollusk dolomite wackestone, mollusk-miliolid wackestone, echinoid-mollusk-miliolid wackestone, laminated and burrowed dolomite mudstone	The thick crossbedded sandstones grade upward into parallel- and ripple-laminated sandstones and siltstones with clay drapes, mudcracks, and nodular anhydrite. This sequence suggests deposition from the lower to upper tidal-flat environment
Hardgrounds, laminations, cross-bedding, and stylolites	None observed.	Baker, Pruitt, Schmidt, Dix, and Mercer	Pellet-mollusk dolomite wackestone, pellet dolomite grainstone, burrowed and laminated dolomite mudstones, skeletal dolomite grainstone	Associated facies indicate deposition within the tidal-flat environment. Abundant large clasts suggest deposition from a high-energy event, probably as a storm lag
Parallel laminations (algal) and burrows most common. Bird's-eye structure, brecciation, clasts, graded beds, mudcracks, hardgrounds, disrupted beds, and stylolites common	Up to 5% moldic and 5% intercrystalline	Schmidt, Baker, Mercer, Dix, and Pruitt	Pellet-mollusk dolomite wackestone, intraclast dolomite wackestone, pellet dolomite grainstone, laminated siltstone, burrowed and laminated sandstones and burrowed dolomite mudstone, skeletal dolomite grainstone	Parallel laminations, mudcracks bird's-eye structures, and oxidation colors indicate an intertidal-supratidal environment. Algal laminations are suggestive of a marsh setting
Burrows, irregular laminations, crossbedding, graded beds, hardgrounds, and stylolites	Up to 15% interparticle and moldic porosity, generally 5% or less	Baker, Mercer, Pruitt, and Schmidt	Pellet dolomite grainstone, pellet-mollusk dolomite wackestone, mollusk-miliolid wackestone, intraclast dolomite wackestone, laminated and burrowed mudstones	Storm or tidal-current deposits on intertidal beach ridges, or tidal-channel bars, and deltas as indicated by grainstone fabric, crossbedding, and associated tidal-flat facies
Crossbedding, ripples, burrows, irregular laminations, clay drapes, disrupted laminations, hardgrounds, and stylolites	5 to 15% moldic porosity	Pruitt, Schmidt, Mercer, Dix, and Baker	Mollusk-miliolid wackestone, intraclast dolomite wackestone, skeletal dolomite grainstone, mollusk dolomite wackestone, and laminated and burrowed dolomite mudstones	Association with typical tidal-flat facies, restricted fauna, crossbedding, and abundance of mud intraclasts suggest deposition predominantly as a winnowed lag on beach ridges. Also in tidal channels, deltas, levees, and as storm deposits on the tidal flat. Muddier units locally occur as storm washovers onto the tidal flat
None observed	None observed	Schmidt and Baker	Burrowed and laminated sandstones	Uncertain, red color, lack of fauna, lack of structures, and coarse grain size imply a braided-stream deposit in an alluvial-fan or fan-delta system
Dominantly horizontal burrows, locally laminated	None observed	Herrera, Belco No. 1 Kincaid, Schmidt, and Dam Site No. 7	Echinoid-mollusk-miliolid wackestone	Horizontal burrows and muddy texture indicate a low-energy subtidal setting. Lateral occurrence and silt content suggest this facies is restricted to an inner-shelf lagoon
Burrows, wavy laminations, stylolites, fractures. Geopetal and fenestral structures in Watkins and Alvarado. Hardgrounds occasionally present updip	Up to 12% moldic, 5% vuggy, and 10% interparticle porosity is present although porosity is usually less than 5% moldic	Present in all wells with core except Friedrichs, Roessler, Baker, and Reuthinger	Oolite grainstone, coated-grain packstone, skeletal grainstone, pellet packstone, pellet grainstone, fossiliferous lime mudstone, silty lime mudstone, oyster-miliolid wackestone, toulasid wackestone, oncolite packstone, caprinid packstone, coral-caprinid packstone and grainstone, and pellet-mollusk wackestone	Burrows, diverse fauna, and muddy texture indicate deposition in shallow, quiet waters 10 to 15 ft (3 to 4.6 m) deep on the outer shelf and in the shelf lagoon
Crossbedding, burrows, irregular laminations, stylolites, and graded beds	Less than 3% moldic porosity, up to 5% interparticle porosity	Pruitt, Canales, Wilson (La Salle Co.), Dix, Crowell, Handy, Washburn, and Reuthinger	Mollusk-miliolid wackestone, mollusk wackestone, pellet wackestone, oyster-miliolid wackestone, echinoid-mollusk-miliolid wackestone, skeletal grainstone, coated-grain packstone, and fossiliferous lime mudstone	Diverse fauna indicates deposition in an open-shelf setting. The grainstone fabric probably resulted from strong tide and storm currents effectively winnowing the fines
Wavy laminations burrows, vertical fractures—some of which are large and filled by the overlying facies, stylolites	None observed	Ney, P. R. Smith, J. J. Smith, Collins, Finch, Climer, Pruitt, Herrera, Rogers, Wilbeck, Wilson (Medina Co.), Sirianni, Wilson (La Salle Co.), Canales, Rolf, O'Neal, Handy, Alvarado, and McDowell	Oyster-miliolid wackestone, mollusk-miliolid wackestone, miliolid wackestone, echinoid-mollusk-miliolid wackestone, pellet grainstone, coated-grain packstone, skeletal grainstone, toulasid wackestone, oncolite packstone, coral-caprinid grainstone and packstone, and caprinid grainstone and packstone	Abundant burrows, diverse fauna, and muddy texture suggest deposition in a low-energy setting. Associated facies are from outer-shelf and shelf-margin environments indicating a similar depositional setting
Borings into hardgrounds, bird's-eye, fenestral, stylolites, some geopetal, clayey laminations, and vertical fractures	None observed	Mercer, Wilson (La Salle Co.), Canales, Carrol, Washburn, Watkins, Handy, and Reuthinger	Mollusk-miliolid wackestone, echinoid-mollusk-miliolid wackestone, miliolid wackestone, fossiliferous lime mudstone, toulasid wackestone, pellet grainstone, skeletal grainstone, oncolite packstone, pellet packstone, and coated-grain packstone	Presence of oysters suggests deposition on a restricted shallow shelf with water depths commonly less than 10 ft (3 m). Occasional influx of fresh water based on abundance of oysters in growth position. Bird's-eye structures and abundant oysters and bored hardgrounds indicate possible infrequent subaerial exposure of those parts of the oyster reef that grew up to sea level
Stylolites, fenestral structures	Local microporosity (less than 2% noted)	Watkins, Wilson, Handy, Rolf, and Brown	Echinoid-mollusk-miliolid wackestone, mollusk-miliolid wackestone, oyster-miliolid wackestone, skeletal grainstone, oncolite packstone, caprinid packstone, caprinid-coral grainstone, and fossiliferous mudstone	Toulasids typify a low-energy setting commonly behind shelf-margin sand shoals and rudist-coral banks
Geopetals, bird's-eyes, stylolites, fractures	Up to 5% intraparticle or interparticle porosity	O'Neal, Suggs, Finch, Handy, Washburn, and Brown	Coral-caprinid and skeletal grainstones, caprinid packstone, pellet packstone, oyster-miliolid wackestone, mollusk wackestone, echinoid-mollusk-miliolid wackestone, coated-grain packstone, and fossiliferous lime mudstone	The large oncolites indicate the grains lay on the sea floor in warm, quiet waters. At the shelf margin this facies occurs behind the sand shoals and rudist-coral banks
Laminations and bird's-eye structures characteristic. Brecciation, stylolites, and fractures also observed	None observed	Handy, Ney, and Mercer	Oncolite packstone, pellet packstone, oyster-miliolid wackestone, mollusk-miliolid wackestone, toulasid wackestone, miliolid wackestone and skeletal grainstone	Bird's-eye structures, brecciation, and clasts indicate a tidal-flat environment. Thinness of this facies indicates these tidal flats were never extensive or long lasting. They probably originated leeward of exposed oyster reefs or sand shoals

Table 3

Description and Figure	Lithology	Color	Texture	Fossils	Thickness
Coated-grain packstone Fig. 26 C, D	Limestone, locally up to 5% nodular anhydrite, 20% dolomite or silt, traces of pyrite	Light gray to dark brown	Packstone, locally grainstone or wackestone. Coated grains predominate with oolites in the inner shelf and shoals. Locally up to 50% skeletal, 20% intraclasts, or 20% pellets	Mainly mollusks and miliolids, also echinoids, ostracodes, green algae, oncolites, and worm tubes. Red algae, corals, caprinids, and stromatoporoids are also present at shelf margins	2 to 18 ft (0.3 to 5.5 m)
Pellet packstone Fig. 27 A, B	Limestone and dolomitic limestone; less than 5% nodular anhydrite; traces of pyrite locally	Light to dark gray, light to medium brown	Packstone, locally wackestone. Grains are mainly pellets, but occasionally up to 40% are intraclasts or skeletal debris	Mollusks and miliolids are most common. Green algae, echinoid fragments, oncolites, red algae, and worm tubes are also present. Coral, caprinids, and stromatoporoids are present at shelf margin	1 to 7 ft (0.3 to 2.1 m)
Skeletal grainstone Fig. 27 C, D	Limestone, locally up to 40% dolomite and 10% nodular anhydrite	Light to medium brown, light to dark gray	Grainstone, locally a packstone	Mollusks dominate this facies. Miliolids, echinoid fragments, worm tubes, and green algae are also present	1 to 5 ft (0.3 to 1.5 m) on inner shelf, up to 10 ft (3 m) near shelf margin
Oolite grainstone Fig. 28 A, B, C, D	Limestone and dolomitic limestone	Light brown to dark gray	Grainstone, locally packstone. Although oolites characterize this facies, superficially coated grains and intraclasts are locally important	Fossils usually make up less than 30% of the grains. Those fossils that are common include echinoids, mollusks, miliolids. Other fossils include red algae, oncolites, toudasid shells, worm tubes, ostracodes, and boring pelecypods in local hardgrounds	1 to 30 ft (0.3 to 9.2 m). Thinner beds are locally interbedded with coated-grain packstone. Most oolite-grainstone beds are between 5 and 10 ft (1.5 to 3 m) thick
Caprinid grainstone Fig. 29 A, B, and Coral-caprinid grainstone Fig. 29 C	Limestone	Light to dark gray	Grainstone, locally a packstone. Grains are generally rounded and either well sorted sand size debris or poorly sorted gravel and sand size debris	Mollusks, corals, and caprinids dominate with red algae, encrusting algae, algal oncolites, bryozoa, stromatoporoids, miliolids, green algae, and echinoid fragments present in varying amounts. Caprinids totally dominate the caprinid-grainstone facies	Generally 10 to 40 ft (3 to 12.2 m) but up to 60 ft (18.3 m) and as thin as 1 ft (0.3 m)
Coral-caprinid packstone/ wackestone Fig. 29 D, 30 A and Caprinid packstone/ wackestone Fig. 30 B, C	Limestone, locally traces of pyrite	Light to dark gray	Packstone to wackestone, locally a boundstone. Occasionally up to 20% pellets. Packstone facies strongly bimodal with large caprinids and finer abraded skeletal debris	Large caprinids and colonial or solitary corals dominate. Echinoid fragments, mollusks, miliolids, green algae, red algae, encrusting algae, bryozoa and stromatoporoids common	4 to 40 ft (1.2 to 12.2 m)
Coralgal boundstone Fig. 30 D	Limestone	Light to dark gray	Boundstone with 10 to 60% skeletal material, locally a wackestone	Corals or caprinids and encrusting algae predominate with stromatoporoids, bryozoa, miliolids, forams, mollusks and green algae common. Fragments of oysters occasionally present	Individual units 1 to 5 ft (0.3 to 1.5 m); stacked sequences up to 20 ft (6.1 m)

minimum and maximum observed facies thicknesses are included under "thickness." Porosity types are named according to Choquette and Pray (1970). Percent porosity in the descriptions and in the cross sections is based on visual estimates. "Occurrence" includes only the wells in which a particular facies was described. "Associated facies" includes all facies that are in contact above or below the facies described. Comments under "Depositional environment" are interpretive, and water depths are inferred. All core slabs are actual size.

Facies Distribution

Six cross sections have been constructed to display graphically lateral facies relationships between wells and vertical changes within wells. Because of the great distance between some wells, correlations are not shown on half of the cross

sections. Thirty-two of 50 wells logged in this study are shown on these cross sections, representing 2,100 m (6,887 ft) of the 2,765 m (9,069 ft) examined (76 percent). The datum for all sections except D-D' and E-E' is the top of the Sligo Formation, picked from electric logs.

Hosston and Lower Sligo Facies

The vertical sequence within each core on section B-B' (fig. 31, in pocket) shows the lithologic transition from dominantly terrigenous sandstone and siltstone with anhydrite and dolomite in the Hosston Formation, to dolomite in the lower Sligo Formation, and finally to limestone in the upper Sligo Formation. Within the Hosston Formation a decrease in sandstone and increase in siltstone and dolomite are distinct both downdip (for example, Stanolind No. 1 Schmidt to Humble No. 46 Pruitt) and laterally off the San Marcos Arch (for example, Stanolind No.

(cont.)

Structures	Porosity	Occurrence	Associated Facies	Depositional Environments
Abundant burrows, wavy laminations, fractures, graded beds, stylolites, crossbedding, and geopetals	Less than 8% primary interparticle, 5% intraparticle, 5% moldic, and 10% solution-enlarged interparticle porosity	Edgar, Sirianni, Rowe No. 1 Kincaid, Wilson (Medina Co.), Dam Site No. 7, Dix, Schmidt, No. 1 Goad, Wilbeck, Ney, Hardie, Machen, Roberts, No. 2 Rheiner, Crowell, Mercer, Baker, Dickson, P. R. Smith, J. J. Smith, Powell, Collins, Finch, Climer, Belco No. 1 Kincaid, Herrera, Rogers, Pruitt, Friedrichs, and Washburn	Oolite grainstone, skeletal grainstone, oncolite packstone, coral-caprinid packstone and grainstone, echinoid-mollusk-miliolid wackestone, mollusk-miliolid wackestone, oyster-miliolid wackestone, pellet packstone and grainstone, fossiliferous lime mudstone, pellet-mollusk dolomite wackestone	The muddy, yet grain-supported texture and abundant burrows indicate deposition in banks of stabilized grain flats. These banks occurred in less than 5 ft (1.5 m) of water and were probably cut by channels up to 10 ft deep (3 m). The grain flats developed behind mobile sand shoals, at the shelf margin and behind oolite bars on the inner shelf
Burrows, irregular laminations, bi-directional crossbedding, stylolites, fractures	5% interparticle, 2% moldic porosity	P. R. Smith, Powell, Pruitt, Belco No. 1 Kincaid, Dix, Watkins, Canales, Handy, Washburn, and Rolf	Coated-grain packstone, echinoid-mollusk-miliolid wackestone mollusk-miliolid wackestone, oyster-miliolid wackestone, mollusk-miliolid wackestone, fossiliferous lime mudstone, skeletal grainstone, and oncolite packstone	This facies is commonly adjacent to the coated-grain packstone, yet the greater percentage of mud and pellets suggests deposition in muddy sandflats landward of the stabilized sandflats in 5 to 10 ft (1.5 to 3 m) of water. On the outer shelf and shelf margin the association with the pellet grainstone suggests deposition as winnowed lags probably associated with storms or high current activity
Burrows, irregular laminations, stylolites, graded beds, crossbedding, geopetals, and large veins	Less than 5% interparticle, moldic, and intraparticle porosity. In Shell Alvarado, up to 10%	No. 1 Goad, Wilbeck, Mack, Powell, Kaufmann, Wilson (Medina Co.), Sirianni, Wilson (La Salle Co.), Dix, Carroll, Finch, Climer, Roberts, Pruitt, K. B. & M. Belco No. 1 Kincaid, Schmidt, Dickson, Canales, Handy, Washburn, and Alvarado	Oolite grainstone, pellet grainstone, coated-grain packstone, oncolite packstone, pellet packstone, echinoid-mollusk-miliolid wackestone, oyster-miliolid wackestone, mollusk-miliolid wackestone, toucasid wackestone, and fossiliferous lime mudstone	The grainstone fabric indicates deposition in a strong current-swept shallow subtidal setting. Winnowing of fines due to tidal energy and storms
Stylolites, cross lamination, vertical fractures, and burrows are present	Interparticle and intraparticle porosity of less than 10% is dominant. Oomoldic porosity is less common but locally ranges up to 25% as in the Tenneco-Pennzoil No. 1 Finch	Hardie, Sawicki, Kincaid, Ney, Machen, Roberts, No. 2 Rheiner, Carroll, Collins, Finch, Dickson, Crowell, Climer, Rogers, Pruitt, Herrera, Nixon, Plachy, Wilson (Medina Co.), Dix, No. 1 Goad, Edgar, K. B. & M. Schmidt, and Dam Site No. 7	Coated-grain packstone, skeletal grainstone, echinoid-mollusk-miliolid wackestone, mollusk-miliolid wackestone, and mollusk-pellet dolomite wackestone	The abundance of oolite and cross laminations signifies deposition in a high-energy sand shoal. The facies occurs seaward of the lower-energy coated-grain and pellet packstone facies indicating the mobile oolite bars were along the seaward margin of the larger shoal complex
Burrows, irregular laminations, stylolites, graded beds, geopetals, and large veins	Up to 5% interparticle and intraparticle porosity, 10% moldic porosity cement-reduced in McDowell	Handy, Alvarado, Friedrichs, Brown, and McDowell	Skeletal grainstone, coated-grain packstone, oncolite packstone, coral-caprinid packstone, caprinid packstone, miliolid wackestone, toucasid wackestone, fossiliferous lime mudstone, and corallal boundstone	Grainstone fabric with shelf-margin fauna indicates deposition in strong current-swept sand shoals and spits flanking discontinuous coral-caprinid banks. Winnowing of fines due to high tidal, wave, and storm energy
Geopetals, burrows, stylolites, and fractures	5% moldic and 5% intraparticle porosity commonly observed	Alvarado, Roessler, Brown, Handy, McDowell, and Friedrichs	Coral-caprinid and caprinid grainstones, corallal boundstone, coated-grain packstone, fossiliferous lime mudstone, oncolite packstone, and echinoid-mollusk-miliolid wackestone	Shelf margin in very shallow water. The abundance of large caprinids and corals suggests little transport or reworking. The occasional boundstone fabric and association with other boundstones suggest this facies accumulated as debris from small discontinuous banks. The lack of corals in some of these banks apparently resulted in the caprinid packstone/wackestone facies
Geopetals, stylolites, and fractures	5% intraparticle porosity observed rarely	Brown	Coral-caprinid grainstone, coated-grain packstone, coral-caprinid packstone, and caprinid packstone	Shelf margin in 5 to 15 ft (1.5 to 4.6 m) of water. The boundstone fabric and thin nature of the facies suggest it accumulated in small discontinuous banks

1 Schmidt to Magnolia No. 1 Mercer and No. 1 Baker).

Laminated sandstone and siltstone, burrowed sandstone, laminated dolomitic mudstone, and burrowed dolomitic mudstone constitute the facies from Guadalupe Dam Site No. 7 to Gulf No. 20 Dix in the Hosston. These units are interpreted as having been deposited in a tidal-flat environment.

A progradational unit of the Hosston siliciclastic tidal flats (fig. 32) is marked at its base by extensive burrowing in fine-grained sandstones. This is overlain by thick-bedded, rippled, and crossbedded sandstone with minor burrowing and clay drapes. These sandstones are generally the coarsest observed within the sequence but they never exceed a medium grain size. A very fine grained sandstone caps the upper tidal-flat sequence and is characterized by parallel laminations, mud cracks, clasts, nodular anhydrite, and wispy, irregular laminations.

The Hosston dolomitic tidal-flat sequence (fig. 33) is marked by highly burrowed and bioturbated, organic- and shale-rich dolomite mudstone at its base. The intertidal zone in the middle consists of laminated dolomite mudstones containing minor burrows. The supratidal zone contains bird's-eye structures, mud cracks, clasts, and abundant anhydrite, the presence of which distinguishes this zone from the intertidal sediments. Laminated dolomite mudstone also occurs in the supratidal zone. These supratidal sediments have been interpreted as laterally extensive sabkha deposits. Numerous small scour features characterized by slumped bedding and basal lags of mud clasts suggest the presence of tidal channels.

Intertidal and subtidal sediments in the upper part of the Hosston Formation in the Gulf No. 20 Dix include pellet-mollusk dolomite wackestone indicative of less restrictive conditions occurring

seaward across the tidal-flat complex. This trend is also common in the Humble No. 46 Pruitt. The Hosston Formation in this core resembles the Sligo Formation more than it does the time-equivalent, updip Hosston Formation. Sandstone is very minor, as is the laminated dolomite mudstone. Only the interval from 3,250 to 3,277 m (10,660 to 10,750 ft) consists of the previously described tidal-flat sequences. The remainder of the Hosston Formation in this core consists of partly dolomitized skeletal wackestones and scattered, thin grainstones with mollusks, miliolids, and dasycladacean algae, interpreted as representing nearshore shelf sediments. Burrowing is abundant and anhydrite, rare.

This lateral transition within the Hosston Formation — from the siliciclastic, dolomitic, and anhydritic tidal-flat complex to the calcitic, nearshore, marine-shelf wackestones — also occurs vertically within Stanolind No. 1 Schmidt, Magnolia No. 1 Mercer and No. 1 Baker, and Gulf No. 20 Dix. The transition zone from the Hosston Formation to the Sligo Formation is indicative of facies changes rather than a distinct time-stratigraphic boundary. Terrigenous clastics decrease gradually, and fossil content increases upward and downdip. Facies range from burrowed dolomite mudstone (subtidal) to laminated dolomite mudstone and pellet-mollusk dolomite wackestone (intertidal). Supratidal sediments are no longer exclusively laminated dolomite mudstone deposited in broad sabkhas; they also include local pellet and skeletal dolomite grainstones and packstones that were deposited in beach ridges and overbank tidal-channel levees.

The lower Sligo sedimentation pattern that emerges from this transition zone is a series of progradational cycles (fig. 34). The subtidal units are highly burrowed and organic-rich pellet-mollusk dolomite wackestone and rarely mollusk-miliolid wackestone. Intertidal sediments are laminated and burrowed dolomite mudstone and pellet-mollusk dolomite wackestone. Pellet dolomite grainstone, skeletal dolomite grainstone, laminated dolomite mudstone, and intraclast dolomite wackestone characterize the supratidal deposits. Parallel laminations, clasts, and minor burrows dominate these facies; ripples, crossbedding, mud cracks, and anhydrite are less common. The pellet dolomite grainstone commonly caps the supratidal sequence. Some of the pellet dolomite grainstones and skeletal dolomite grainstones, however, may have been subtidal deposits of tidal-channel deltas.

These supratidal units, interpreted as beach ridge and levee deposits, represent high-energy

deposits above the normal tidal zone. Desiccation produces mud cracks and clasts. Laminated dolomite muds result from algal mats growing on the margins of these ridges, adjacent to the intertidal zone. Some of the packstones probably

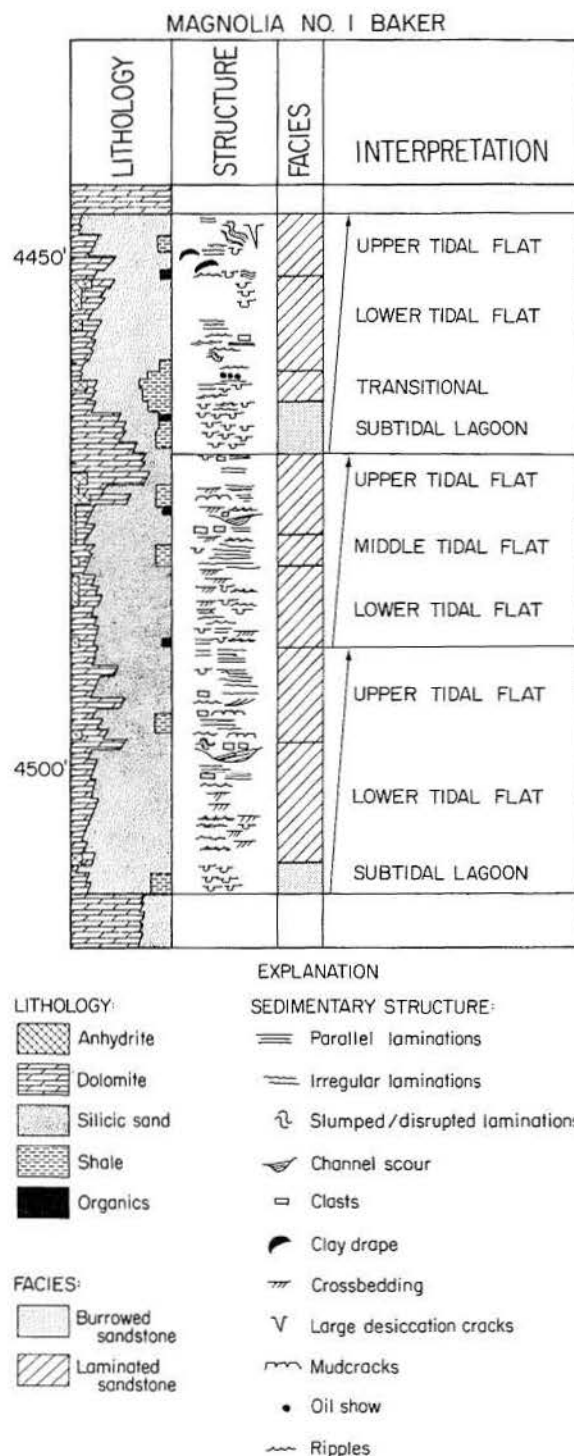
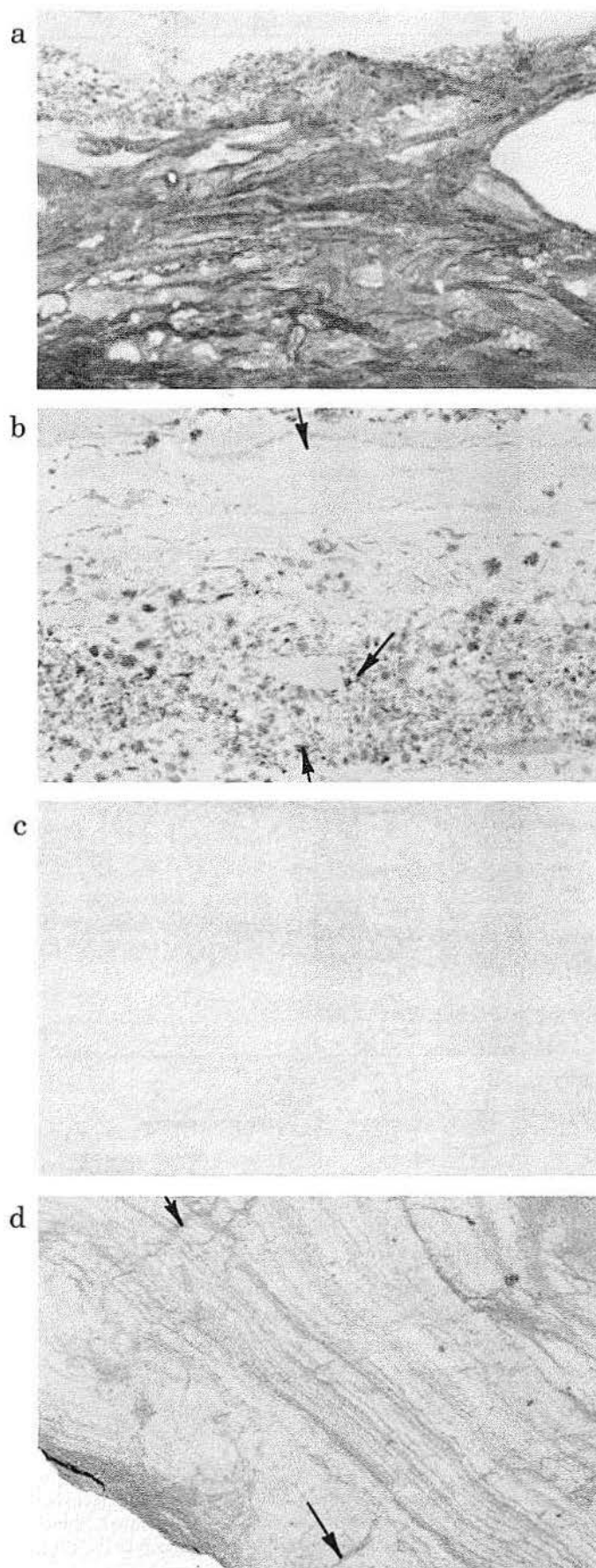


Figure 32A. Vertical succession of facies, interpreted environments, and progradational cycles of the Hosston terrigenous clastic tidal-flat deposits, Magnolia No. 1 Baker, South Texas.



represent overwash onto the intertidal flat. Table 4 summarizes and compares the facies, features, and interpretations of the Hosston and lower Sligo tidal-flat complexes.

Not all the sediments of the lower Sligo Formation are exclusively tidal-flat in origin. As in the Hosston Formation, more normal-marine conditions are present locally, especially downdip in the Humble No. 46 Pruitt. Oolite grainstone, coated-grain packstone, skeletal grainstone, and mollusk-miliolid wackestone compose these facies. The sequences are characterized by a high oolite content and are rarely thicker than 3 m (10 ft), except in the Pruitt core. As stated previously, this facies succession indicates the dominantly transgressive nature of the Sligo Formation. Extensive transgression across the broad, low-relief, tidal flats quickly reestablished subtidal conditions, and rapid progradation similarly returned the sedimentary regime to the tidal zone and tidal-flat sedimentation.

Along section B-B' (fig. 31) the contact between the upper and lower Sligo Formation is as indistinct as that between the lower Sligo and Hosston Formations. The upper Sligo Formation is characterized by an increase in limestone and a decrease in dolomite. Facies also change across the transition zone. The upper Sligo Formation on this section is characterized by mollusk-miliolid and echinoid-mollusk-miliolid wackestone (inner-shelf deposits). Oolite and skeletal grainstones and coated-grain packstone indicate the existence of subtidal shoal complexes. Oyster-miliolid wackestone and laminated lime mudstone are also associated with these shoals, generally capping the sequences. They indicate the stabilization of the shoals and the establishment of local oyster reefs or tidal flats.

The depositional environments and progradational sequences along part of cross section B-B' are summarized in figure 35. Comparison with figure 31 shows the good correlation between facies, depositional environment, and position in the progradational cycles.

Figure 32B. Hosston siliciclastic tidal-flat sequence: a. Basal burrowed sandstone with abundant unoxidized organics and some shale. b. Laminated sandstone with two coarse sand layers (arrows) probably originating from storm tides flooding the lower tidal flat. c. Parallel-laminated sandstone from the upper intertidal zone. Burrowing is absent. d. Laminated sandstone with soft-sediment desiccation cracks (arrows). Slumping into a tidal channel on the upper tidal flat caused the laminations to dip to the right. Darker areas in the photograph are red.

Upper Sligo Facies

Regional Facies Patterns: Echinoid-mollusk-miliolid wackestone dominates on the northern end of dip section C-C' (fig. 36). These muddy sediments were deposited in the quiet-water, inner-shelf lagoon. Locally, skeletal grainstones, such as those in Stanolind No. 1 Schmidt, probably represent winnowing by tidal currents in channels between the adjacent large shoal complexes. The transgressive nature of these shoal complexes is clearly documented on the central part of the section, based on the landward shift of the high-energy oolite grainstone facies.

A wide belt of coated-grain packstone flanks the oolite-grainstone facies on its landward side. Occurrence of coated-grain packstone without associated oolites could be the result of storm and tidal destruction of oolite bars and mixing of oolites with nearby muddy sediments. Finer grained carbonates, including pellet grainstone and pellet packstone, occur on the lobate landward margin of the oolite-shoal complex. A thin fringe of skeletal grainstone lies just shelfward of the oolite grainstone, separating the high-energy oolite grainstone and packstone trend from the outer-shelf wackestone and lime mudstone that were deposited in a low-energy environment. The similarity of these individual shoal complexes to the ooid sand shoal of Joulter's Cay on the Great Bahama Bank (Harris, 1979) is striking and has been discussed by Bebout and Schatzinger (1978).

The thickening of the outer-shelf wackestones and lime mudstones toward the shelf edge indicates that water deepened away from the oolite-shoal complexes. Echinoids, mollusks, and miliolids dominate the fauna across the shelf to the Texaco No. 1 Canales core. A subsequent shallowing is indicated as the wackestones and lime mudstones thin toward the shelf edge. A faunal change also accompanies this shallowing as first oysters then toudasids become the dominant mollusks in the "back-reef" environment (Texaco No. 1 Canales and No. 1 Watkins). Skeletal grainstone, pellet packstone, and intraclast packstone occur locally, probably as a result of storm washover from the shelf margin.

The shelf margin itself is represented on section C-C' by the Gulf No. 1 Friedrichs. Whereas the oolite shoals obviously transgressed landward across the broad shelf, the shelf margin appears to have built vertically through upper Sligo time. Coral-caprinid grainstone is the dominant lithology. This facies lies atop the actual shelf edge and represents the high-energy margin.

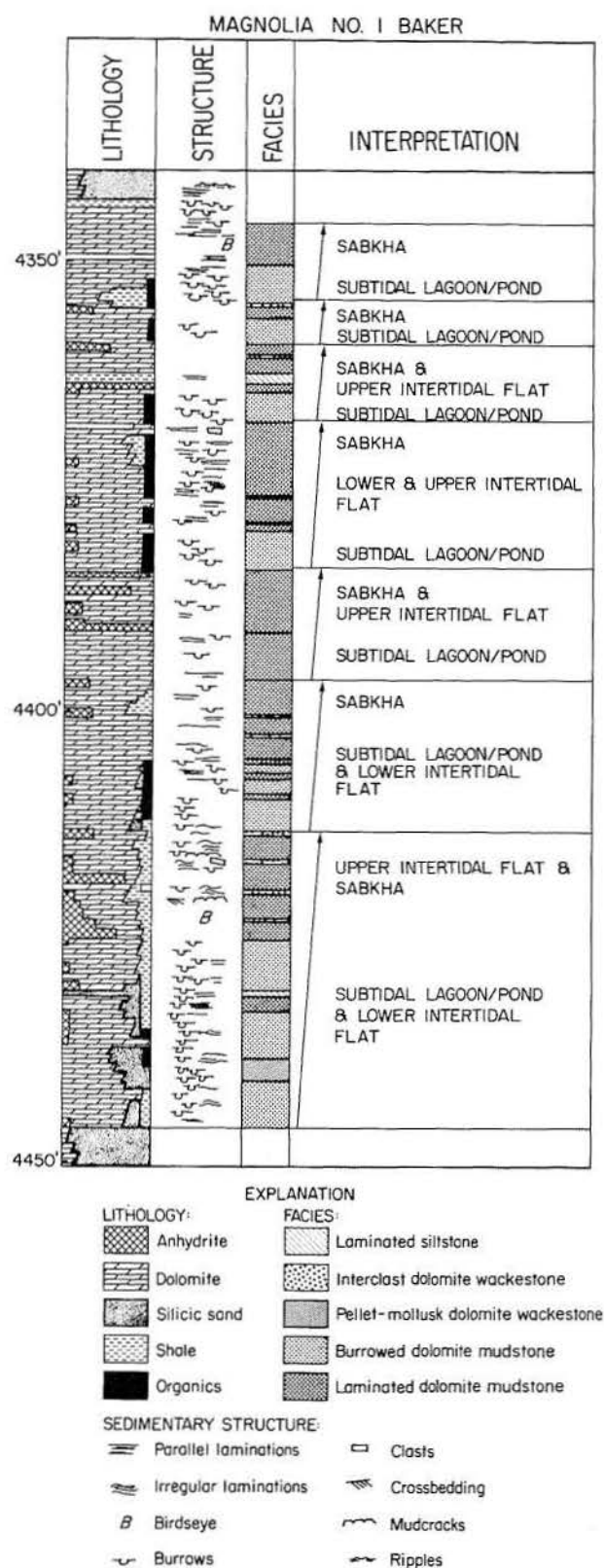
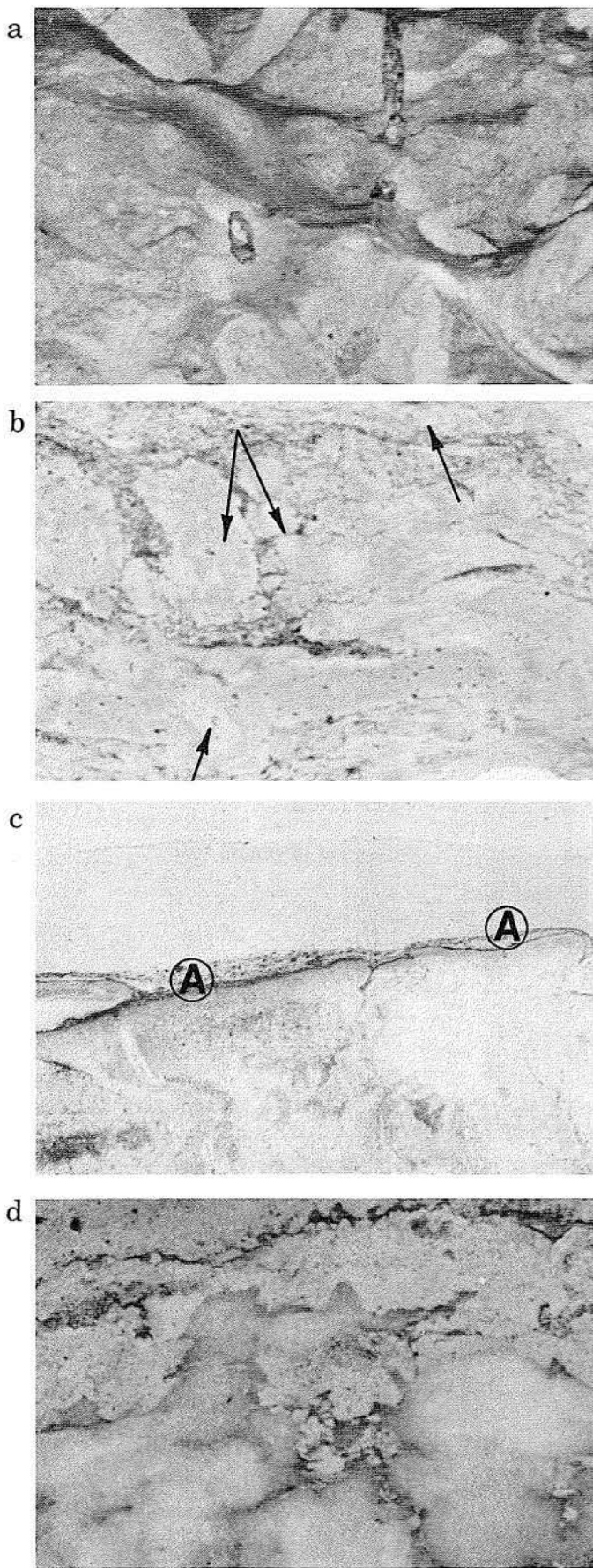


Figure 33A. Vertical succession of facies, interpreted environments, and progradational cycles of the Hosston dolomitic tidal-flat deposits, Magnolia No. 1 Baker, South Texas. See figure 31 for relationship of this section to the Sligo and Hosston depositional wedge.



Immediately seaward of these grainstones coral-caprinid packstone/wackestone and caprinid packstone/wackestone were deposited in association with laterally discontinuous biological buildups. In the Friedrichs core these facies transgressed twice over the grainstones, which subsequently prograded back over the skeletal packstone/wackestone. In this manner the shelf edge accreted nearly vertically.

One anomaly on section C-C' is the presence of oolite grainstone and coated-grain packstone in the extreme updip Guadalupe Dam Site No. 7 core. The vertical facies arrangement suggests an ooid-shoal complex that Amsbury (1974) interpreted as tidal-delta deposits; the oolite grainstones represent the high-energy seaward margin of the tidal bars, and the packstone, the low-energy landward segment. It cannot be determined whether this oolite unit was deposited on ebb or flood deltas or where associated channel deposits are located.

Oolite-Shoal Complex: Dip sections D-D' and E-E' through the oolite-shoal complex show the internal anatomy of the complex in greater detail. The facies are distributed in a manner similar to that described for section C-C'. From these sections, however, it is obvious that the coated-grain packstone and oolite grainstone constitute the major components of the shoals. It is also apparent that the entire complex comprises a vertical succession of several oolite shoals. Each oolite sequence is separated from the next by skeletal wackestones that represent drowning of the shoal by transgression and the deposition of muddy outer-shelf sediments. Shoaling is reestablished with the oolite grainstones on the seaward margin and coated-grain packstone on the landward margin. The vertical accumulation of these individual sequences into the larger total complex is clearly visible in section D-D' (fig. 37), where four shoals are separated by skeletal wackestones. The largest oolite unit is 9.2 m (30 ft) thick and can be correlated laterally for 48.3 km (30 mi) (in the Tenneco No. 1 Roberts well). The associated coated-grain packstone gradually thins updip.

Figure 33B. Hosston dolomitic tidal flat: a. Subtidal burrowed dolomite mudstone. b. Minor bioturbation has disrupted but not destroyed parallel laminae (arrows) in this laminated dolomite mudstone. Coarser layers of pellets, bioclasts, and organic flecks have been somewhat homogenized throughout the mud by the burrowing. White areas in the center of the photograph are artifacts of sample preparation. c. Laminated dolomite mudstone with small anhydrite nodules, indicative of upper intertidal to sabkha deposition. Exposure is evidenced by unconformity between laminae. d. Mosaic anhydrite overlain by laminated dolomite mudstone from a sabkha environment.

**Table 4. Comparison
of tidal-flat sequences,
Hosston and lower Sligo Formations.**

Hosston Siliciclastic Tidal-Flat			Hosston Dolomitic Tidal-Flat			Lower Sligo Tidal-Flat		
Subtidal	Dep. Setting	Extensive flat or sabkha	Dep. Setting	Extensive flat or sabkha	Dep. Setting	Beach ridges and tidal-channel levees flanking intertidal flats		
	Features	Mud cracks, clasts, anhydrite, irregular and parallel laminations	Features	Mud cracks, anhydrite, clasts, bird's-eye structures	Features	Parallel laminations, clasts, and burrows dominant. Also ripples, cross-bedding, mud cracks, and anhydrite		
	Facies	Laminated sandstone and siltstone	Facies	Laminated dolomite mudstone	Facies	Pellet dolomite grainstone, skeletal dolomite grainstone, laminated dolomite mudstone, and intra-clast dolomite wackestone		
Intertidal	Dep. Setting	Intertidal flat	Dep. Setting	Intertidal flat	Dep. Setting	Intertidal flat		
	Features	Ripples, crossbedding, less burrowing, thick-bedded	Features	Minor burrows	Features	Parallel laminations and burrows		
	Facies	Laminated sandstone and siltstone	Facies	Laminated dolomite mudstone	Facies	Laminated dolomite mudstone and pellet-mollusk dolomite wackestone		
Supratidal	Dep. Setting	Pond	Dep. Setting	Pond	Dep. Setting	Pond, adjacent marine and rare tidal-channel deltas (grainstones)		
	Features	Highly bioturbated	Features	Highly bioturbated, organics	Features	Highly bioturbated, organics, and some crossbedding (grainstones)		
	Facies	Burrowed sandstone	Facies	Burrowed dolomite mudstone	Facies	Pellet-mollusk dolomite wackestone, mollusk-miliolid wackestone, pellet and skeletal dolomite grainstones		

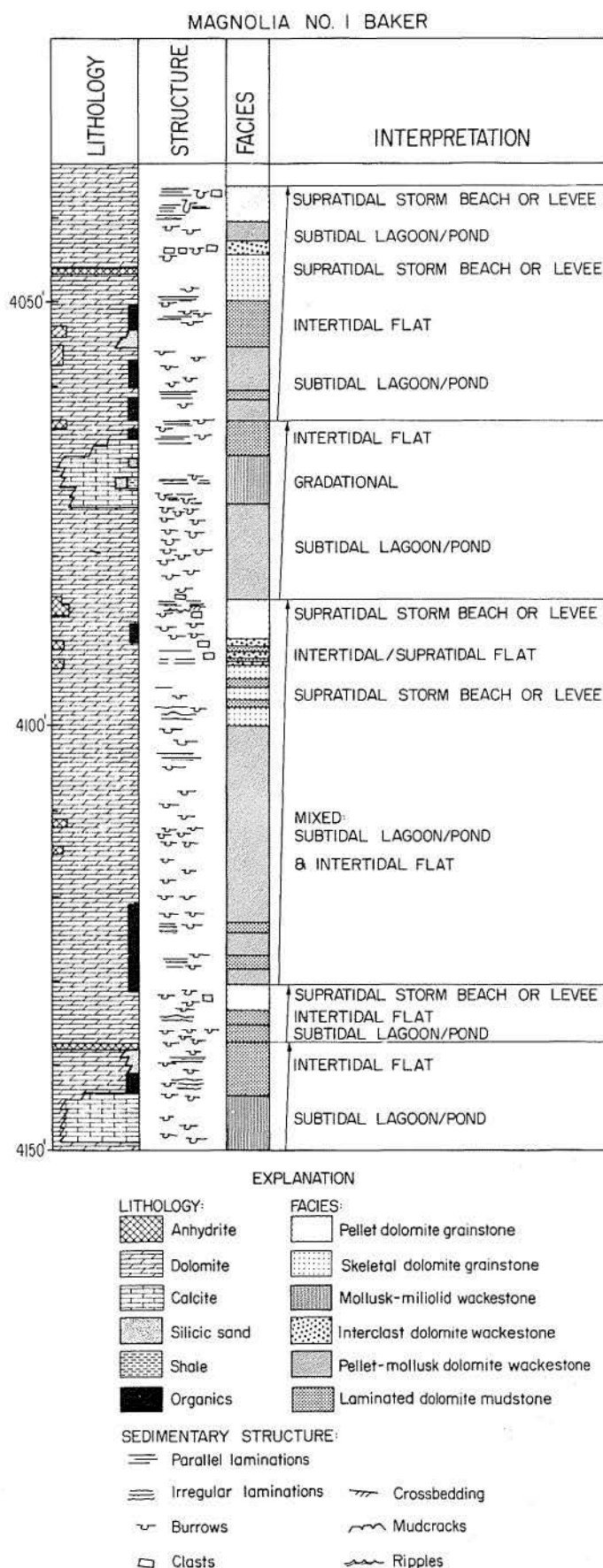


Figure 34A. Vertical succession of facies, interpreted environments, and progradational cycles of the lower Sligo tidal-flat deposits, Magnolia No. 1 Baker, South Texas. See figure 31 for relationship of this section to the Sligo and Hosston depositional wedge.

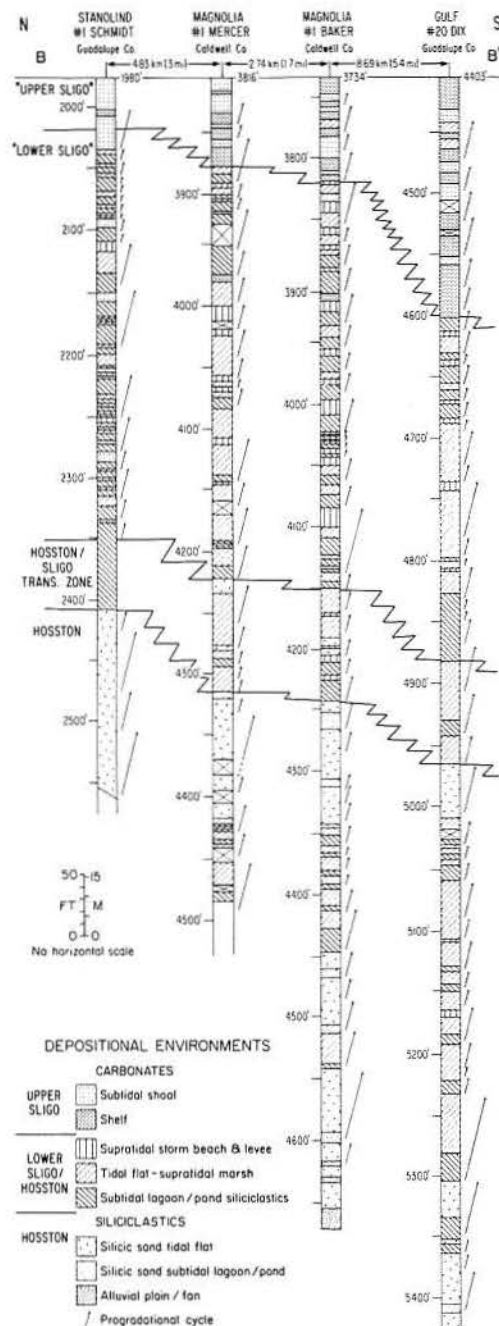
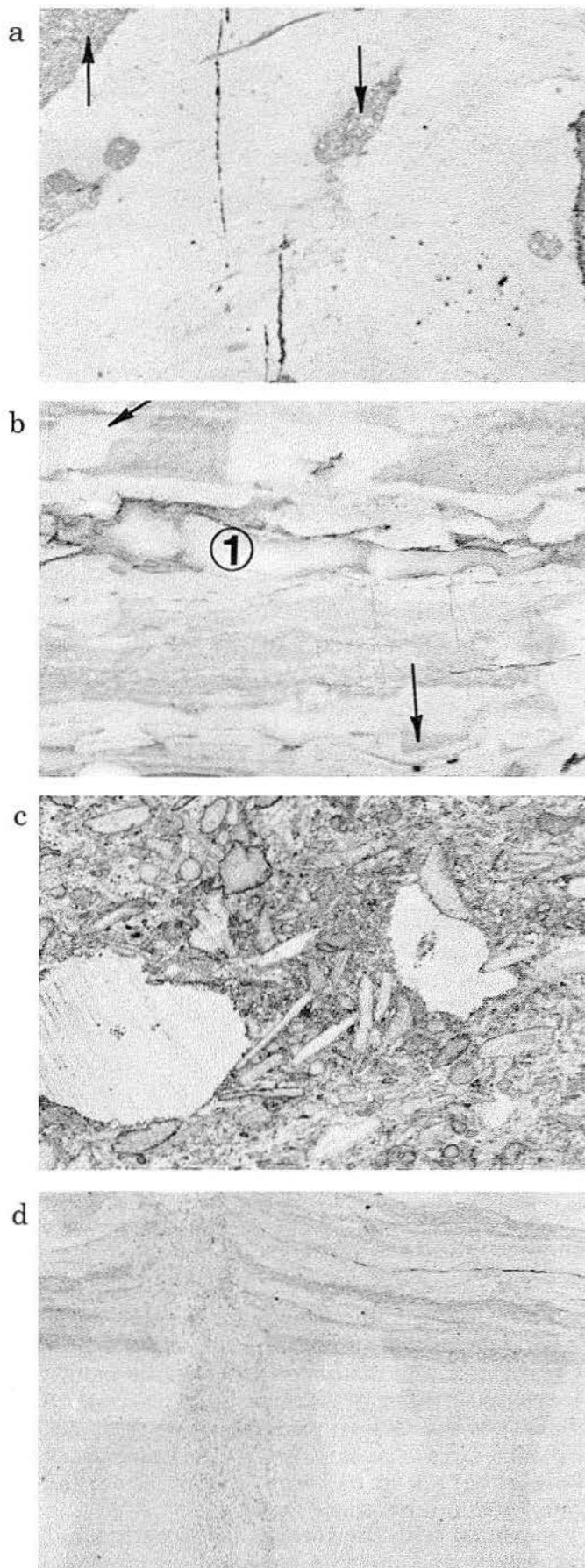


Figure 35. Dip section B-B', Sligo and Hosston Formations, over the San Marcos Arch with interpreted depositional environments and corresponding progradational cycles.

Figure 34B. (left) Lower Sligo dolomitic tidal-flat sequence: a. Large burrows (arrows) filled with pellets and bioclasts in a dolomite mudstone from the lower intertidal zone. Vertical fractures (?) occur solely in the mud. b. An upper intertidal to supratidal, laminated dolomite mudstone. Oxidation rims (arrows) indicate exposure and anhydrite (1) indicates an arid climate. c. Large storm deposit of intraclasts on a channel levee or beach ridge. Nearly all the clasts are dolomite mudstones, derived from the laminated mudstone facies. d. Low-angle crossbedding and vertical escape structure in a finely sorted pellet grainstone. Oxidation of minor organic debris gives a faint red tint to the sample. These high-energy beach deposits cap the tidal-flat sequences.

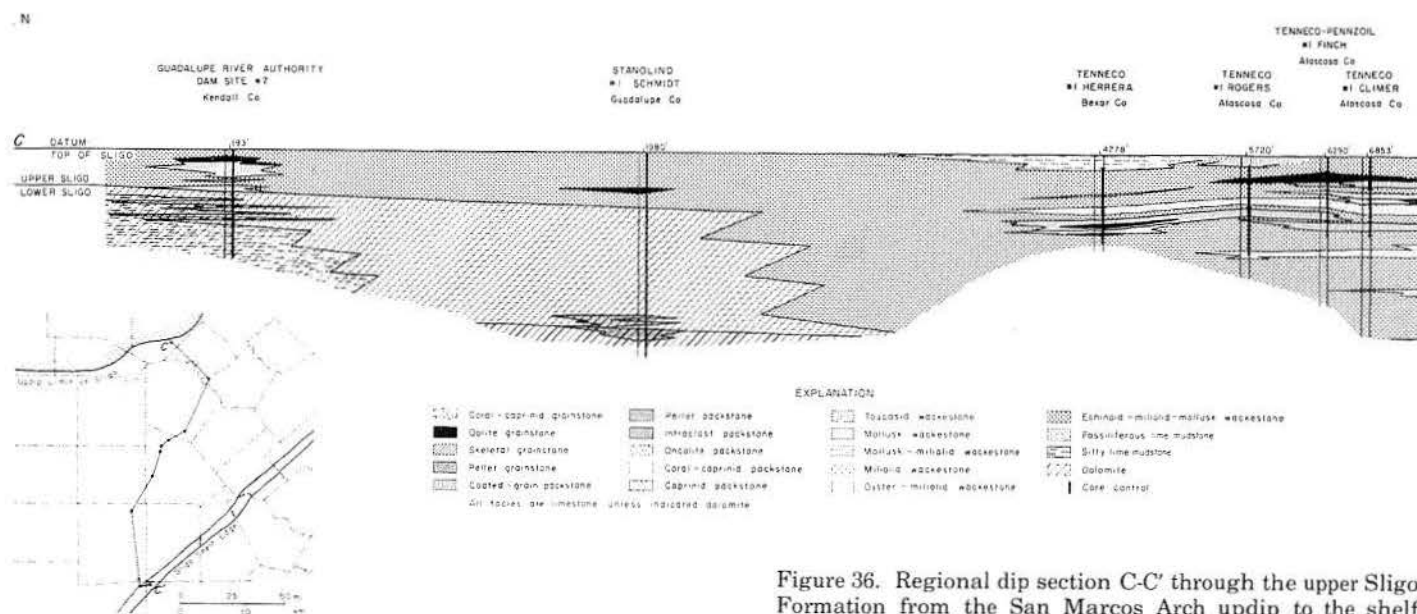


Figure 36. Regional dip section C-C' through the upper Sligo Formation from the San Marcos Arch updip to the shelf

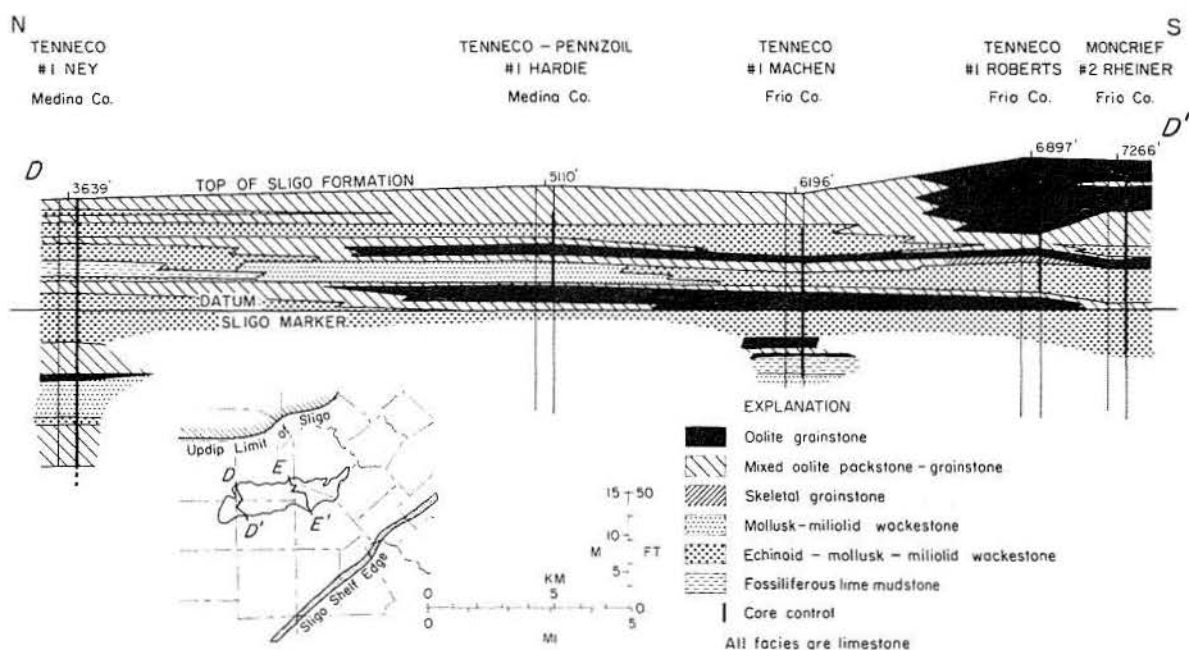
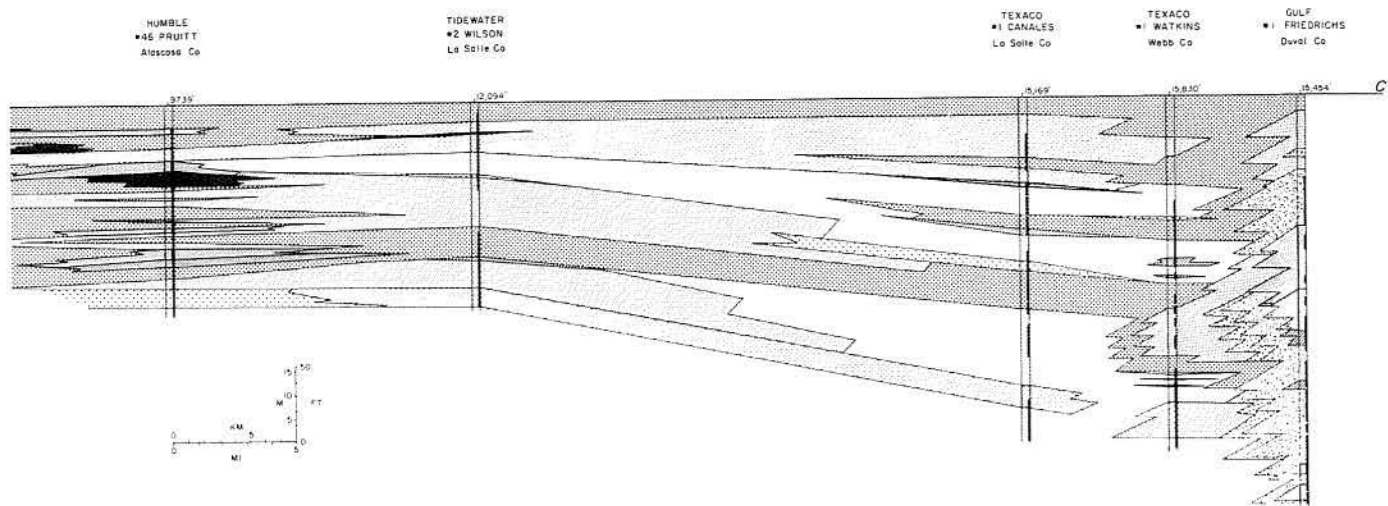


Figure 37. Facies section D-D' through the oolite-shoal complex in the upper Sligo Formation. Datum is an electrical-log marker within the upper Sligo Formation used here to show the lateral relationship between facies as they existed at the time of deposition; the use of the top of the Sligo Formation as a datum slightly distorts these relationships at this scale.

Shelf Margin: Only four wells have cores from the shelf-margin facies; these are shown on strike section F-F' (fig. 39). Two facies sequences alternate throughout each core. The coral-caprinid grainstone and lesser amounts of caprinid grainstone and coated-grain packstone represent the shelf-edge sand shoals. This sequence is very thick in the Gulf No. 1 Friedrichs and in parts of the Shell No. 1 Brown. Grainstones range from very coarse grained and poorly sorted

to fine-grained and well-sorted skeletal hash. Varying grain size and sorting reflect the degree of reworking and distance from organic banks. The coarse-grained grainstone units are near or adjacent to the skeletal packstones/wackestones (organic banks or reefs), whereas the fine-grained skeletal grainstone was never observed juxtaposed against those facies.

Associated with the coral-caprinid packstone/wackestone and caprinid packstone/wackestone



margin downdip. A nearly complete spectrum of facies, and subsequently depositional environments, is represented.

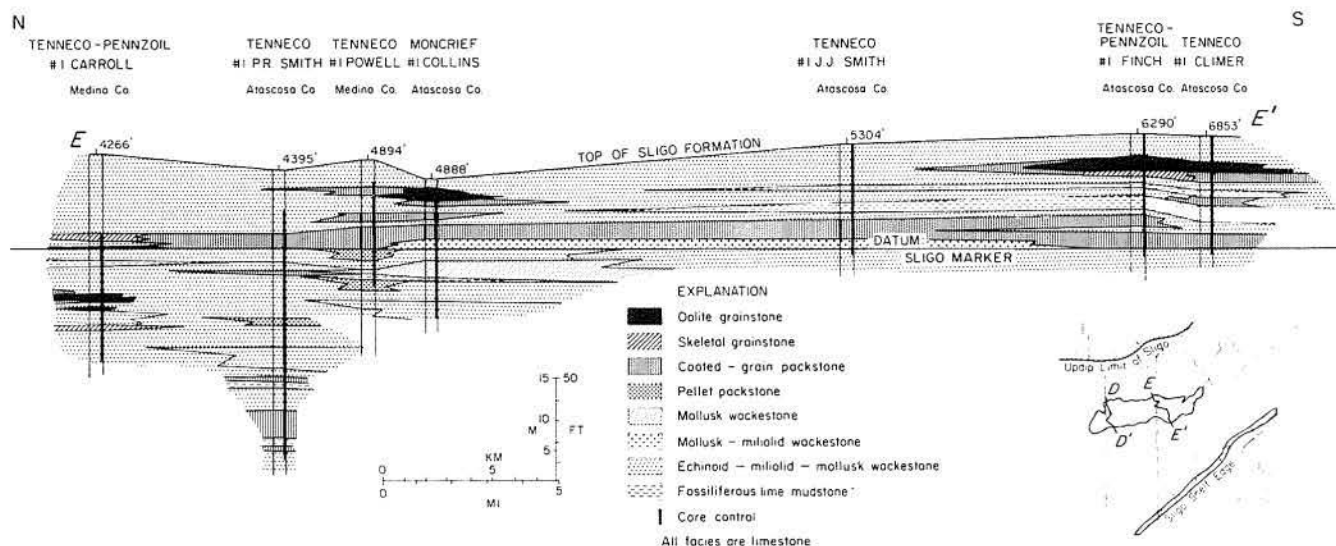


Figure 38. Facies section E-E' through the oolite-shoal complex in the upper Sligo Formation. Datum is an electrical-log marker within the upper Sligo Formation used here in order to show the lateral relationships between facies as they existed at the time of deposition; use of the top of the Sligo Formation as a datum slightly distorts these relationships at this scale.

are corallgal boundstone, fossiliferous lime mudstone, mollusk-miliolid wackestone, and echinoid-mollusk-miliolid wackestone. The wackestone facies reflect the deepening of water down the shelf slope, gulfward of the shelf edge. These units were deposited below wave base and probably grade downslope into fossiliferous pelagic lime mudstones and black, shaly, lime mudstones.

The coral-caprinid and caprinid packstone/wackestone represent debris from small,

discontinuous organic banks. Generally the skeletal material shows some breakage and minor transport and rarely shows any organic binding. Boundstones are common but difficult to recognize in core.

Coralgal boundstones occur in the Shell No. 1 Brown core and are associated with both the skeletal packstones and coarse grainstones. Corals, stromatoporoids, and caprinids are the major framebuilders but encrusting algae are

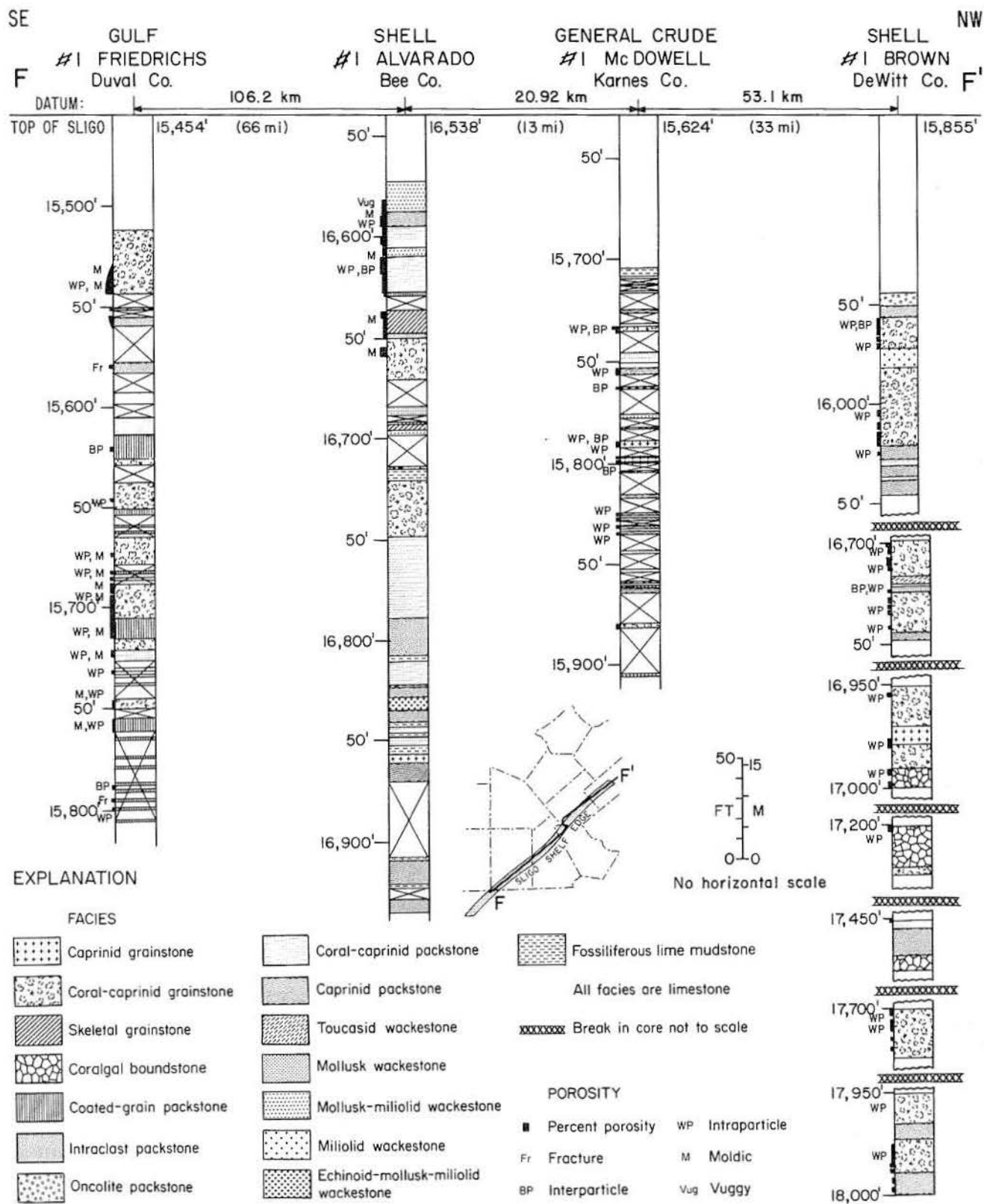


Figure 39. Strike section F-F' along the Sligo shelf margin showing the vertical distribution of facies within individual cores. The lack of systematic progradational or transgressive patterns suggests vertical accretion along the Sligo shelf margin. Large distances between wells prevent detailed facies correlations.

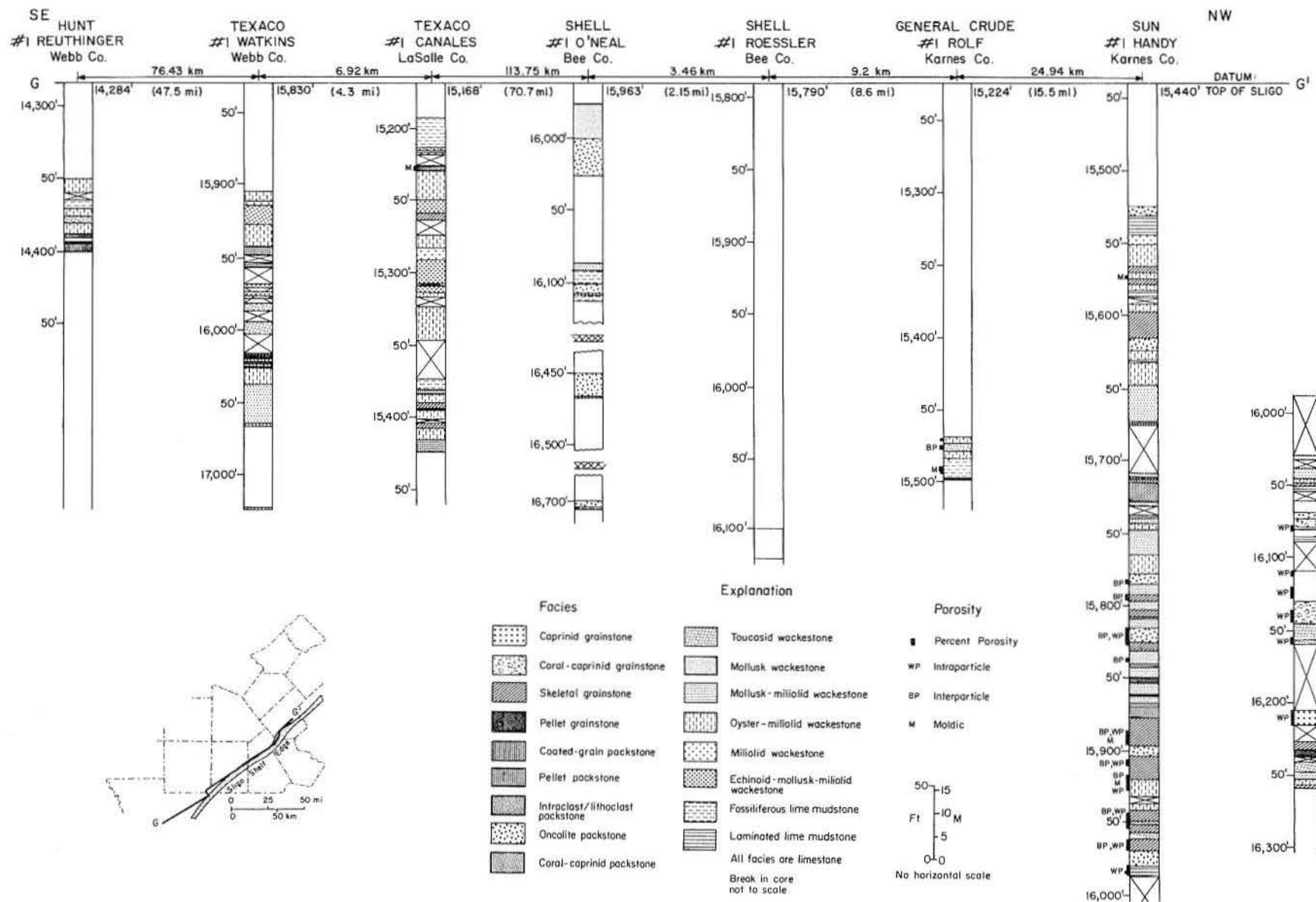


Figure 40. Strike section G-G' immediately behind the Sligo shelf margin. The lack of shelf-edge facies is striking. The large distance between wells prohibits facies correlations.

responsible for binding the predominantly wackestone matrix.

There does not appear to be any systematic pattern of transgression or progradation across the shelf margin in this section. In the Shell No. 1 Brown core the grainstones overlie the skeletal packstone/wackestone facies (progradation) and are, in turn, overlain by the packstones/wackestones (transgression). This is the same cyclical pattern that characterizes the entire Sligo Formation at the shelf edge, but each successive transgressive unit does not extend farther landward. Rather, a balance appears to have existed between organic productivity and relative rise of sea level, keeping the shelf margin geographically constant and accretion vertical.

Less cyclicity occurs in the other three cores, perhaps because of well location. The Shell No. 1 Alvarado core contains more packstone/wackestone as a result of being located farther seaward of the Sligo shelf edge than the Gulf No. 1 Friedrichs and Shell No. 1 Brown wells, which contain more grainstones.

The Sligo Formation immediately behind the shelf edge is represented by seven wells with cores shown on strike section G-G' (fig. 40). Although many of these wells are within a few miles of the shelf edge, a nearly total lack of the shelf-edge facies is striking, and mollusk-miliolid wackestone and oyster-miliolid wackestone dominate. The latter facies normally contains oysters in growth position and associated laminated mudstone. These oyster banks apparently grew near sea level and adjacent to laterally discontinuous tidal flats. The presence of toucasid wackestone and oncolite packstone indicates shallow, relatively quiet water near the shelf margin. The few skeletal grainstones that are present, particularly in the upper part of Sun No. 1 Handy, are composed of mollusks, miliolids, oysters, toucasids, green algae, and echinoids — an outer-shelf platform fauna considerably different from the shelf-margin fauna. These

DIAGENESIS

More than 190 thin sections were prepared from throughout the entire Sligo and Hosston Formations. Thin sections were not prepared for every facies described in this report, and the grainstones and packstones of the upper Sligo oolite-shoal complex and shelf-edge facies are disproportionately represented. Similar diagenetic sequences occurring in different facies are described together. Significant variations in

grainstones represent the landward edge of the shelf-margin sand shoals and indicate periodic high-energy conditions; the grainstone facies are commonly overlain by laminated lime mudstone representing a tidal-flat environment.

No systematic vertical sequence of facies is apparent from these cores other than a pattern of subtidal shelf wackestones alternating with oyster banks, sand shoals, and/or tidal flats. A laterally complex system of highly variable, very shallow-water sediments apparently produced no repeatable vertical patterns. Shallow-water sediments consisting of burrowed skeletal wackestones and oncolite packstones in association with scattered islands and local oyster and toucasid banks characterize the upper Sligo "back-reef" environments.

In the Sun No. 1 Handy core there is evidence of an overall progradation of these "back-reef" facies over the shelf-margin facies. Below 4,893 m (16,050 ft) in the Handy, caprinid and coral-caprinid grainstone and packstone/wackestone are interbedded with the toucasid wackestone and oncolite packstone. This occurrence indicates that the toucasid and oncolite facies are immediately adjacent to the shelf-margin facies. The vertical arrangement of these facies also suggests that after minor transgressive-progradation cycles between the shelf-margin facies and toucasid and oncolite facies, a large-scale progradation seaward of the shelf margin placed the oyster banks, sand shoals, and tidal flats in the geographic location of the Handy well. These facies then vertically accreted during the remaining Sligo deposition.

The apparent overall progradation in the Handy core is contrary to that observed in all other cores, especially Shell No. 1 Brown (section F-F'). Thus, it is probable that parts of the Sligo shelf edge reacted differently to transgressive pulses throughout Sligo time; irregularities along the shelf edge can therefore be expected.

the paragenetic sequences of the Hosston tidal flat, Sligo shelf-lagoon and oolite-shoal complex, and Sligo shelf margin justify their separate analysis. Cementation histories of the various upper Sligo depositional environments are compared.

Sligo Paragenetic Sequences

Sligo Shelf-Lagoon and Oolite-Shoal Complex

The upper Sligo oolite-shoal complex and adjacent shelf deposits are quite similar

diagenetically to the shoal complexes in the overlying Pearsall Formation (Loucks, 1977) and lower Glen Rose Formation (Bay, 1980). Submarine diagenesis, the first stage, was not extensive. However, the second stage, early meteoric-phreatic diagenesis, was extensive. The third stage, a late meteoric-phreatic event, possibly associated with a regional ground-water system, was followed by the final stage, deep subsurface diagenesis.

Submarine Stage: Submarine diagenesis consists dominantly of micrite rim formation. Well-preserved microborings (fig. 41a) suggest the importance of boring algae and fungi in grain micritization, as has been suggested by Bathurst (1966, 1971), Golubic and others (1975), and Kobluk and Risk (1977).

After deposition in the marine environment, grain breakage also occurred, and adjacent broken pieces were cemented by later meteoric-phreatic cements (fig. 41b). Intraclasts derived from nearby hardground areas show breakage between as well as across grains. Many intraclasts are oolitic in the upper Sligo, have a mud matrix, and contain abundant peloids. Pyrite is also common in intraclasts.

Internal sediment is irregularly distributed in the grainstones but not separated from grain edges by cement. Randomly oriented geopetal structures and grainstone texture indicate the continual reworking of skeletal fragments by wave and tidal action, which allowed no submarine cementation (Shinn, 1969; Purser, 1969).

The presence of the oolite intraclasts and bored surfaces (fig. 41c) may reflect submarine hardground cementation (Bathurst, 1971, p. 395); however, no petrographic fabrics characteristic of seafloor cements were observed. Both the intraclasts and hardgrounds have mud matrices; thus, the apparent lithification may also reflect evaporation and consolidation with a short period of exposure. Inferred shallow water depths across much of the outer shelf make this a possibility.

Early Meteoric-Phreatic Stage: Prolonged exposure of supratidal sediments or the emergence of islands along the Sligo oolite shoal could have led to the development of a localized meteoric-water system. Although caliche, meniscus cement (Dunham, 1971), and dripstone cement (Müller, 1971), characteristic of the vadose zone, were not observed in the Sligo, there is abundant evidence of meteoric-phreatic diagenesis. The lack of vadose-zone indicators is not surprising. According to the Ghyben-Herzberg relation, a fresh-water table only 0.3 m (1 ft) above sea level is accompanied by a fresh-water lens extending 12.2 m (40 ft) into the underlying salt-water body

(Freeze and Cherry, 1979). Thus, in a situation with low-lying islands, such as an island 1.8 m (6 ft) above sea level, a very minor vadose zone, 1.5 m (5 ft), could overlie a considerably thicker phreatic zone, 12.5 m (41 ft). Sampling the poorly cemented vadose-zone rocks would then be much less probable than sampling or preserving a large part of the well-cemented phreatic-zone rocks.

In the meteoric-phreatic zone, stabilization of carbonate mineralogy to calcite is extremely rapid (Land, 1970). Aragonite shells were dissolved with subsequent breakage of micrite rims (fig. 42a, b) and collapse. Most of the ooids, however, were not leached; they retain their fine radial and concentric structure and have, at most, recrystallized nuclei. This suggests that the ooid's original mineralogy was not aragonite, but rather Mg-calcite (Sandberg, 1975). Inversion of aragonite to calcite with the retention of shell microstructure is not common in the Sligo. However, magnesium calcite skeletal fragments, predominantly echinoid fragments, did undergo exsolution to calcite (Land, 1967).

Early, shallow meteoric-phreatic cements are of two kinds: large, interlocking syntaxial overgrowths around echinoderm fragments, and isopachous rim cements. Both cement types are typical of Holocene and Pleistocene rocks that have undergone meteoric-phreatic diagenesis (Land, 1970; Steinen, 1974; Harris, 1979; Longman, 1980). The overgrowths grew around and enveloped intraclasts and interfered with the rim cement (fig. 41d), an indication that they are contemporaneous cements. Loucks (1977) reported the same relationship in grainstones from the overlying Pearsall Formation.

The isopachous cement is composed of subequant to bladed, fine- to medium-crystalline calcite. It coats the outside of all types of allochems and also lines the inside of leached skeletal grains (fig. 42a, b). This rim cement is well-developed in the oolite grainstone and skeletal grainstone facies and also occurs in pelletal facies.

Evidence for compaction immediately subsequent to the precipitation of the isopachous calcite is abundant and diverse. In the oolite grainstone this rim cement is present on the margins of grains embaying one another (fig. 42c). The ooids involved show plastic deformation and, consequently, molding of shapes to one another, which suggests mechanical compaction of grains rather than chemical pressure solution. Outer layers of some ooids were spalled off and deformed between other allochems (fig. 42d).

An unusual "stringy" structure (fig. 43a, b) is also attributed to collapse of well-developed iso-

pachous rim cement prior to the precipitation of later cements. This feature is present in skeletal grainstones, pellet grainstones, and pellet packstone facies. This texture may alternatively represent well-calcified chasmolithic algal filaments (Schroeder, 1972; Kobluk and Risk, 1977).

Compaction affected the pelletal facies the most. Squeezing of soft pellets and intraclasts between harder pellets, cemented intraclasts, and skeletal fragments (fig. 43c, d) resulted in very irregularly shaped, often wispy, peloids. Plastically deformed intraclasts and peloids are separated from one another by aligned fragments of isopachous rims. Less deformed intraclasts or peloids were apparently hardened by earlier selective cementation (Shinn and others, 1980).

Early dolomitization occurred primarily in ooid and pelletal facies in association with the establishment of meteoric-phreatic conditions (Folk and Land, 1975). The dolomite ranges from "dirty" microcrystalline dolomite in pellets and micrite to fine- to coarse-crystalline, clear, euhedral to subhedral dolomite. This variation in texture probably reflects the difference between penecontemporaneous dolomitization on a tidal-flat and later dolomitization in a fresh-water/salt-water mixing zone (Land, 1973a, b). None of the dolomite is so clear as to be considered fresh-water (phreatic) limpid dolomite (Folk and Siedlecka, 1972).

The progressive dolomitization of the microcrystalline pellets and interstitial mud has preserved pellets with variable amounts of calcite, ranging from those with calcite cores only (fig. 44a), to those with sparse calcite in dominantly dolomite pellets (fig. 44b), and to those that are completely dolomitized (fig. 44c, d). Likewise, in some samples of the oolite grainstone, only the ooid exteriors (possibly including the isopachous cement layer) were affected, whereas at other locations the isopachous rim, ooid cortex, and nucleus were dolomitized.

The exact timing of dolomitization varies. In some oolite grainstones (fig. 45a), it must have occurred before compaction or the oomolds would have been flattened. However, the dolomite postdates the isopachous calcite because that rim cement is itself dolomitized in both pelletal and oolitic (fig. 45b) facies. However, many of the dolomitized pellet grainstones show compaction effects, suggesting that dolomitization postdates compaction. In many of these same samples, dolomite pore filling is the final diagenetic product, and the isopachous rim is lacking (or at best poorly developed; fig. 45c). This relationship suggests that dolomitization predates the formation of the calcite rim.

This apparent contradiction in timing of dolomitization can be resolved if consideration is given to original depositional environments. The most extensive, and apparently earliest, dolomite is associated with tidal-flat deposits. Because the potential for repeated flushing with salt water and fresh water would have been high in these sediments, early mixing-zone dolomites could easily have formed. However, in the oolite-shoal complex, dolomitization is much less extensive, even absent, in more than half of the samples analyzed. Repeated establishment of a mixing zone was not as likely, nor would it necessarily have been as areally extensive. Because the dolomite in these samples postdates the isopachous calcite, it is probable that the dolomitization represents the migration of the mixing zone into the former phreatic-meteoric lens. This migration implies the destruction of the fresh-water lens and/or initiation of a transgressive event. The latter would result in renewed sedimentation, increased overburden, and the subsequent compaction observed.

Late Meteoric-Phreatic Stage: There is a sharp break between the isopachous rim cement and the coarse-crystalline anhedral calcite cement that occurs within fossil molds (fig. 46a), beneath skeletal shelters (fig. 46b), between grains, and within collapsed structures. The lack of transitional grain sizes between cements indicates that the coarse-crystalline calcite formed at a later time. This coarse-crystalline anhedral calcite tends to show straight crystal borders.

Loucks (1976, 1977) noted that in the Pearsall Formation early equant calcite stages of cementation may be distinguished from late equant calcite by finer crystal size and more irregular grain contacts. In addition, early equant cements were more gradational in size with the earlier isopachous calcite. Loucks (1977) thus interpreted coarse-crystalline calcite in the Pearsall Formation to have originated either in a regional ground-water system (if Fe-poor) or in the deeper subsurface (if Fe-rich). A similar interpretation is possible for the coarse-crystalline calcite in the Sligo Formation. However, this cement apparently predates the features of the subsequent diagenetic phase, deep subsurface, which suggests that it originated as a late (regional?) meteoric-phreatic event. Such a conclusion is also supported by Longman and Mench's (1978) observations in the Edwards Formation along the Balcones Fault Zone: coarse calcite spar occurs within the regional meteoric-phreatic zone on the upthrown block and is absent in the bad-water zone on the downthrown block.

Deep Subsurface Stage: The final stage of cementation included deposition of coarse-crystalline calcite, baroque dolomite, and anhydrite. Replacement by authigenic quartz is known as well. The anhydrite and baroque dolomite are most common in the lower Sligo skeletal grainstones. Each of these cements appears to postdate the meteoric-phreatic cements and each has a generally uneven distribution. Anhydrite and baroque dolomite are thus considered collectively to represent deeper subsurface cementation. Loucks (1977) observed similar late-stage events in the Pearsall Formation and defined deep subsurface diagenesis generally to include all events occurring with burial below 610 m (2,000 ft). Loucks noted that such features have not been observed in rocks of the Trinity Group unless they have been buried below 610 m (2,000 ft) at some time in their history.

Calcite, commonly euhedral fine- to coarse-crystalline, is associated with but predates anhydrite. This euhedral calcite (fig. 45d) partly filled the voids remaining after phreatic-meteoric-zone, coarse-crystalline calcite precipitation. Poikilotopic anhydrite then eliminated the remaining porosity.

Baroque or saddle-shaped, curved dolomite (Folk and Assereto, 1974) most commonly occurs as large intergranular crystals that fill leached intraparticle and primary interparticle pores (fig. 46c, d). This cement obviously formed after the meteoric-phreatic cements and leaching of allochems. In some cases baroque dolomite and anhydrite cement both occur within the same fossil mold (fig. 47a). The anhydrite cement, commonly poikilotopic, is coarse-crystalline and is widely scattered throughout the grainstone facies, filling pores incompletely filled by earlier cements. Although neither is consistently euhedral against the other, the dolomite was observed in some samples to be clearly euhedral against the anhydrite (fig. 47a, b), which may imply that the baroque dolomite grew somewhat faster than the anhydrite.

Anhydrite nodules, mainly less than 3 cm (1 inch) in diameter, with well-developed felted texture locally replace dolomitized micrite and allochems (fig. 47c) in muddy shelf-lagoon facies. In the grainier facies this replacement texture cuts across the edges of oolites (fig. 47d) and skeletal fragments (fig. 48a). Dolomitic ghosts of previous allochems as well as finely preserved opaques (organics?) on the edge of partly replaced ooids testify to the lack of a void during replacement.

Authigenic quartz, less than 0.5 mm long, is sparse in all shelf-lagoon and oolite-shoal complex

facies. It occurs within pellets and ooids (fig. 48b), cuts across isopachous calcite, geopetal fill, coarse equant spar, and baroque dolomite, and indicates the end of diagenesis. Widely separated crystals of authigenic quartz were occasionally observed in optical continuity (fig. 48c), and probably formed in response to directed pressure on the sediments at the time of quartz growth.

Sligo Shelf-Margin Grainstones

The diagenetic history of Sligo shelf-margin grainstones seems quite similar to that of the overlying Stuart City Trend (Bebout and Loucks, 1974; Bebout and others, 1977). Rudists are the dominant skeletal contributors but corals, *Solenopora*, gastropods, stromatoporoids, and possible algal produced textures (fig. 48d) occur. Less common in the grainstones of the shelf margin are miliolids and dasycladacean algae.

Submarine Stage: Common borings (macro and micro) produced thick micrite rims on allochems (fig. 49a). Some well-preserved macroborings from the Gulf No. 1 Friedrichs (fig. 49b, c) show micrite fill of tubular borings and two generations of geopetal mud fill. The two generations of mud fill are separated by a layer of thin, fine-grained, isopachous calcite that indicates the rapid development of cement between and within allochems composing these shelf-margin grainstones. This internal sediment is especially prevalent within the body cavities of rudists. Figure 49d shows micrite and neomorphosed grains with micrite rims partly filling a rudist body cavity. A thin, fine-grained isopachous layer (possibly marine cement) separated the geopetal fill from coarse-crystalline radiaxial cement that fills the remainder of the body cavity. The initial isopachous cement occurs rarely throughout the grainstone facies, immediately postdates micritic rim formation, and may represent a neomorphosed Mg-calcite submarine cement.

Rarely observed ghosts of square-ended fibrous crystals (fig. 50a, b) in an inclusion-rich, bladed radiaxial calcite (Bathurst, 1959, 1971) indicate that a submarine aragonite cement was also present along some horizons (Assereto and Folk, 1976; Loucks and Folk, 1976). The aragonite cement is interpreted to have subsequently neomorphosed to the radiaxial calcite. Achauer (1977) and Shinn and others (1974) considered *all* the radiaxial calcite in the Sligo shelf-margin grainstones to be a neomorphosed submarine cement. We have noted various features, however, that indicate that much of the radiaxial calcite may not have had a submarine cement precursor:

- (1) The radiaxial calcite is ubiquitous throughout the thick shelf-margin grainstones, yet

thick sequences of submarine cemented rocks are uncommon in modern carbonate environments. Modern submarine cements precipitate at or near the sediment-water interface and, thus, form a cap over the underlying uncemented sediments (Shinn, 1969; Neumann and others, 1977; James and others, 1976).

- (2) Modern submarine cemented rocks commonly break into intraclasts, are abundantly bored through both grains and cements, and are associated with encrusting and attached marine organisms (Bathurst, 1971; Longman, 1980), features not observed in the Sligo shelf-margin grainstones.
- (3) Some of the radiaxial calcite occurs within originally aragonitic skeletal grains, either as an inversion product or as a pore-filling cement after leaching.
- (4) The radiaxial calcite is gradational into equant calcite rather than in sharp contact as one might expect with a submarine cement.

This radiaxial calcite is discussed further in the following section on the meteoric-phreatic diagenetic environment, the zone in which we believe it originated.

Early Meteoric-Phreatic Stage: Leaching of allochems with the influx of fresh water clearly occurred, as evidenced by disrupted micrite rims and interpenetrating broken micrite rims (fig. 50c, d). In some samples, where the radiaxial calcite is lacking, a thick layer of pore-filling, fine-grained, equant to slightly bladed calcite cement exists (fig. 50c, d). This layer is sharply overlain by coarse-crystalline spar. The fine grain size of this sparry calcite typifies early meteoric cements (Land, 1970; Steinen, 1974; Harris, 1979). The lack of characteristic vadose-zone indicators, such as meniscus or gravitational cements (Dunham, 1971; Muller, 1971), suggests that this is a meteoric-phreatic zone cement. This cement apparently precipitated only where no initial marine cement was present.

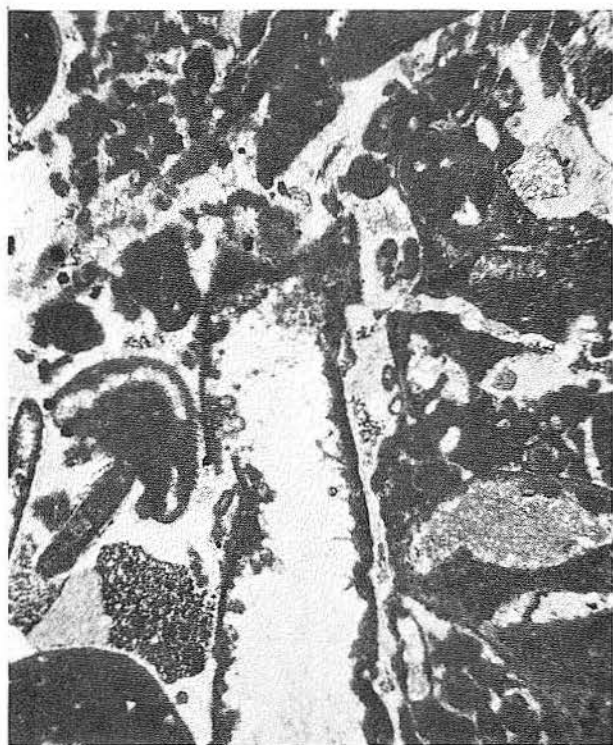
In most cases, however, the first cement is a layer of the inclusion-rich radiaxial calcite, commonly up to 4 mm thick. In some large interparticle pore spaces the radiaxial calcite grades into coarse-crystalline equant sparry calcite (fig. 51a, b) or less commonly into a dirty-yellow, medium-crystalline calcite with undulose extinction (fig. 51c). In figure 51d, the outermost segment of the thick, interparticle radiaxial calcite layer is stained dark brown, probably by abundant organic material. Similar radiaxial calcites occur widely (Bathurst, 1971, 1979) and are almost uniformly interpreted to be

neomorphosed submarine cement (Bathurst, 1959, 1971; Kendall and Tucker, 1973; Davies, 1977; Achauer, 1977; Walls and others, 1979).

The origin of the radiaxial calcite in the Sligo is apparently varied and debatable. Some is possibly a primary pore-filling cement, and some is definitely the product of inversion. Besides the previously described inversion of some aragonitic submarine cement, aragonitic skeletal fragments also inverted to the radiaxial calcite (or, less commonly, a dirty yellow, medium-crystalline calcite spar with undulose extinction, as in figure 51a). The clearest evidence of this inversion is: (1) skeletal fragments with preserved ghosts of original microarchitecture clearly inverted to radiaxial calcite (fig. 52a), (2) masses of radiaxial calcite containing caprinid wall structure and growth bands visible under crossed nicols (fig. 52b), and (3) radiaxial calcite grading inward from allochem borders to dirty neomorphic sparry calcite, as well as outward into the interparticle space (fig. 51c, d). From these examples it is apparent that radiaxial inversion began at the grain edge and proceeded inward into the grain. In figure 51c, a faintly preserved growth band in the neomorphic spar and radiaxial "cement" of the grain indicates that partial dissolution of the allochem was not responsible for the space in which the radiaxial "cement" grew.

The evidence for some of the radiaxial calcite in interparticle and shell moldic pores originating as pore-filling cement is not as conclusive. If there was no submarine cement or skeletal precursor for some of the interparticle radiaxial calcite, then it must be either (1) a primary pore-filling cement or (2) a neomorphosed nonmarine cement. It is unclear, however, why a nonmarine cement, presumably calcite, would subsequently neomorphose to a bladed radiaxial calcite. Thus we believe that some of the intraparticle bladed radiaxial calcite originated as a primary pore-filling cement.

Bebout and Loucks (1974) described similar radiaxial calcite in skeletal moldic pores in the Stuart City Trend, which they also interpreted to be a primary precipitate in the meteoric-phreatic zone. However, the bladed habit of the radiaxial calcite suggests to us that the Mg/Ca ratio of the pore fluid was intermediate between marine (high Mg/Ca ratio) and meteoric (low Mg/Ca ratio) waters (Folk, 1974), for example, brackish or mixing-zone waters. A mixing zone would have been established with the invasion of meteoric-phreatic waters into the Sligo shelf margin, and any subsequent cement, such as radiaxial calcite, would be closely related to the meteoric-phreatic zone diagenetic products.



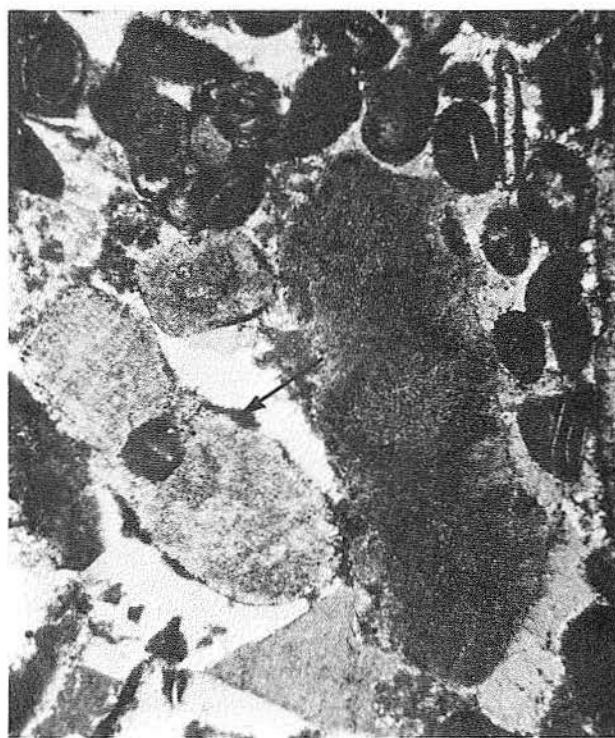
a



b



c



d

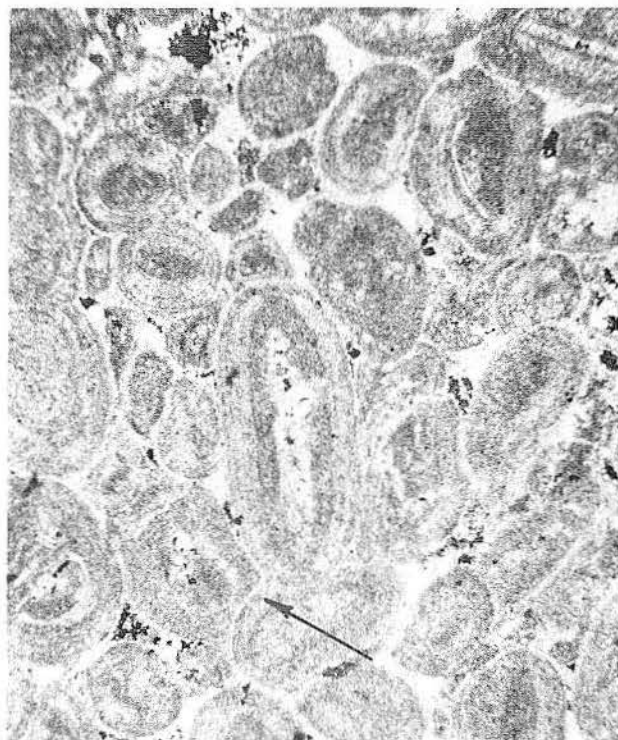
Figure 41. a. Numerous well preserved microborings coalesce to form a micrite rim on a broken mollusk shell. b. Grains broken in the marine environment were later cemented by phreatic-zone sparry calcite. c. Hardground shows truncated grains and a possible pellet-filled boring (arrows). d. Syntaxial overgrowth around an echinoderm fragment (arrow) also enveloped small intraclasts and interfered with rim cement; thus, the two cements must have been contemporaneous.



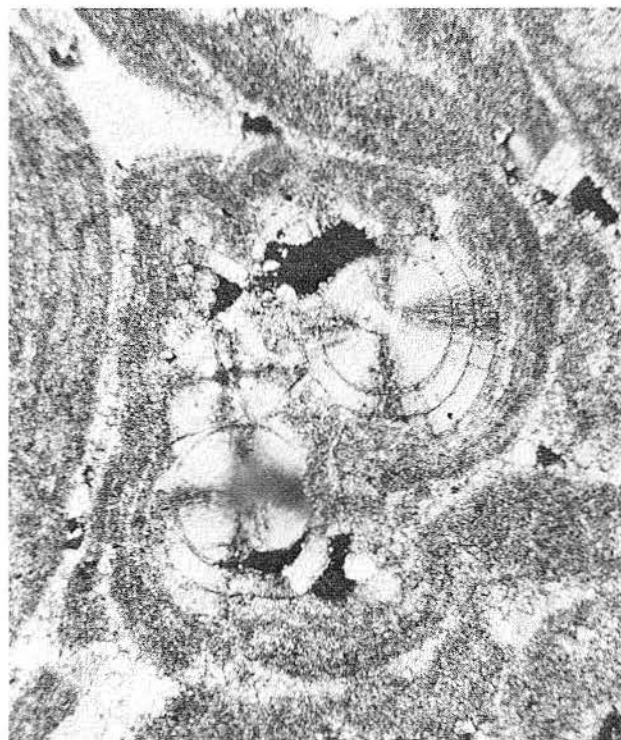
a



b

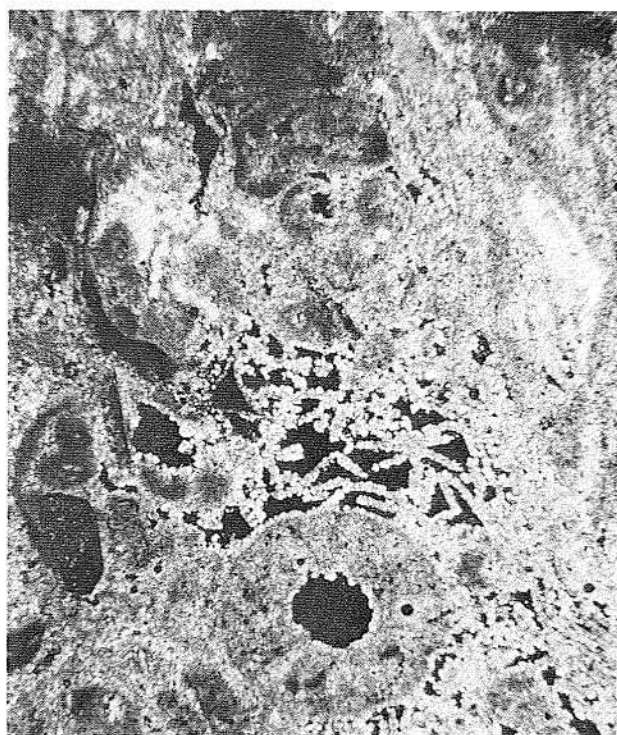


c



d

Figure 42. a and b. Only micritic rims remain from leached aragonitic shells. Here, dissolution led to collapse of the unsupported rims (arrow). Later fine-grained, bladed to subequant, isopachous rims of calcite grew into both interparticle and moldic pores. Large interlocking spar crystals filled the remaining porosity. c and d. Compaction immediately postdated rim cement formation. The rim cement is present (arrow) even where ooids interpenetrate. Plastic deformation resulted in elongate ooids and some spalled laminae.



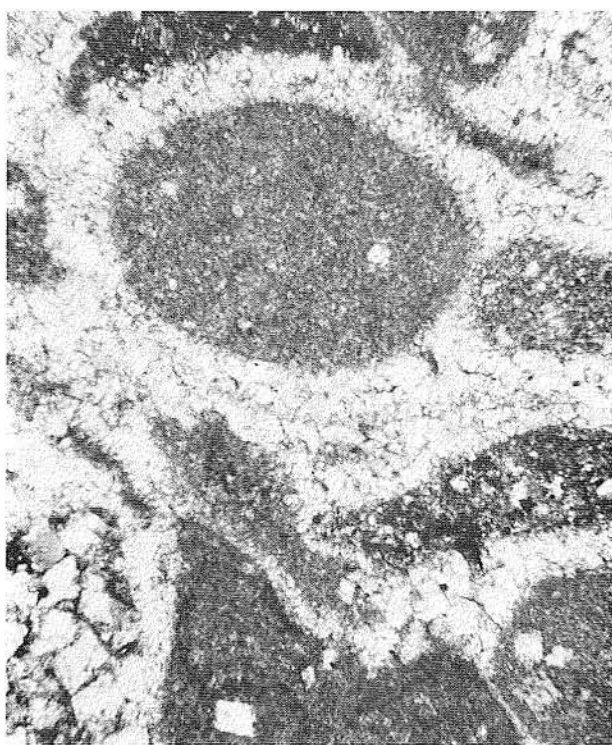
a



b

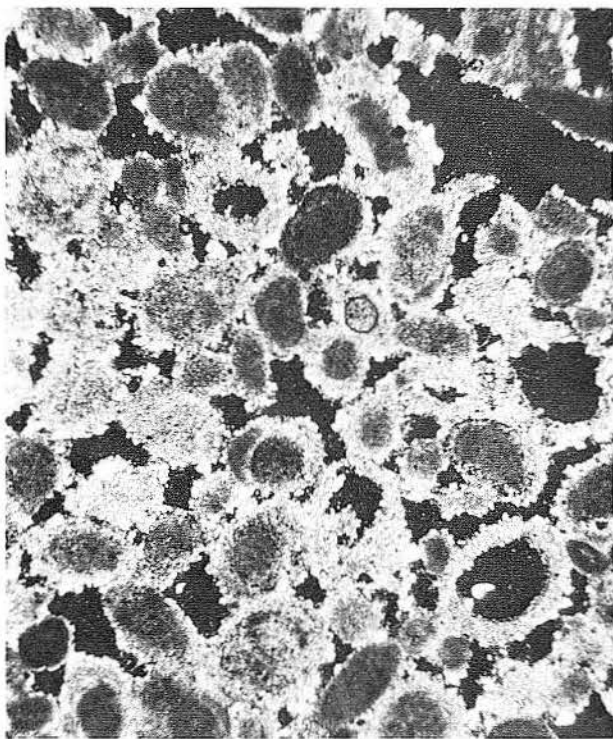


c



d

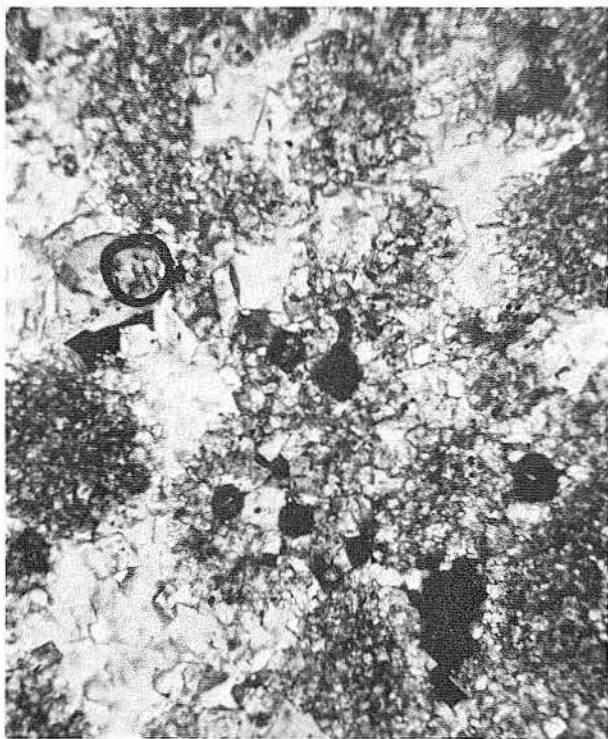
Figure 43. a and b. Superficially algal-like layers of cement are probably the result of collapsed isopachous rims after allochems were leached. The distribution and shape of the former rims suggest that other cements were not yet present. c and d. Compacted pellets. Less deformed pellets, d, may have been hardened earlier.



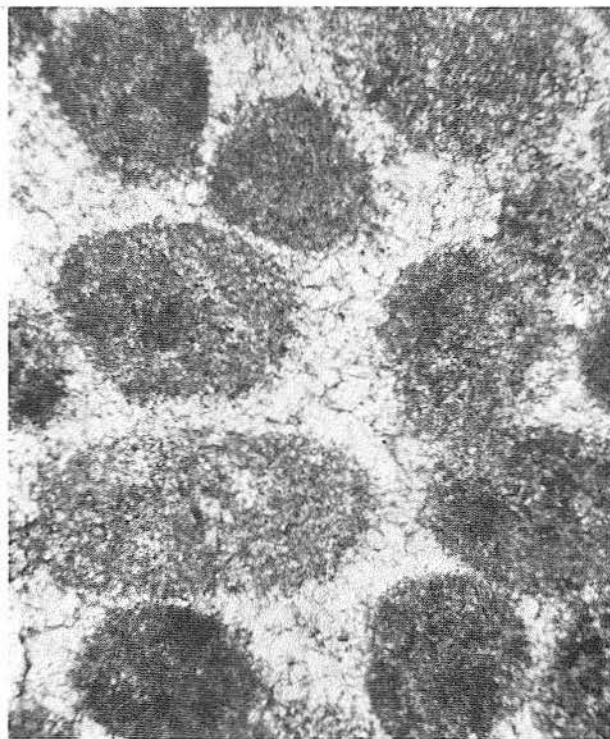
a



b

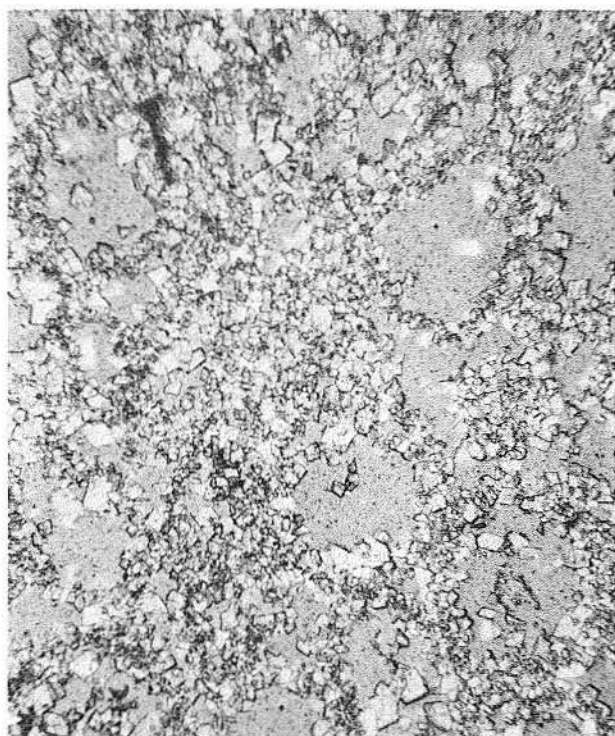


c

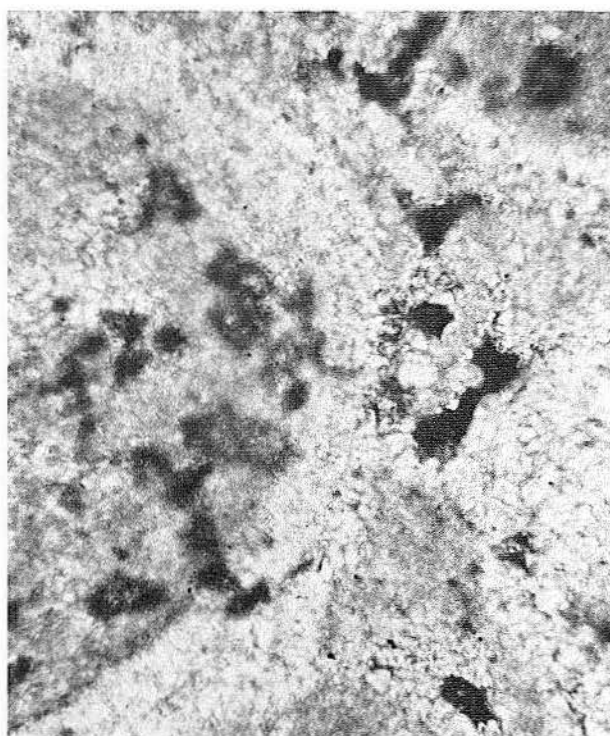


d

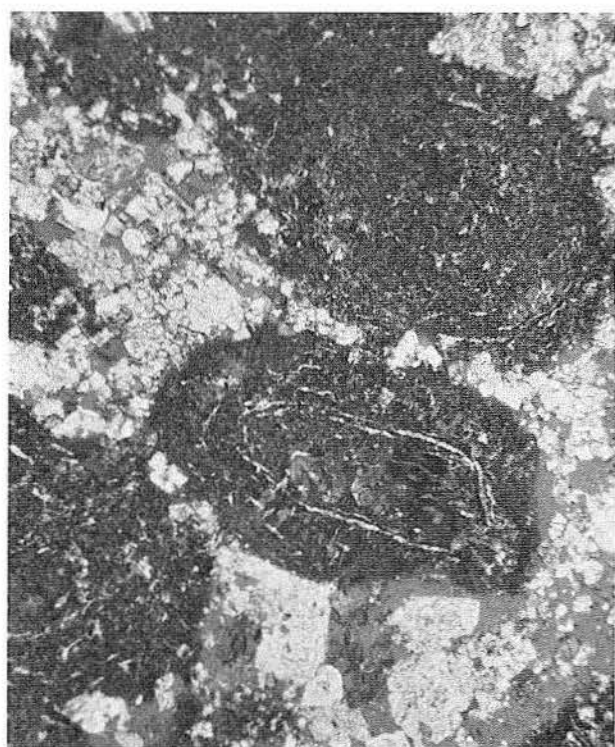
Figure 44. Dolomite content of pellet grainstone ranges from only dolomite rims with calcite cores, a, to dominantly dolomite pellets, b, to completely dolomitized pellets, c and d. Note the larger and more clearly defined euhedral shape of dolomite crystals as dolomitization progressed.



a



b



c

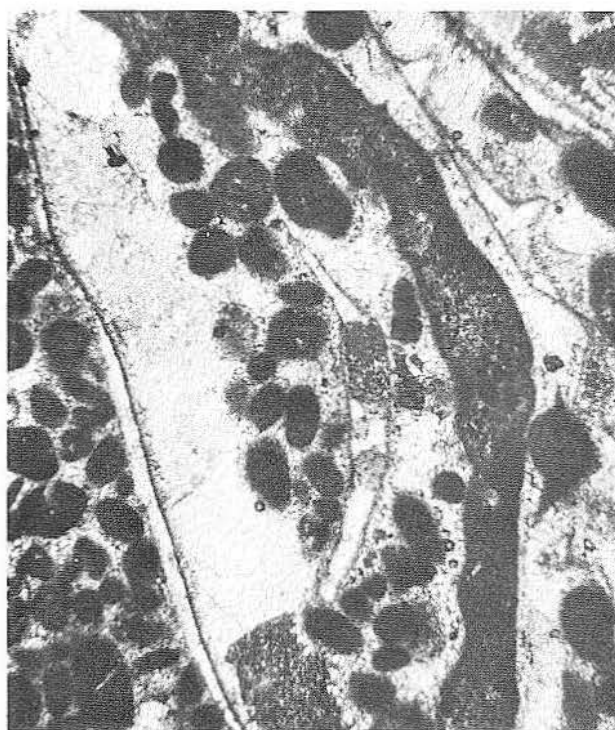


d

Figure 45. a and b. Unflattened oomolds and dolomitized rim cement indicate dolomitization occurred before leaching a but after precipitation of rim cement b. c. Pellet grainstone with no isopachous rim cement. Pellets retain calcite mineralogy, white cement is entirely dolomite. d. Poikilotopic anhydrite (light areas) precipitated in the deep subsurface after coarse equant calcite cement (darker areas, arrow). Note the inclusion of the broken and distorted isopachous rim cement in the anhydrite.



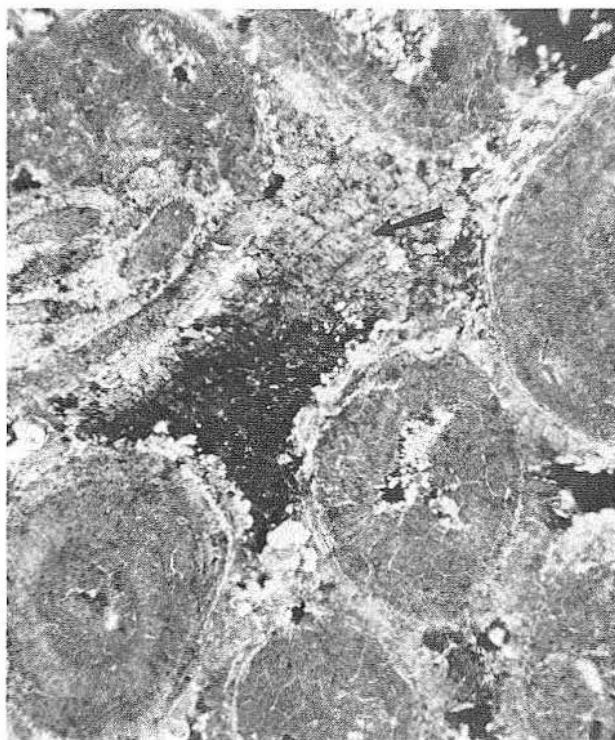
a



b



c

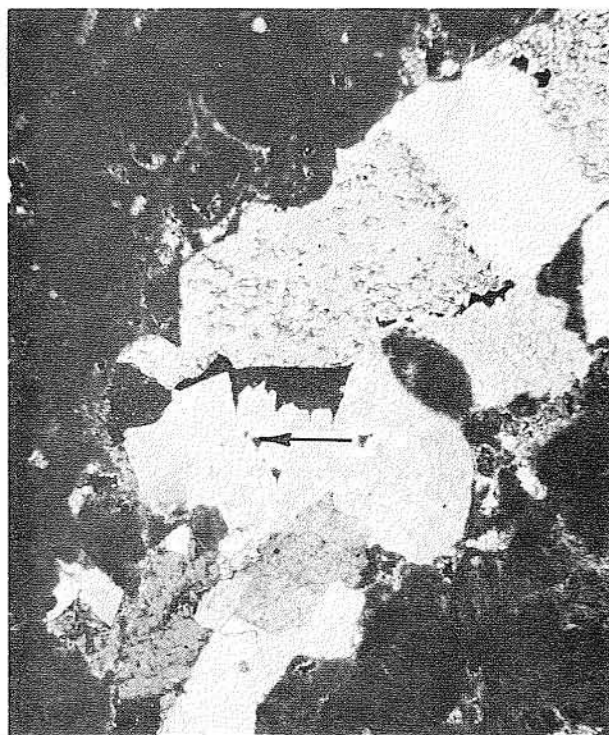


d

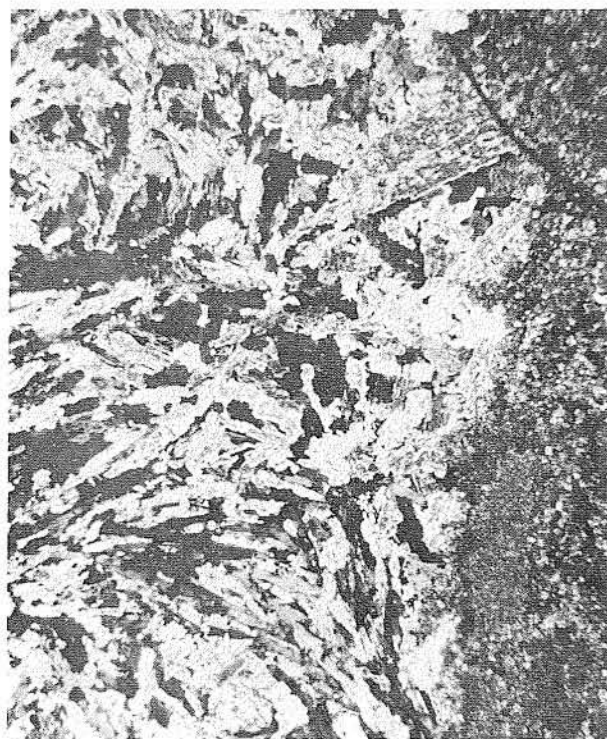
Figure 46. a and b. Sharp break between coarse-crystalline calcite and isopachous rim cement in fossil molds, a, interparticle pores, a, and geopetal structures, b. c and d. Interparticle pore spaces filled with a late-stage baroque dolomite (arrows).



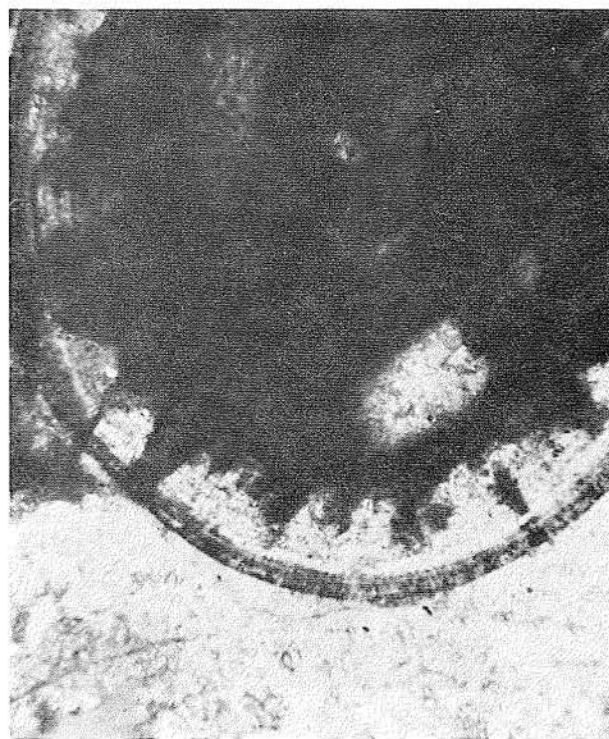
a



b



c

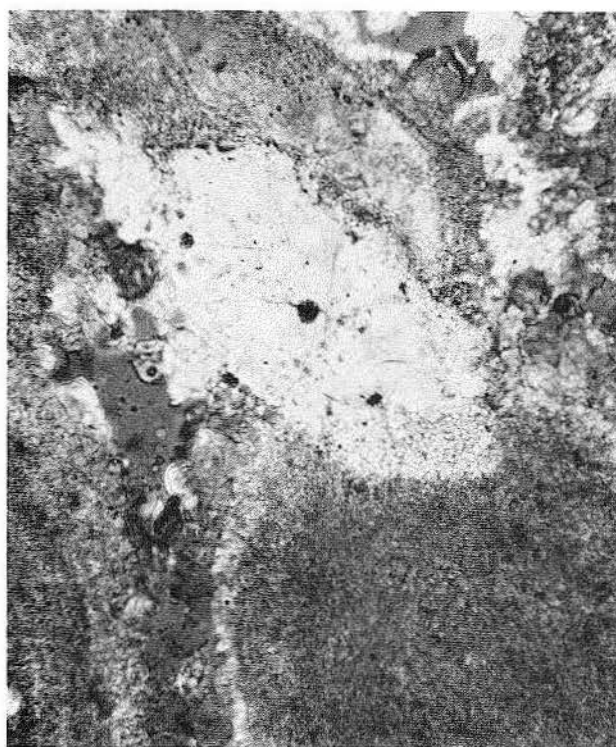


d

Figure 47. a and b. Baroque dolomite also occurs in intraparticle pores, a, and in fracture fill, b. It is occasionally in contact with and euhedral against anhydrite in such pores (arrows). c. Felted texture of a small anhydrite nodule. The nodule has replaced dolomitized micrite. d. Replacement by anhydrite is proven where ooid microstructure is still present within anhydrite.



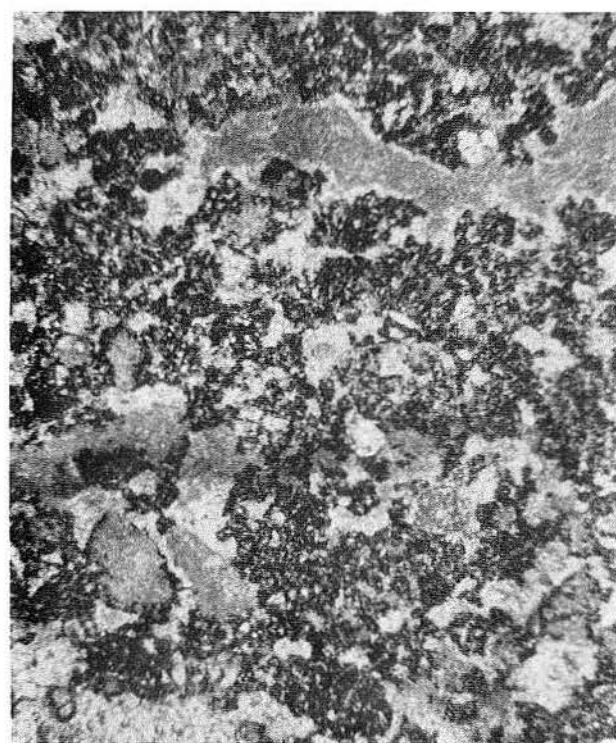
a



b



c



d

Figure 48. a. Dasycladacean alga is replaced by anhydrite (arrow) yet its mud-filled pores remain unaltered. b. Authigenic quartz (highly magnified) cuts across ooids as well as isopachous rim cement and later anhydrite. c. Three widely separated authigenic quartz crystals, two in sparry cement and one in a mud geopetal, are optically continuous. Note that the authigenic quartz cuts across the mud/spar boundary (center) and apparently bisects a muddy intraclast (top right). d. Nebulous algal textures present in shelf-margin facies.



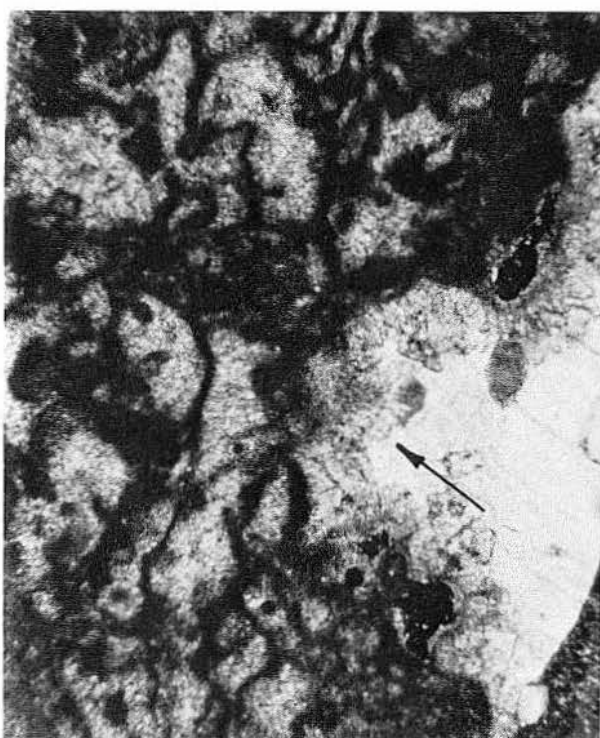
a



b



c



d

Figure 49. a. Thick micrite rims enveloping a coral fragment (arrow). b and c. Well preserved macroborings, rimmed with micrite and with multiple stages of internal sediment. In c each generation of mud infilling is separated from the next by bladed to subequant isopachous cement (submarine cement, arrow). d. Allochems within rudist body cavity are commonly neomorphosed and deformed against one another so that only the micrite rims mark their presence. A fine-grained isopachous cement (marine?) separates micrite rims from radiaxial cement (arrow).



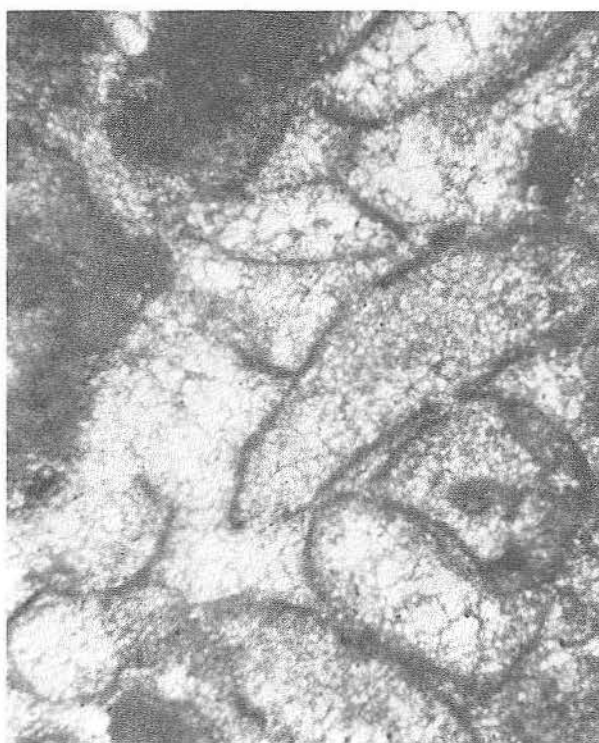
a



b

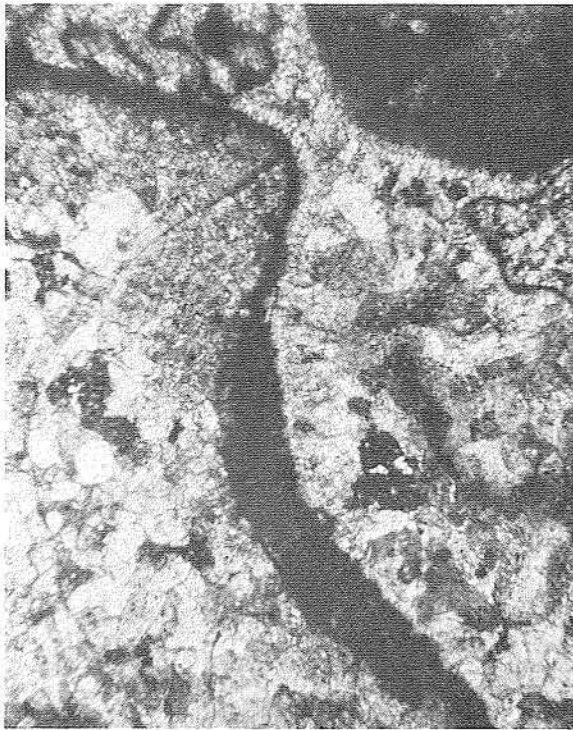


c



d

Figure 50. a. Apparent square-ended terminations in the radiaxial cement indicate the incorporation of original aragonitic submarine cement (arrows). b. Polygonal cement junctions and radiaxial cement in intergranular pores. c and d. Leaching of skeletal grains with fresh-water influx commonly resulted in broken micrite rims and interpenetrating grains. Fine-crystalline calcite, an uncommon cement in the shelf-margin grainstones, occurs where radiaxial cement is absent.



a



b

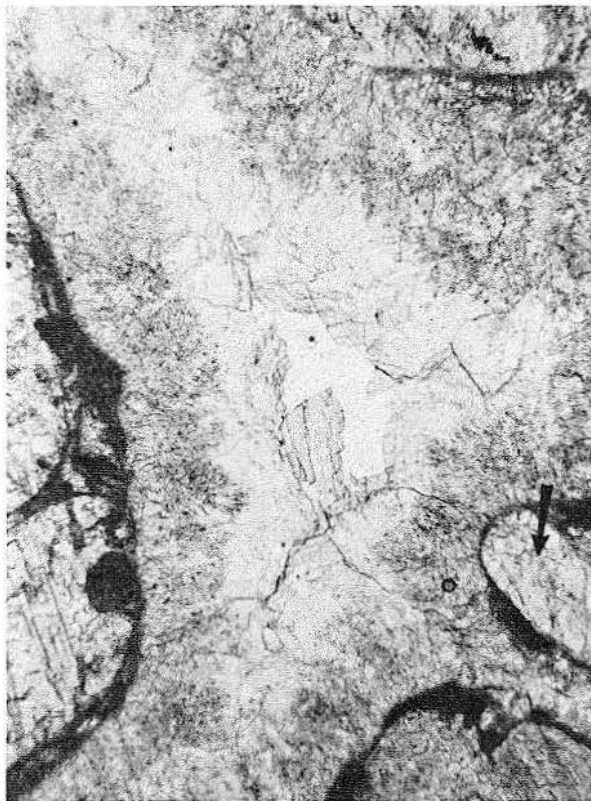


c

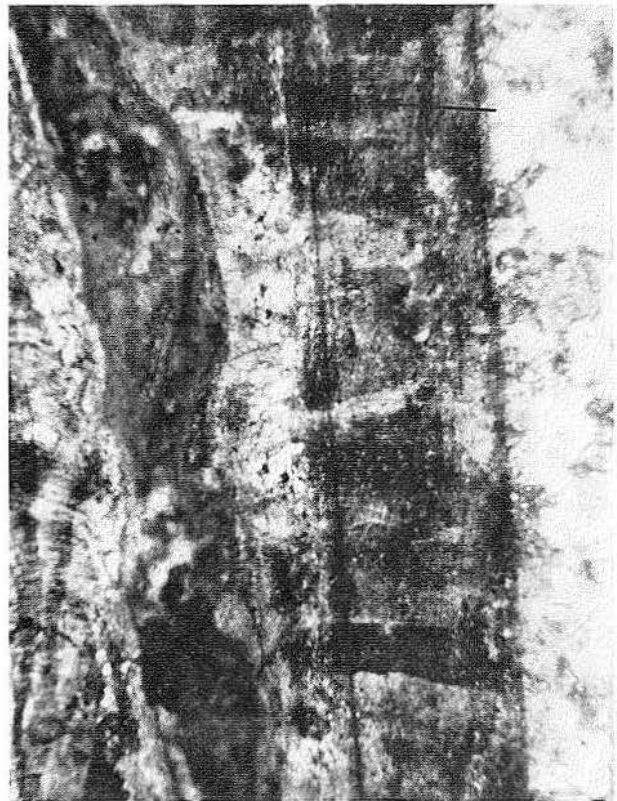


d

Figure 51. a and b. Radiaxial cement overlain by coarse-crystalline calcite (a, plane polarized, and b, crossed nicols). c. Radiaxial cement grades into a rare undulose, dirty yellow, medium-crystalline calcite spar. d. Outer part of the radiaxial spar is stained dark brown, probably due to organic inclusions. The polygonal juxtaposition of cement crystals indicates a possible submarine cement precursor for the radiaxial cement (see also fig. 50b).



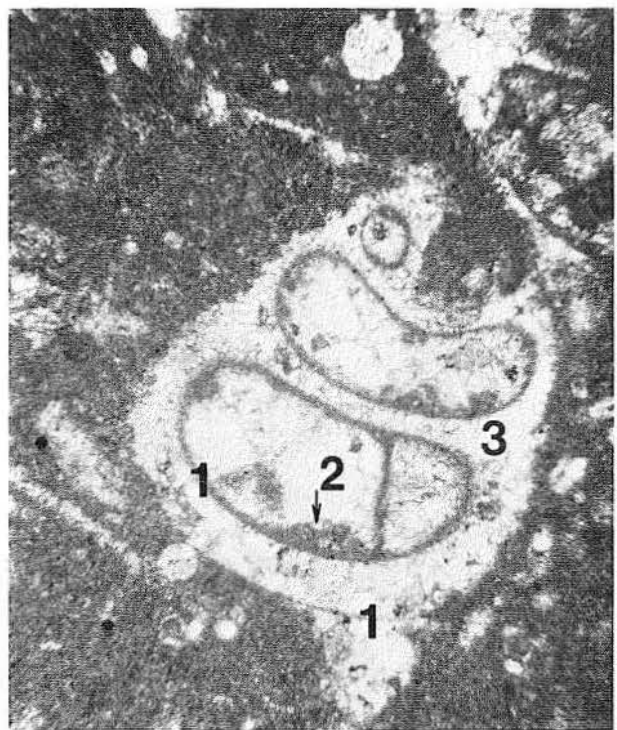
a



b



c



d

Figure 52. a and b. Strong evidence that at least some radial cement had an inversion origin includes the preservation of ghosts of original skeletal microstructure (arrows). c. Radial inversion of rudist shells, marked by the ghost of shell microstructure (arrow), is also common in the "cleaner" packstones of the shelf-margin facies. d. Micritization of skeletal walls (1), internal sediment (2), and neomorphism of allochems (3) occur in the shelf-margin wackestones.

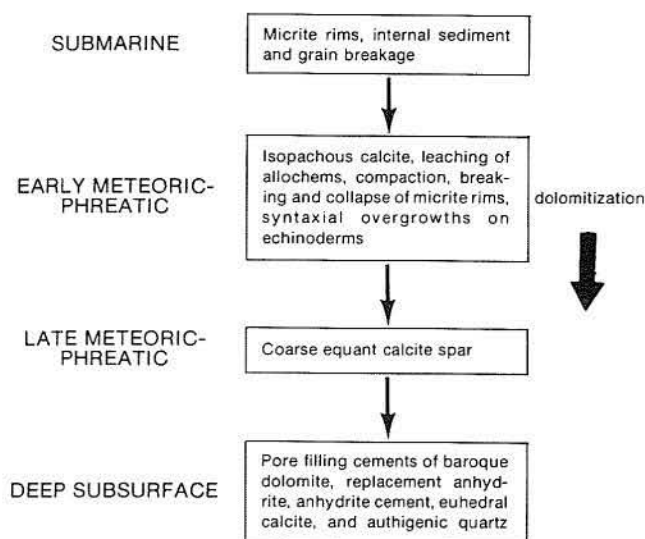


Figure 53. General composite sequence of diagenetic events in the upper Sligo oolite-shoal complex and adjacent subtidal skeletal wackestones. Variability is the norm, and no sample shows all features. Dolomitization stages yield successively larger rhombs and are generally restricted to the skeletal wackestone and pelletal facies.

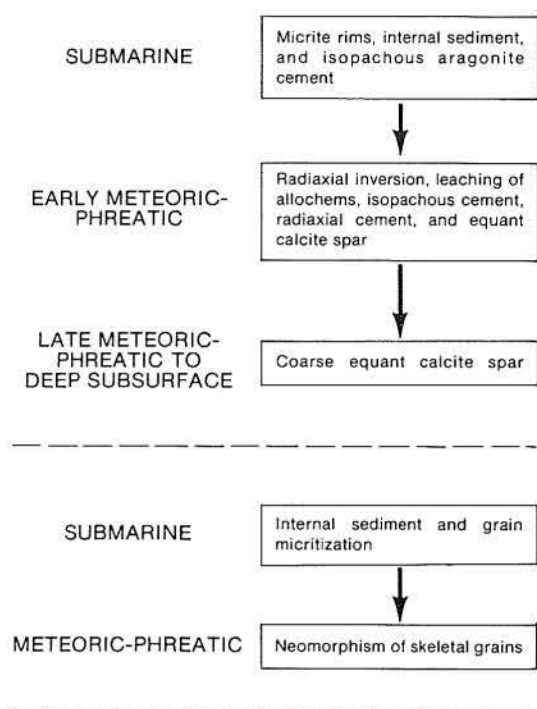


Figure 54. General sequence of diagenetic events in the Sligo shelf-margin grainstones and "cleaner" packstones (upper) and in the shelf-margin wackestones and "muddier" packstones (lower). Much less variability occurs in these rocks than in those from the oolite-shoal complex (fig. 53), and subsurface diagenesis is less pronounced.

Late Meteoric-Phreatic to Deep Subsurface Stage: Coarse-crystalline calcite spar (fig. 51a, b) overlies all previous cements and is thus interpreted to be a later cement. Achauer (1977) reports that this cement is iron-poor, which indicates it formed in either an oxidizing environment, such as a regional meteoric-phreatic zone, or an Fe-poor environment, which could include the deeper subsurface (below 610 m; 2,000 ft). Authigenic quartz laths are sparsely present. Their occurrence is irregular, and the laths cut across all cement and allochem borders.

Sligo Shelf-Margin Wackestones and Packstones

Mollusks, corals, and dasycladacean algae, along with echinoderm debris, *Solenopora*, oysters, and irregular stromatoporoid-like encrusting organisms are the dominant floral and faunal constituents of the wackestone and packstone facies. They show micritization of skeletal exteriors, micrite infilling of body chambers, and neomorphism of skeletal calcite (fig. 52d). Crushing of allochems is generally limited to pellets and micritic intraclasts. The shelf-margin wackestone and packstone facies contrast with the associated grainstones in the nearly complete lack of radial "cement" in the micritic facies. Fewer original voids and less marine cementation in the micritic facies may be the reason for this. However, radial inversion of rudist shells does occur (fig. 52c) in the less mud-rich packstones.

Summary: Sligo Diagenesis

The diagenetic history of the oolite-shoal complex is markedly different from that of the adjacent shelf-lagoon and outer-shelf facies (fig. 53). Oolite-shoal complex facies all show the imprint of a meteoric-phreatic water system. On the other hand, most shelf sediments were high in carbonate mud and underwent a limited postdepositional diagenesis including some dolomitization, skeletal leaching, and subsequent cementation. Aside from micritized rims and local bored hardground-like structures, there is little evidence for submarine cementation in either shelf or oolite-shoal complex facies. Submarine cementation was only locally significant.

Within the oolite-shoal complex three stages of diagenetic alteration occurred. The first, which took place either on the exposed substrate or with very shallow burial, includes the formation of micrite rims, some grain breakage, production and addition of internal sediments, and compaction.

Timing of compaction overlaps with the early features of meteoric-phreatic diagenesis, the

second stage of diagenesis. The fine- to medium-crystalline, equant to subequant (rarely bladed) isopachous calcite was involved in compaction. Therefore, although compaction may have begun very early in soft pellet-rich facies, the phreatic-zone rim cements were already present. Other features considered indicative of meteoric-phreatic diagenesis in the Sligo oolite-shoal facies include leaching of allochems, breaking and collapse of micrite rims, and interference in growth between isopachous calcite and syntaxial calcite around echinoderm fragments. Coarse-crystalline calcite is considered to have originated in the meteoric-phreatic zone, but at a later time.

The third phase of diagenesis, presumed to have occurred deeper in the subsurface than the meteoric-phreatic zone, includes events that post-date leaching of grains and are, in most cases, later than the precipitation of coarse equant calcite. Included here are several cementation products that cannot in all cases be dated relative to one another: baroque dolomite, replacement anhydrite, anhydrite cement, and authigenic quartz.

Facies of the oolite-shoal complex differ in their cement content. Clearly, meteoric-phreatic events, particularly isopachous calcite, are significant in all oolite-shoal facies; however, coarse-crystalline calcite cements are better developed in the grainstone facies. Anhydrite cement, although widespread in all Sligo facies, also appears to be greatest and most prevalent in the oolite grainstone.

Shelf-edge facies contrast diagenetically with the oolite-shoal complex as well as with shelf-lagoon and outer-shelf facies (fig. 54). Submarine cements, both aragonite and Mg-calcite, were locally present. Bladed, radial calcite is characteristic of the shelf-margin grainstones. This cement is interpreted to have multiple origins, including the inversion of submarine cements and rudist shells and precipitation as a pore-filling cement. Deep subsurface diagenesis — including abundant anhydrite and baroque dolomite — is also lacking in the shelf-margin grainstones. Late meteoric-phreatic coarse-crystalline equant calcite marks the final important stage of shelf-margin diagenesis.

Shelf-margin wackestone and packstone had a limited postdepositional history — much like the shelf-lagoon and outer-shelf wackestones that they border. The greatest difference between shelf-lagoon and outer-shelf wackestones and shelf-margin wackestones is the lack of anhydrite cement in the latter.

Finally, there appears to be a greater degree of crushing in the pellet-rich facies. Isopachous cement in the pelleted facies is due to meteoric-phreatic diagenesis and is intimately associated

with the crushed pellets. In contrast, pelleted facies are lacking on the shelf margin. Crushing of grains in shelf-margin facies was probably inhibited by the ubiquitous radial calcite. Grain leaching and compaction in the meteoric-phreatic zone are restricted to local shelf-margin grainstones, probably due to growth of irregularly spaced shoals above sea level and consequent subaerial exposure. Apparently such islands were not common along the shelf margin.

Hosston Formation

Siliciclastics

Nelsen (1978) examined thin sections of the Hosston siliciclastics from the Stanolind Schmidt, Gulf Dix, and Magnolia Baker and Mercer cores. The major cement type in the laminated sandstone facies is fine- to medium-crystalline dolomite. Nelsen (1978) observed that the dolomite commonly corrodes the quartz grains, resulting in serrated and embayed grains.

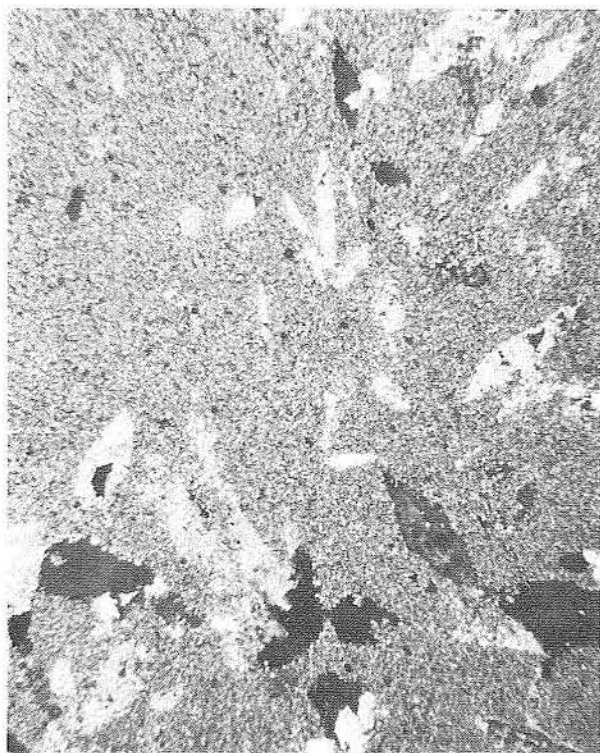
Anhydrite is the second most abundant cement. It displays a typical pseudocubic cleavage and apparently occurs as a later (postdolomite) void fill. Nelsen reports patchy to total destruction of porosity and permeability in some units by this cement.

Quartz is the last significant cement type in the clastic tidal flats recorded by Nelsen (1978). Quartz was precipitated as an overgrowth and appears to be associated with welded grain contacts and sutured grains. Nelsen reports that this type of siliceous cementation occurs in all the sandstones examined but is not extensive. In some cases quartz cementation occurs prior to the final pore-fill anhydrite cement.

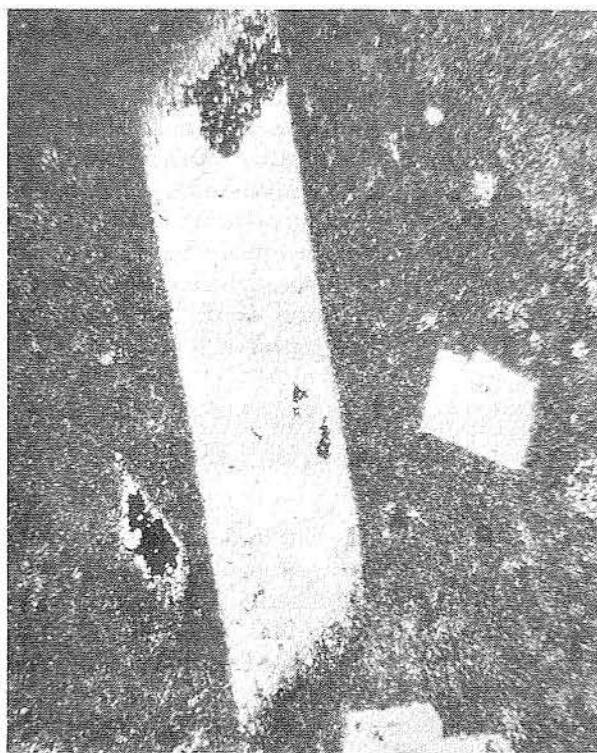
Minor pore-filling cements recorded by Nelsen (1978) include celestite, pyrite, and iron oxide. Iron oxide is very common in the conglomeratic sandstone facies and basal laminated sandstones. Nelsen documents a thin, circumgranular dolomite cement followed by a massive, pore-filling, iron-oxide cement.

Carbonates

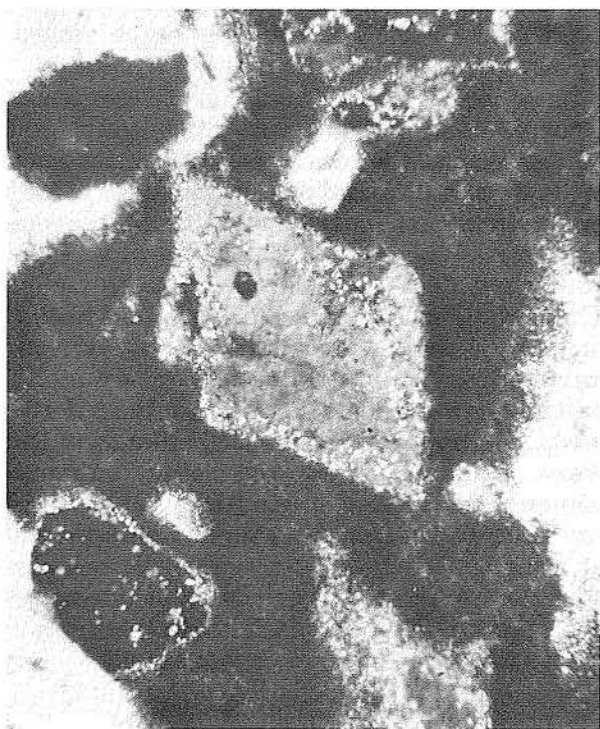
Diagenetic events observed in the Hosston dolomitic tidal-flat facies are similar to the diagenetic sequences documented for similar facies in the Sligo; therefore, the details will not be repeated. Briefly, the Hosston dolomitic tidal-flat units are characterized by (1) early dolomitization of pellets, (2) an isopachous, subequant calcite cement in some of the grainstones, (3) leaching of the aragonitic shell material, (4) compaction, (5) a later, coarse-crystalline, equant spar, (6) complete dolomitization, and (7) coprecipitation of baroque dolomite and anhydrite cements, often in shell-moldic voids. The resulting porosity is a



a



b



c



d

Figure 55. a and b. Anhydrite that has replaced the original gypsum laths in the Hosston mud-rich tidal-flat facies. c. Zonation of dolomite inclusion in gypsum lath indicates that there never was a period of leaching, and the laths have retained their original mineralogy. d. Rounded crystal edges suggest that some of the laths were windblown across the tidal flats.

combination of shell-moldic in the grainier facies and intercrystalline in the muddier dolomites. The dominant dolomite crystal size is fine to medium, and the rhombs always show some inclusions.

Although more thoroughly dolomitized, the micrite-rich carbonates (mudstones) underwent less postdepositional change than did other facies. The finer grain size is probably responsible for this phenomenon. The most significant diagenetic alterations are associated with the evaporite nodules. Anhydrite has replaced gypsum laths in

CONCLUSIONS

The Sligo and Hosston depositional wedge extends over thousands of square miles in South Texas. The wedge thickens from its pinch-out updip to greater than 300 m (1,000 ft) thick downdip at the shelf edge. It can be subdivided into three major coeval parts on the basis of facies and interpreted depositional environments: Hosston, lower Sligo, and upper Sligo.

Overall the Sligo and Hosston depositional wedge is time-transgressive; however, this transgression was punctuated by several progradational cycles, each of which was shifted farther landward.

Six major environments are recognized: alluvial plain, tidal-flat complex, inner-shelf lagoon, oolite-shoal complex, outer-shelf platform, and shelf margin. These environments occurred over a broad, shallow, very gently sloping shelf. The great variability of facies between environments reflects the wide spectrum of physical and biological conditions influencing deposition. The shelf margin is very narrow, elongate, and irregular. The entire complex is characterized by abundant coral and caprinid skeletal debris. Strike-oriented sand shoals dominate, and actual preserved reefs or bioherms are few. No systematic pattern of transgression or progradation occurs. In general, the shelf margin accumulated nearly vertically. The strike-trending oolite-shoal complex is many miles wide and tens of miles long. The entire complex comprises a vertical succession of several distinct shoals. Each shoal is similar in facies arrangement to the modern Joulter's Cay shoal of the Bahamas. Seaward each

fine dolomite (fig. 55a, b), although in one case (fig. 55c) gypsum crystals are still present. These gypsum crystals are zoned with fine to very fine dolomite, indicating that there never was a period of leaching that would have allowed the dolomite within the gypsum to fall to the bottom of the void. Rounded corners of the gypsum (fig. 55d) and sorting in some slabs may mean that gypsum laths were windblown across the tidal or supratidal flats to accumulate in windrows.

shoal is characterized by high-energy skeletal and oolite grain belts. Behind these facies, moderate- to low-energy coated-grain and pellet packstones were deposited on stabilized grain flats. The oolite-shoal complex separates the inner-shelf lagoon and outer-shelf platform. Highly burrowed skeletal wackestones containing mollusks, miliolids, and echinoids were deposited in both of these low-energy settings. The tidal-flat complex is very broad and comprises both siliciclastic and dolomitic sequences in the Hosston Formation. Burrowed, subtidal dolomite mudstone and sandstone are overlain by laminated dolomite mudstone and sandstone. Landward, the supratidal zone was a broad evaporitic sabkha. In the lower Sligo tidal-flat sequences, the subtidal and intertidal facies are more abundant, and the supratidal facies, deposited in beach ridges or channel levees, were less extensive.

In general, four stages of diagenesis are recognized throughout the Sligo and Hosston strata: submarine, early meteoric-phreatic, late meteoric-phreatic, and deep subsurface. There is a marked contrast, however, between the diagenetic histories of the oolite-shoal complex, inner- and outer-shelf deposits, and shelf-margin complex. The oolite-shoal complex shows the imprint of meteoric-phreatic water diagenesis, including mixing-zone dolomitization, whereas most shelf sediments were subjected to limited postdepositional diagenesis. Shelf-margin facies were also modified by some submarine cementation. The precipitation of bladed radiaxial calcite cements along with the inversion of some rudist shells and aragonitic submarine cements to radiaxial calcite characterizes the shelf-margin grainstones. The shelf margin also shows less deep subsurface diagenesis.

ACKNOWLEDGMENTS

We acknowledge the cooperation of C. R. Burnett (formerly with Tenneco Oil Company), R. L. Nicholas (Shell Oil Company), P. L. Keyes (Exxon Company, U.S.A.), D. P. McGooky (Texaco), and P. C. Smith (Amoco Oil Company), all of whom aided us in obtaining cores and subsurface data. J. Klutsch (Cities Service) provided some thin sections.

We wish to thank F. Wilson, D. Feray, L. Wooten, and R. G. Loucks for helpful discussions concerning this study. Sincere appreciation is also expressed to R. G. Loucks, C. R. Handford, C. D. Winker, and L. F. Brown, Jr., who read the

manuscript and made many helpful suggestions. M. W. Longman, R. G. Loucks, and F. C. Lucas aided in logging some of the cores while employed as Research Assistants at the Bureau of Economic Geology.

Several of the illustrations in this report have been published previously by Bebout (1977) and Bebout and Schatzinger (1978).

The manuscript was edited by Amanda R. Masterson, typeset by Charlotte Frere, and designed by Judy P. Culwell, assisted by Jamie S. Haynes, under the supervision of Susie Doenges, Lucille Harrell, and James W. Macon.

REFERENCES

- Achauer, C. A., 1977, Contrasts in cementation, dissolution, and porosity development between two Lower Cretaceous reefs of Texas, in Bebout, D. G., and Loucks, R. G., eds., *Cretaceous carbonates of Texas and Mexico, applications to subsurface exploration: The University of Texas at Austin, Bureau of Economic Geology Report of Investigations No. 89*, p. 127-137.
- Amsbury, D. L., 1974, Stratigraphic petrology of Lower and Middle Trinity rocks on the San Marcos platform, south-central Texas, in Perkins, B. F., ed., *Geoscience and Man: v. VII, Aspects of Trinity Division geology: Louisiana State University, School of Geoscience*, p. 1-35.
- Assereto, R., and Folk, R. L., 1976, Brick-like texture and radial rays in Triassic pisolites of Lombardy, Italy: a clue to distinguish ancient aragonitic pisolites: *Sedimentary Geology*, v. 16, p. 205-222.
- Bathurst, R. G. C., 1959, The cavernous structure of some Mississippian *Stromatactis* reefs in Lancashire, England: *Journal of Geology*, v. 67, p. 506-521.
- , 1966, Boring algae, micritic envelopes, and lithification of molluscan biosparites: *Geological Journal*, v. 5, p. 15-32.
- , 1971, Carbonate sediments and their diagenesis: *Developments in Sedimentology* 12, New York, Elsevier, 620 p.
- , 1979, Diagenesis in carbonate sediments: a review: *Geologische Rundschau*, v. 68, p. 848-855.
- Bay, A. R., 1980, Deposition of prograding carbonate sand shoals and their subsequent diagenesis — lower Glen Rose (Cretaceous), South Texas: The University of Texas at Austin, Master's thesis, 189 p.
- Bebout, D. G., 1974, Lower Cretaceous Stuart City shelf margin of South Texas: its depositional and diagenetic environments and their relationship to porosity: *Gulf Coast Association of Geological Societies Transactions*, v. 24, p. 138-159.
- , 1977, Sligo and Hosston depositional patterns, subsurface of South Texas, in Bebout, D. G., and Loucks, R. G., eds., *Cretaceous carbonates of Texas and Mexico, applications to subsurface exploration: The University of Texas at Austin, Bureau of Economic Geology Report of Investigations No. 89*, p. 79-96.
- Bebout, D. G., and Loucks, R. G., 1974, Stuart City Trend, Lower Cretaceous, South Texas: a carbonate shelf-margin model for hydrocarbon exploration: The University of Texas at Austin, Bureau of Economic Geology Report of Investigations No. 78, 80 p.
- Bebout, D. G., and Loucks, R. G., eds., 1977, *Cretaceous carbonates of Texas and Mexico, applications to subsurface exploration: The University of Texas at Austin, Bureau of Economic Geology Report of Investigations No. 89*, 332 p.
- Bebout, D. G., and Schatzinger, R. A., 1978, Distribution and geometry of an oolite-shoal complex — Lower Cretaceous Sligo Formation, South Texas: *Gulf Coast Association of Geological Societies Transactions*, v. 28, p. 33-45.
- Bebout, D. G., Schatzinger, R. A., and Loucks, R. G., 1977, Porosity distribution in the Stuart City Trend, Lower Cretaceous, South Texas, in Bebout, D. G., and Loucks, R. G., eds., *Cretaceous carbonates of Texas and Mexico, applications to subsurface exploration: The University*

- of Texas at Austin, Bureau of Economic Geology Report of Investigations No. 89, p. 234-256.
- Choquette, P. W., and Pray, L. C., 1970, Geologic nomenclature and classification of porosity in sedimentary carbonates: American Association of Petroleum Geologists Bulletin, v. 54, no. 2, p. 207-250.
- Conklin, J., and Moore, C., 1977, Paleoenvironmental analysis of the Lower Cretaceous Cupido Formation, Northeast Mexico, in Bebout, D. G., and Loucks, R. G., eds., Cretaceous carbonates of Texas and Mexico, applications to subsurface exploration: The University of Texas at Austin, Bureau of Economic Geology Report of Investigations No. 89, p. 302-323.
- Cook, T. D., 1979, Exploration history of South Texas Lower Cretaceous carbonate platform: American Association of Petroleum Geologists Bulletin, v. 63, no. 1, p. 32-49.
- Davies, G. R., 1977, Former magnesium calcite and aragonite submarine cements in upper Paleozoic reefs of the Canadian Arctic: a summary: Geology, v. 5, p. 11-15.
- Dunham, R. J., 1962, Classification of carbonate rocks according to depositional texture, in Freidman, G. M., ed., Depositional environments in carbonate rocks: Society of Economic Paleontologists and Mineralogists Special Publication 14, p. 182-191.
- , 1971, Meniscus cement, in Bricker, O. P., ed., Carbonate Cements: Johns Hopkins University, Studies in Geology no. 19, p. 297-300.
- Enos, P., 1977, Holocene sediment accumulations of the South Florida shelf margin, in Enos, P., and Perkins, R. D., eds., Quaternary sedimentation in South Florida: Geological Society of America Memoir 147, p. 1-130.
- Enos, P., and Perkins, R. D., 1979, Evolution of Florida Bay from island stratigraphy: Geological Society of America Bulletin, part I, v. 90, p. 59-83.
- Evans, G., Schmidt, V., Bush, P., and Nelsen, H., 1969, Stratigraphy and geologic history of the sabkha, Abu Dhabi, Persian Gulf: Sedimentology, v. 12, p. 145-159.
- Folk, R. L., 1974, The natural history of crystalline calcium carbonate: effect of magnesium content and salinity: Journal of Sedimentary Petrology, v. 44, p. 40-53.
- Folk, R. L., and Assereto, R., 1974, Giant aragonite rays and baroque white dolomite in tepee-fillings, Triassic of Lombardy, Italy: American Association of Petroleum Geologists Abstracts with Programs, v. 1, no. 1, p. 34-35.
- Folk, R. L., and Land, L. S., 1975, Mg/Ca ratio and salinity: two controls over crystallization of dolomite: American Association of Petroleum Geologists Bulletin, v. 59, no. 1, p. 60-68.
- Folk, R. L., and Siedlecka, A., 1972, The "schizohaline" environment: its sedimentary and diagenetic fabrics as exemplified by late Paleozoic rocks of Bear Island, Svalbard: Sedimentary Geology, v. 11, p. 1-15.
- Freeze, R. A., and Cherry, J. A., 1979, Groundwater: Englewood Cliffs, New Jersey, Prentice-Hall, 604 p.
- Ginsburg, R. N., 1956, Environmental relationships of grain size and constituent particles in some South Florida carbonate sediments: American Association of Petroleum Geologists Bulletin, v. 40, no. 11, p. 2384-2427.
- , ed., 1964, South Florida carbonate sediments: Miami Beach, Florida, Geological Society of America Guidebook, Field Trip I, 72 p.
- Golubic, S., Perkins, R. D., and Lukas, K. J., 1975, Boring microorganisms and microborings in carbonate substrates, in Frey, R. W., ed., Trace fossils: New York, Springer-Verlag, p. 229-259.
- Hardie, L. A., and Garrett, P., 1977, General environmental setting, in Hardie, L. A., ed., Sedimentation on the modern carbonate tidal flats of northwest Andros Island, Bahamas: Johns Hopkins University, Studies in Geology, no. 22, p. 12-49.
- Harris, P. M., 1979, Facies anatomy and diagenesis of a Bahamian ooid shoal: University of Miami, Sedimenta VII, 163 p.
- Heckel, P. H., 1974, Carbonate buildups in the geologic record: a review, in Laporte, L. F., ed., Reefs in time and space: Society of Economic Paleontologists and Mineralogists, Special Publication no. 18, p. 90-154.
- Hine, A. C., and Neumann, A. C., 1977, Shallow carbonate-bank-margin growth and structure, Little Bahama Bank, Bahamas: American Association of Petroleum Geologists Bulletin, v. 61, no. 3, p. 376-406.
- James, N. P., Ginsburg, R. N., Marszalek, D. S., and Choquette, P. W., 1976, Facies and fabric specificity of early subsea cements in shallow Belize (British Honduras) reefs: Journal of Sedimentary Petrology, v. 46, p. 523-544.
- Kendall, A. C., and Tucker, M. E., 1973, Radial fibrous calcite: a replacement after acicular carbonate: Sedimentology, v. 20, p. 365-389.
- Kendall, C. G. St. G., and Skipworth, P. A. D'E., 1969, Holocene shallow-water carbonate and evaporite sediments of Khor al Bazam, Abu Dhabi, Southwest Persian Gulf: American Association of Petroleum Geologists Bulletin, v. 53, no. 4, p. 841-869.

- Kobluk, D. R., and Risk, M. J., 1977, Micritization and carbonate-grain binding by endolithic algae: *American Association of Petroleum Geologists Bulletin*, v. 61, no. 7, p. 1069-1082.
- Land, L. S., 1967, Diagenesis of skeletal carbonates: *Journal of Sedimentary Petrology*, v. 37, p. 914-930.
- 1970, Phreatic versus vadose meteoric diagenesis of limestones: evidence from a fossil water table: *Sedimentology*, v. 14, p. 175-185.
- 1973a, Holocene meteoric dolomitization of Pleistocene limestone, North Jamaica: *Sedimentology*, v. 20, p. 411-424.
- 1973b, Contemporaneous dolomitization of middle Pleistocene reefs by meteoric water, North Jamaica: *Bulletin of Marine Science*, v. 23, p. 64-92.
- Longman, M. W., 1980, Carbonate diagenetic textures from nearsurface diagenetic environments: *American Association of Petroleum Geologists Bulletin*, v. 64, no. 4, p. 461-487.
- Longman, M. W., and Mench, P. A., 1978, Diagenesis of Cretaceous limestones in the Edwards aquifer system of South-Central Texas: a scanning electron microscope study: *Sedimentary Geology*, v. 21, p. 241-276.
- Loucks, R. G., 1976, Pearsall Formation, Lower Cretaceous, South Texas — depositional facies and carbonate diagenesis and their relationship to porosity: The University of Texas at Austin, Ph.D. dissertation, 362 p.
- 1977, Porosity development and distribution in shoal-water carbonate complexes — subsurface Pearsall Formation (Lower Cretaceous), South Texas, in Bebout, D. G., and Loucks, R. G., eds., *Cretaceous carbonates of Texas and Mexico, applications to subsurface exploration*: The University of Texas at Austin, Bureau of Economic Geology Report of Investigations No. 89, p. 97-126.
- Loucks, R. G., and Folk, R. L., 1976, Fanlike rays of former aragonite in Permian Capitan reef pisolite: *Journal of Sedimentary Petrology*, v. 46, p. 483-485.
- Maxwell, W. G. H., 1968, *Atlas of the Great Barrier Reef*: New York, Elsevier, 258 p.
- McBride, M. W., Woodruff, C. M., Jr., and Craig, L. E., 1979, Facies distribution within the Hosston Formation, Central Texas — implications to low-temperature geothermal waters: *Gulf Coast Association of Geological Societies Transactions*, v. 29, p. 172-179.
- Muller, G., 1971, "Gravitational" cement: an indicator for the vadose zone of the subaerial diagenetic environment, in Bricker, O. P., ed., *Carbonate cements*: Johns Hopkins University, *Studies in Geology*, no. 19, p. 301-302.
- Myerhoff, A. A., 1967, Future hydrocarbon provinces of Gulf of Mexico - Caribbean region: *Gulf Coast Association of Geological Societies Transactions*, v. 17, p. 217-260.
- Nelsen, R. L., 1978, Facies and depositional environments of the Hosston Formation (Lower Cretaceous), South-Central Texas: The University of Texas at Arlington, Master's thesis, 148 p.
- Neumann, A. C., Kofed, J. W., and Keller, G. H., 1977, Lithohierms in the Straits of Florida: *Geology*, v. 5, p. 4-10.
- Purdy, E. G., 1963, Recent calcium carbonate facies of the Great Bahama Bank: 2. Sedimentary facies: *Journal of Geology*, v. 71, p. 472-497.
- Purser, B. H., 1969, Syn-sedimentary marine lithification of Middle Jurassic limestones in the Paris Basin: *Sedimentology*, v. 12, p. 205-230.
- Purser, B. H., and Evans, G., 1973, Regional sedimentation along the Trucial Coast, Southeast Persian Gulf, in Purser, B. H., ed., *The Persian Gulf*: New York, Springer-Verlag, p. 211-232.
- Pusey, W. C., 1975, Holocene carbonate sedimentation on northern Belize shelf, in Wantland, K. F., and Pusey, W. C., eds., *Belize shelf-carbonate sediments, clastic sediments, and ecology*: *American Association of Petroleum Geologists, Studies in Geology* no. 2, p. 131-233.
- Sandberg, P. A., 1975, New interpretations of Great Salt Lake ooids and of ancient non-skeletal carbonate mineralogy: *Sedimentology*, v. 22, p. 497-537.
- Schroeder, J. H., 1972, Calcified algal filaments of an endolithic alga in recent Bermuda reefs: *Neues Jahrbuch Fur Geologie und Palaontologie Monatshefte*, no. 1, p. 16-22.
- Shinn, E. A., 1969, Submarine lithification of Holocene carbonate sediments in the Persian Gulf: *Sedimentology*, v. 12, p. 109-144.
- Shinn, E. A., Bloxson, W. E., and Lloyd, R. M., 1974, Recognition of submarine cements in Cretaceous reef limestone from Texas and Mexico: *American Association of Petroleum Geologists, Abstracts with Programs*, v. 1, no. 1, p. 82.
- Shinn, E. A., Lloyd, R. M., and Ginsburg, R. N., 1969, Anatomy of a modern carbonate tidal-flat, Andros Island, Bahamas: *Journal of Sedimentary Petrology*, v. 39, p. 1202-1228.
- Shinn, E. A., Robbin, D. M., and Steinen, R. P., 1980, Experimental compaction of lime sediment (abs.): *American Association of Petroleum Geologists Bulletin*, v. 64, no. 5, p. 783.
- Stabler, C. L., and Marquez, D., 1977, Initiation of Lower Cretaceous reefs in Sabinas Basin, Northeast Mexico, in Bebout, D. G., and Loucks, R. G., eds., *Cretaceous carbonates of Texas and*

Mexico, applications to subsurface exploration: The University of Texas at Austin, Bureau of Economic Geology Report of Investigations No. 89, p. 299-301.

Steinen, R. P., 1974, Phreatic and vadose diagenetic modification of Pleistocene limestone: petrographic observations from subsurface of Barbados, West Indies: American Association of Petroleum Geologists Bulletin, v. 58, no. 6, p. 1008-1024.

Stricklin, R. L., Smith, C. I., and Lozo, F. E., 1971, Stratigraphy of Lower Cretaceous Trinity deposits of Central Texas: The University of Texas at Austin, Bureau of Economic Geology Report of Investigations No. 71, 63 p.

Texas Railroad Commission, Oil and Gas Division, Annual Reports, 1960 through 1979.

Walls, R. H., Mountjoy, E. W., and Fritz, P., 1979, Isotopic composition and diagenetic history of carbonate cements in Devonian Golden Spike reef, Alberta, Canada: Geologic Society of America Bulletin, part I, v. 90, p. 963-982.

Wilson, J. L., 1974, Characteristics of carbonate platform margins: American Association of Petroleum Geologists Bulletin, v. 58, no. 5, p. 810-824.

Wilson, J. L., and Piali, G., 1977, A Lower Cretaceous shelf margin in Northern Mexico, in Bebout, D. G., and Loucks, R. G., eds., Cretaceous carbonates of Texas and Mexico, applications to subsurface exploration: The University of Texas at Austin, Bureau of Economic Geology Report of Investigations No. 89, p. 286-294.

APPENDIX I:

Materials and Procedures

This report is based on analysis of core and core chips of 2,765 m (9,069 ft) from 50 wells (fig. 4). Most of these cores are stored at the Bureau of Economic Geology's Well Sample and Core Library.

All the cores were sawed lengthwise, and one sawed surface was etched with dilute hydrochloric acid. The etched surface was examined under low magnification with a binocular microscope, and the following features were recorded on a graphic logging form at the scale of 1 inch = 10 feet: mineral composition, pore type, porosity, nature of contacts, structures, texture, fabric, grain size, crystal size, crystal shape, color, fossils, and cement. More than 190 thin sections were prepared from 31 wells for the identification of diagenetic fabrics. Using the detailed information obtained above, the rocks studied were grouped into general facies types, and these were used on the cross sections included in this report.

Detailed graphic logs of cores in the study are not included in this report. However, those interested in more detail may obtain copies of these logs from the Bureau of Economic Geology's open files for the cost of reproduction.

Well	Core Interval (ft)	Total Footage
1. Stanolind No. 1 Schmidt, Guadalupe Co.	1,953 - 2,574	621
2. Magnolia No. 1 Mercer, Caldwell Co.	3,780 - 3,933 3,950 - 3,973	516

Well	Core Interval (ft)	Total Footage
	3,978 - 4,013 4,019 - 4,159 4,170 - 4,282 4,287 - 4,372 4,386 - 4,396 4,409 - 4,445 4,455 - 4,464 4,466 - 4,472 4,479 - 4,486	
3. Magnolia No. 1 Baker, Guadalupe Co.	3,715 - 4,671	956
4. Gulf No. 20 Dix, Guadalupe Co.	4,386 - 5,018 5,026 - 5,426	1,032
5. Humble No. 1 Pruitt, Atascosa Co.	9,754 - 9,940 9,946 - 9,984 9,996 - 10,351 10,400 - 10,750	929
6. Sun No. 1 Handy, Karnes Co.	15,526 - 15,676 15,708 - 15,730 15,736 - 15,985 16,038 - 16,054 16,060 - 16,088 16,108 - 16,160 16,206 - 16,216 16,226 - 16,236 16,240 - 16,260	557
7. Shell No. 1 Alvarado, Bee Co.	16,572 - 16,628 16,236 - 16,270 16,284 - 16,288 16,292 - 16,298 16,704 - 16,870 16,908 - 16,924 16,928 - 16,934	286
8. Shell No. 1 Roessler, Bee Co.	16,098 - 16,118	20

Well	Core Interval (ft)	Total Footage	Well	Core Interval (ft)	Total Footage
9. Shell No. 1 O'Neal, Bee Co.	15,976 - 16,025 16,085 - 16,112 16,450 - 16,466 16,700 - 16,706	98		15,605 - 15,628 15,638 - 15,654 15,660 - 15,678 15,688 - 15,738 15,746 - 15,750 15,755 - 15,760	
10. Shell No. 1 Brown, DeWitt Co.	15,944 - 16,044 16,696 - 16,748 16,950 - 17,000 17,200 - 17,226 17,450 - 17,474 17,700 - 17,726 17,950 - 18,000	328	26. Texaco No. 1 Watkins, Webb Co. (core chips)	15,906 - 15,949 15,955 - 15,959 15,970 - 15,980 15,984 - 15,989 15,996 - 16,004 16,018 - 16,069	121
11. Smith and Starr No. 1 Crowell, Caldwell Co.	5,340 - 5,384 5,394 - 5,432 5,830 - 5,844	96	27. Hunt No. 1 Reuthinger, Webb Co.	14,350 - 14,400	50
12. Tenneco No. 1 Dickson, Caldwell Co.	6,120 - 6,180		28. Texaco No. 1 Canales, LaSalle Co. (core chips)	15,190 - 15,215 15,224 - 15,260 15,270 - 15,314 15,320 - 15,342 15,370 - 15,418	175
13. Tenneco No. 1 Kauffman, Bastrop Co.	5,995 - 6,058	63	29. Tidewater No. 1 Wilson, LaSalle Co. (core chips)	12,100 - 12,154 12,182 - 12,230	102
14. Tenneco No. 1 Sawicki, Bastrop Co.	7,780 - 7,812	32	30. Tenneco-Pennzoil No. 1 Edgar, Frio Co.	6,076 - 6,136	60
15. Guadalupe 13 River Authority, Dam Site No. 7, Kendall Co.	190 - 266 270 - 278 284 - 288 290 - 294	92	31. Tenneco No. 1 Sirianni, Frio Co.	6,440 - 6,500	60
16. Tenneco No. 1 Herrera, Bexar Co.	4,785 - 4,836	51	32. Tenneco-Pennzoil No. 1 Wilbeck, Frio Co.	6,666 - 6,770	164
17. Tenneco No. 1 McKenzie, Wilson Co.	7,125 - 7,200	75	33. Tenneco-Pennzoil No. 1 Goad, Frio Co.	6,292 - 6,345	54
18. Tenneco-Pennzoil No. 1 Suggs, Atascosa Co.	7,216 - 7,266	50	34. Tenneco No. 1 Machen, Frio Co.	6,210 - 6,270	60
19. Tenneco No. 1 Rodgers, Atascosa Co.	5,725 - 5,786	61	35. Tenneco No. 1 Roberts, Frio Co.	6,896 - 6,950	54
20. Tenneco No. 1 P. R. Smith, Atascosa Co.	4,420 - 4,540	20	36. Moncrief No. 2 Rheiner, Frio Co.	7,260 - 7,344	84
21. Tenneco-Pennzoil No. 1 J. J. Smith, Atascosa Co.	5,300 - 5,354	54	37. Tenneco No. 1 Mack, Frio Co.	7,435 - 7,850	415
22. Tenneco-Pennzoil No. 1 Finch, Atascosa Co.	6,274 - 6,325	51	38. Tenneco No. 1 Ney, Medina Co.	3,630 - 3,752	102
23. Tenneco No. 1 Climer, Atascosa Co.	6,645 - 6,706	61	39. Tenneco-Pennzoil No. 1 Hardie, Medina Co.	5,120 - 5,159	39
24. Phillips No. 1 Washburn, McMullen Co. (cuttings)	14,000 - 14,010 14,015 - 14,082 14,088 - 14,150 14,155 - 14,232 14,240 - 14,295 14,315 - 14,346 14,370 - 14,475 14,485 - 14,494 14,505 - 14,530 14,575 - 14,612 14,620 - 14,680 14,704 - 14,770 14,814 - 14,836	726	40. Tenneco No. 1 Wilson, Medina Co.	4,524 - 4,566	42
25. Gulf No. 1 Friedrichs, Duval Co.	15,512 - 15,544 15,552 - 15,560 15,580 - 15,584 15,594 - 15,600	166	41. Tenneco-Pennzoil No. 1 Carroll, Medina Co.	4,300 - 4,360	60
			42. Hughes and Hughes No. 1 Plachy, Medina Co.	4,768 - 4,790	22
			43. Tenneco No. 1 Powell, Medina Co.	4,088 - 4,148	60
			44. Moncrief No. 1 Collins, Medina Co.	4,894 - 4,950	56
			45. Rowe No. 1 Kincaid, Zavala Co.	6,396 - 6,456	60

Well	Core Interval (ft)	Total Footage	Well	Core Interval (ft)	Total Footage
46. Tenneco No. 1 Nixon, Zavala Co.	7,330 - 7,372	42		15,752 - 15,756	
47. Tenneco-Pennzoil No. 1 K, B and M, Zavala Co.	6,404 - 6,454	50		15,776 - 15,778	
48. Belco No. 1 Kincaid, Maverick Co.	7,716 - 7,836	120		15,786 - 15,792	
49. General Crude No. 1 McDowell, Karnes Co.	15,704 - 15,708	48		15,798 - 15,800	
	15,712 - 15,714			15,813 - 15,817	
	15,732 - 15,736			15,823 - 15,832	
	15,745 - 15,749			15,860 - 15,865	
				15,880 - 15,882	
			50. General Crude No. 1 Rolf, Karnes Co.	15,470 - 15,498	28

